

**A Precision Search for Exotic Scalar and Tensor Couplings in
the Beta Decay of Polarized ^{37}K**

by

Melissa Anholm

A Thesis submitted to the Faculty of Graduate Studies of
The University of Manitoba
in partial fulfillment of the requirements of the degree of

DOCTOR OF PHILOSOPHY

Department of Physics and Astronomy
University of Manitoba
Winnipeg

Abstract

The nuclear weak interaction is known to feature both vector and axial-vector couplings in a dominant role, however the presence of scalar and tensor couplings cannot be ruled out entirely. In beta decay physics, the Fierz interference, b_{Fierz} , is an observable comprised of a linear combination of scalar and tensor couplings, and can be measured as an adjustment to the shape of the resultant beta energy spectrum. A precision measurement experiment is conducted to observe the β^+ decay of spin-polarized ^{37}K from an atom cloud intermittently confined by a magneto-optical trap, and the beta energy spectra are observed in two detectors on opposing sides of the cloud, along the axis of polarization. This geometry, combined with a knowledge of the polarization, allows the superratio asymmetry to be constructed, providing an observable which is particularly sensitive to the value of b_{Fierz} , while simultaneously eliminating contributions from a variety of systematic effects. Geant4 simulations are used to model scattering effects that could mimic the signal being searched for. The resulting measurement gives $b_{\text{Fierz}} = +0.033 \pm 0.084(\text{stat}) \pm 0.039(\text{syst})$, consistent with the Standard Model.

Acknowledgements

People to acknowledge here include: John Behr, Gerald Gwinner, Dan Melconian.
Also: Spencer Behling, Ben Fenker, Alexandre Gorelov, James McNeil, Danny Ashery.

Contents

Abstract	ii
Acknowledgements	iii
Contents	vi
List of Figures	vii
List of Tables	x
Shit To Do	xxxiii
1 Background	1
1.1 Beta Decay within the Standard Model	1
1.2 A Generalized Description of the Weak Interaction	3
1.3 Mathematical Formalism	4
1.4 Our Decay	6
1.5 The Shake-off Electron Spectrum	7
1.6 Fierz Interference – The Physical Signature	9
1.7 On the Superratio, the Supersum, and the Constructed Asymmetry .	11
2 Considerations and Implementation of Atomic Techniques	12
2.1 An Overview of Magneto-Optical Traps	12
2.1.1 Zeeman Splitting	13
2.1.2 Doppler Cooling	14
2.1.3 Atom Trapping with a MOT	15
2.2 Optical Pumping	17
2.3 An Overview of the Double MOT System and Duty Cycle	18
2.4 The AC-MOT and Polarization Setup	22
2.5 Measurement Geometry and Detectors	25
2.5.1 Microchannel Plates and Electrostatic Hoops	25
2.5.2 Beta Detectors	28

2.5.3	The Photoionization Laser	29
3	Calibrations and Data Selection	32
3.1	An Overview of Available Data	32
3.2	Preliminary Data Selection with the rMCP	34
3.3	Calibrations with the rMCP	37
3.4	Measurements of the Atom Cloud	42
3.5	Electron Run Data Selection and Preliminary Cuts	48
3.6	Further Cuts Using the DSSD	50
3.7	Timing Improvements with the Leading Edge and Scintillator Walk Correction	52
4	Simulations	58
4.1	Considerations for Software Upgrade Implementation	58
4.2	The Simple Monte Carlo and Response Function	61
4.3	Evaluating Scattering Effects from the Cloud	76
4.4	Simulating the Background and Time of Flight	80
5	Analysis and Estimates of Systematic Effects	84
5.1	Overview	86
5.2	Comparing Simulations to Experimental Data	87
5.3	BB1 Radius, Energy Threshold, Agreement	89
5.4	Background Modeling – Decay from Surfaces within the Chamber	90
5.5	Quantifying the Effects of Backscatter with Geant4	90
5.6	Lineshape Reconstruction	90
5.6.1	What is it and how does it work?	90
5.6.2	The Results – Things That Got Evaluated This Way	90
5.6.3	The low-energy tail uncertainty, and what it does	91
6	Results and Conclusions	94
6.1	Measured Limits on b_{Fierz} and A_β	94
6.2	Discussion of Corrections and Uncertainties	94
6.3	Relation to Other Measurements and New Overall Limits	95
6.4	Other Possible Future Work for the Collaboration: R_{slow}	102
6.4.1	Motivation	102
6.4.2	The Decay Process	103
6.4.3	Status of the R_{slow} Measurement	104
6.5	Conclusions	105
Bibliography		106
Appendices		110

A Notable Differences in Data Selection between this and the Previous Result	110
A.1 Polarization Cycle Selection	110
A.2 Leading Edge / Trailing Edge and Walk Correction	111
A.3 TOF Cut + Background Modelling	111
A.4 BB1 Radius	111
A.5 BB1 Energy Threshold	111
B A PDF	112
B.1 JTW	112
B.2 Holstein	114
C Notation	120
C.1 Comparison Guide	120
C.2 Imported from Another Appendix	120
D SuperRatio	130

List of Figures

1.1	A level diagram for the decay of ^{37}K	7
1.2	Levinger TOF	9
1.3	Here's why it's better to extract b_{Fierz} from an asymmetry, in this case.	10
2.1	Components of a magneto-optical trap, including current-carrying magnetic field coils and counterpropagating circularly polarized laser beams. Diagram taken from [1]	16
2.2	An atomic level diagram for the optical pumping of ^{37}K , taken from [2].	18
2.3	The TRINAT experimental set-up, viewed from above. The two MOT system reduces background in the detection chamber. Funnel beams along the atom transfer path keep the atoms focused.	20
2.4	The 2014 duty cycle for transferring, cooling, trapping, and optically pumping ^{37}K	21
2.5	One cycle of trapping with the AC-MOT, followed by optical pumping to spin-polarize the atoms. After atoms are transferred into the science chamber, this cycle is repeated 100 times before the next transfer. The magnetic dipole field is created by running parallel (rather than anti-parallel as is needed for the MOT) currents through the two coils.	22
2.6	A scale diagram of the interior of the TRINAT detection chamber, shown edge-on with a decay event. After a decay, the daughter will be unaffected by forces from the MOT. Positively charged recoils and negatively charged shake-off electrons are pulled towards detectors in opposite directions. Although the β^+ is charged, it is also highly relativistic and escapes the electric field with minimal perturbation.	27

2.7	Inside the TRINAT science chamber. This photo is taken from the vantage point of one of the microchannel plates, looking into the chamber towards the second microchannel plate. The current-carrying copper Helmholtz coils and two beta telescopes are visible at the top and bottom. The metallic piece in the foreground is one of the electrostatic hoops used to generate an electric field within the chamber. The hoop's central circular hole allows access to the microchannel plate, and the two elongated holes on the sides allow the MOT's trapping lasers to pass unimpeded at an angle of 45 degrees 'out of the page'.	31
3.1	Timing sums for the rMCP, run 447.	36
3.2	Cloud Position for run 447 for various rMCP timing sum cuts	37
3.3	rMCP Calibration	40
3.4	Photoion Hit Positions in 2D	41
3.5	Photoion Hit Positions at 535 V/cm, as a function of AC-MOT Time	43
3.6	Trap Position along TOF Axis	45
3.7	Trap Position from Camera	46
3.8	Vertical Trap Position from rMCP	47
3.9	Position as measured on the eMCP, after some data cleaning.	53
3.10	Beta-electron TOF, for events with and without eMCP hit position information. A cut will eventually be taken to accept only events sufficiently near the largest peak – in this case the number of events is ‘only’ decreased by a factor of 2.	54
3.11	SOE TOF peaks (eMPC - Scintillator), using the leading edge (LE) and using the trailing edge (TE). Data is sorted according to sunset. For each individual sunset, the TE peak is broader than the LE peak. The centroid of each sunset is also more variable in the TE plots.	55
3.12	SOE TOF walk, before (left) and after (right) applying a quartic adjustment to straighten out the effective TOF.	56
3.13	Experimental Scintillator Spectra	57
4.1	Fit to Mono-Energetic Spectrum, 5000 keV	67
4.2	Fit to Mono-Energetic Spectrum, 3000 keV	68
4.3	Fit to Mono-Energetic Spectrum, 1500 keV	69
4.4	Fit to Mono-Energetic Spectrum, 1000 keV	70
4.5	Fit to Mono-Energetic Spectrum, 750 keV	71
4.6	Lineshape Parameter Fits (Part 1)	72
4.7	Lineshape Parameter Fits (Part 2)	73
4.8	Lineshape Parameter Fits (Part 3)	74
4.9	Lineshape Parameter Fits (Part 4)	74
4.10	Goodness of Fit for Modeled Response Functions	75

4.11	Simulated Beta emission angle w.r.t. the detector vs adjusted Levinger SOE TOF	78
4.12	Simulated Beta emission angle w.r.t. the detector vs adjusted 0eV SOE TOF	79
4.13	SOE TOF – Model and Data	82
4.14	The superratio asymmetry, averaged over all scintillator energies between 400-4800 keV, is used to compare the experimental data and simulated TOF model as a proxy for the quality of the model to estimate the background. All other cuts have been applied.	83
5.1	Scattering Effects in the Asymmetry	88
5.2	Lineshape Comparison	91
5.3	A_β Position Error	92
5.4	b_{Fierz} Position Error	93
6.1	SetB Superratio Asymmetry	95
6.2	SetC Superratio Asymmetry	96
6.3	SetD Superratio Asymmetry	97
6.4	χ^2 Map for Runset B	98
6.5	χ^2 Map for Runset C	99
6.6	χ^2 Map for Runset D	100
6.7	χ^2 Map for All Data	101
C.1	"Notes 0"	124
C.2	"Notes 1"	125
C.3	"Notes 2"	126
C.4	"Notes 3"	127
C.5	"Notes 4"	128
C.6	"Notes 5"	129

List of Tables

3.1	List of Electron Runs	33
3.2	List of Recoil Runs	33
3.3	Cloud Position and Size	44
5.1	Error Budget	87
C.1	Kinematic Terms Guide	121
C.2	Angular Momentum Notation	121
C.3	Multipole Notation	122
C.4	Selected Integrals from Holstein's Eq. (51)	123

Shit To Do

■ Seriously, this section needs some citations. Notably, C.S. Wu [3] (done) and Lee+Yang [4] (done). Perhaps also Hong+Sternberg+Garcia [5]. Probably a bunch more people too though.	4
■ Write a paragraph about what we're looking for with this experiment. . . .	4
■ JB on intuitive concepts that are missing: The SM couples to left-handed neutrinos and right-handed antineutrinos. Since the neutrinos only have weak interactions, there are no right-handed nu's nor left-handed antinu's in nature. The neutrino asymmetry B_ν is a number with no energy dependence. Similarly, the SM weak interaction only couples to right-handed positrons and left-handed electrons. Since these are massive particles, the average helicity of positrons is not 1, but instead v/c. One can always boost to a frame where the positron keeps its circulation but is moving in the opposite direction. This is why the beta asymmetry is A v/c, not just A. The Fierz term's additional energy dependence of m/E also comes from helicity arguments, stemming from the fact that it still is coupling to SM nu's and antinu's only, so the beta's are generated with wrong handedness. The details are built at 4th-year undergrad level in Garcia's paper with his student and postdoc [5].	4
■ Unfortunately, the outgoing (anti-)neutrino is very difficult to detect directly, and we make no attempt to do so in this experiment. Instead, we might look for coincidences between an outgoing beta and a recoiling nucleus, and use that information to reconstruct the kinematics of the neutrino.	5
■ Do it! Do the master equation!	5
■ JB: cut "so we will simply provide the combined master equation here" Don't. The equation you have is all you need.	5

█ JB on intuitive concepts that are missing:	
The beta asymmetry dependence on the Fierz term only comes through the normalization of $W(\theta) = 1 + b_{\text{Fierz}}m/E + A_\beta \cos(\theta)$.	
i.e.:	
$W'(\theta) = 1 + A_\beta/(1 + b_{\text{Fierz}}m/E) \cos(\theta)$. (the angular distribution must be unity where cos(theta) vanishes, by definition).	6
█ Is it definitely true that the nuclear structure corrections are *smaller*? Or is it just that they're better understood?	7
█ Also, ^{37}K is a really nice isotope for this, because its big A_β value means we have a big thing to multiply any b_{Fierz} value there might be when we construct the superratio asymmetry to eliminate systematics.	7
█ Do I want to re-assign N somehow so the notation works better?	8
█ cite someone!! I don't know who.	8
█ In the end, we used $(0.09) * (0\text{eV}) + (0.91) * (0.85 * (4\text{S}) + 0.15 * (3\text{P}))$. But I say that in the other section. Also, John used Eq.20 for the 4S, and Eq.24 for the 3P.	8
█ Comment on how well this matches our data? Somehow?	8
█ Maybe just kill this picture? At least reference it in the text somewhere.	9
█ JB on that missing figure that I've now put in: "A dependence of Abeta on beta energy is also introduced. UCNA fits energy spectrum and Abeta[Ebeta] simultaneously now."	9

■ The point is, the presence of either scalar or tensor interactions will produce a b_{Fierz} term in the decay PDF. It has other effects on the PDF, but those come in at higher-order in the tiny scalar and tensor couplings. So, the Fierz term would be by far the biggest thing that changes in the PDF. The PDF describes the energy and momentum of the outgoing beta w.r.t. a variety of other things. Notably, we can write an elegant-ish description of beta momentum w.r.t. nuclear polarization direction, and ignore the neutrino completely after integrating over it. We have a PDF in beta <i>direction</i> (w.r.t. polarization), and beta <i>energy</i> . To lowest order (and lowest order is best order) the distribution w.r.t. polarization direction doesn't change, but the distribution w.r.t. energy does change. Or ... something? The point is, it makes a change in the beta energy spectrum. This change is most pronounced at low energies, because the Fierz term is scaled by $(1/E_\beta)$. However, the asymmetry is also a function of E_β . A different function of E_β . In fact, it is scaled by (p_β/E_β) within the PDF, which is distinctly different than b_{Fierz} . So, one might ask what effect a b_{Fierz} term would produce on a constructed asymmetry spectrum.This explanation has gone way off track.	10
■ Here's a reference to the picture that shows the result of a non-zero b_{Fierz} term. It's Fig. 1.3.	10
■ JB: You need to at some point say that the supersum is the beta energy spectrum. There are experiments trying to do this method better, but they are very difficult. UCNA published a combined energy spectrum and Abeta[Ebeta] analysis on the neutron in March 2020 [7]. ... MJA: I can't help but also notice the follow-up article from September 2020 [8]. Ugh.	11
■ I need to organize the sections/subsections in this chapter/section better, and generally just de-Frankenstein it.	12
■ Needs a level diagram. Maybe.	13

When this is combined with a circularly polarized laser beam, the effect is to move the atomic resonance closer to- or farther from- the frequency of the laser. The circular polarization, combined with some selection rules, means a circularly polarized laser will only couple to one particular transition, w.r.t. angular momentum. ie, for a σ_+ polarized laser, the atom's overall angular momentum projection (along some axis) will be incremented by +1. The Zeeman shift means that in a magnetic field, this transition ($M=+1$) not be the same as the $M=1$ transition. So, if you have a magnetic field that changes linearly across space, you can make it so that in $+B_z$ regions, the laser beam with one certain polarization is closer to resonance and therefore more likely to be absorbed – and similarly, in $-B_z$ regions, a different laser with the opposite polarization will be more likely to be absorbed. Again, if the B-field is linear in space, you can do it so that as the atoms get further and further from the ‘centre’ region, the effect gets progressively stronger. So, if you’ve done this right, you can make it so that the atoms get a stronger “push” back towards the center the farther away they’ve drifted.

They still get the optical molasses cooling effect for free. 13

...and opposite polarization. Or something. I have to talk about the selection rules somewhere else. 14

Optical molasses equation? Maybe? 15

“...This will slow the atom down, at least up to a limit related to the linewidth of the atomic transition and/or the laser. There’s something to look up.” 15

Removed ‘Angular Momentum and Selection Rules’ section. Because it was super wrong. 15

The laser, which must be circularly polarized in the appropriate directions and tuned slightly to the red of an atomic resonance, is split into three perpendicular retroreflected beams, doppler cooling the atoms and (with the appropriate magnetic field) confining them in all three dimensions (see Figure 2.1). 15

JB: on 3.3 (now 2.3) “Atom Trapping with a MOT” ((that’s here!)): The content and scope are ok, but the informal phrasing is going to confuse people. You have to pay some attention and rephrase these sections. . . 15

■ Do I *have* an equation I can put here? Surely there must be one somewhere, but I really don't want to dig it up, and I don't think it's really necessary.	15
■ Needs work.	15
■ Upon decay, atoms literally aren't trapped anymore by the trap. No trapping forces, no slowing forces, because it's all isotope-specific. This is super useful for us.	15
■ Ignore the repumper.	15
■ Removed 'Photoionization as a Probe' section from the 'Intro to Atomic Physics' section, because John says it's horribly wrong anyhow. Plus, it's redundant with the 'Photoionization Laser' section (2.5.3).	15
■ Direct quote from John follows below:	17
■ End quote from John. But also!: “...Then you can refer to that (ie, John’s red quoted mini-blurb about optical pumping, (which I may relocate to Sec. 2.5.3? Or not?) in section 3.4 (now 2.4, about the AC-MOT – ie, Sec. 2.4, (even though I might remove that section entirely and put all its content into Sec. 2.4)), where you’re trying to now but the phrasing is poor.”	17
■ “Until recently, one limitation of such samples was the necessity for the presence of a relatively large magnetic field, which is expected to partially destroy atomic polarization, limiting the precision of many types of measurements. Here we discuss the construction of a newer type of MOT, the AC-MOT, which minimizes residual magnetic fields. The guys in [9] came up with the idea of the AC-MOT. They made it work and did some stuff with it. Good for them.”	17

█ JB says: "I would say you don't need an atomic level diagram. You could just describe in words the semiclassical picture of atoms absorbing photons until they are nearly fully polarized, then they stop absorbing. The optical pumping + photoionization is then an <i>in situ</i> probe of the polarization. ... You would need to add in words that quantum mechanical corrections to this picture are in the optical Bloch equation approach in B. Fenker et al. The depolarized states still have high nuclear polarization (1/2 for $F = 2, M_F = 1$, 5/6 for $F = 1, M_F = 1$) and determining the ratio of those two populations provides most of the info we need – we model with the O.B.E, measure the optical pumping light polarization, and float an average transverse magnetic field. This is adequate to determine the depolarized fraction to 10% accuracy, which is all that is needed." . . .	17
█ Describe what's going on here! Alternately, cut the whole image. It's from that paper anyway.	18
█ put this in! "...and is designed to operate at ultra-high vacuum (UHV) to minimize trap losses from collisions." Also, I think it helps prevent sparking? .	18
█ JB: ...You could call the first half of such a chapter "General considerations of Atomic techniques used" and the 2nd half "Experimental Implementation of Atomic Techniques used"	18
█ Supersection: Experimental Implementation of Atomic Techniques Used . .	18
█ Remember the pulser LED! To evaluate the stability of the scintillator gain!	18
█ JB says: chapter (((this section))) is really good, and in good shape for the committee	18

■ We obtain a sample of neutral, cold, nuclear spin-polarized ^{37}K atoms with a known spatial position, via the TRIUMF accelerator facility, by intermittently running a magneto-optical trap (MOT) to confine and cool the atoms, then cycling the trap off to polarize the atoms. With β detectors placed opposite each other along the axis of polarization, we are able to directly observe the momenta of β^+ particles emitted into 1.4% of the total solid angle nearest this axis. We also are able to extract a great deal of information about the momentum of the recoiling ^{37}Ar daughters by measuring their times of flight and hit positions on a microchannel plate detector with a delay line. Because the nuclear polarization is known to within < 0.1% [2], and we are able to account for many systematic effects by periodically reversing the polarization and by collecting unpolarized decay data while the atoms are trapped within the MOT, we expect to be well equipped to implement a test of ‘handedness’ within the nuclear weak force.	18
■ Surely most of this paragraph goes in an intro chapter somewhere.	19
■ Cite a bunch of papers here.	19
■ made possible by UHV!	19
■ Figure was originally created by Alexandre, modified by ... someone else? Or Alexandre? And I got it from ... probably an experimental proposal? I should figure out how to cite a proposal.	20
■ discussed ... idk, somewhere else.	20
■ I *do* discuss this, right? Right??	21
■ JB on Ch. 3.4 (now 2.4) ((now Ch. 2.4)) “The AC-MOT” (that’s this section!): The content and scope are ok, but the informal phrasing is going to confuse people. You have to pay some attention and rephrase these sections.	22
■ John suggests that maybe I should just refer directly to his red, quoted OP blurb in the chapter about the AC-MOT.	22
■ This content *came from* that other section, and needs to go in here somewhere: “Many laser ports to make the MOT functional, and for optical pumping. Fancy mirror geometry to combine optical pumping and trapping light along the vertical axis. Water-cooled (anti-)Helmholz coils within the chamber for the AC-MOT, fast switching to produce an optical pumping field.”	22

█ “...where you’re trying to now but the phrasing is poor.”	22
█ How much do we lose? Have we quantified that somewhere? Probably.	23
█ begin content of the historical other AC-MOT+Polarization section.	23
█ Probably document things about the waveform and frequency used for the beamtime, since I don’t think it’s in my MSc.	23
█ John objects to the phrasing of the following paragraph, because you fundamentally need polarized atoms to measure b_{Fierz}	23
█ Plus, it barely makes sense to talk about measuring b_{Fierz} if you don’t know A_β	23
█ End paragraph that John hates.	24
█ JB says: “Since you worked hard on the logic triggers, a photoion spectrum with duty cycle would be appropriate if you want.”	24
█ Note that because the atoms within a MOT can be treated as following a thermal distribution, some fraction of the fastest atoms continuously escape from the trap’s potential well. Even with the most carefully-tuned apparatus, the AC-MOT cannot quite match a similar standard MOT in terms of retaining atoms. The TRINAT AC-MOT has a ‘trapping half-life’ of around 6 seconds, and although that may not be particularly impressive by the standards of other MOTs, it is more than adequate for our purposes. ^{37}K itself has a radioactive half-life of only 1.6 seconds (cite someone), so our dominant loss mechanism is radioactive decay rather than thermal escape.	24
█ At some point I have to decide if that’s going to be a section or a subsection.	25
█ Do I talk about how this works somewhere? Probably in that section on cuts.	26
█ Reference that one table.	26
█ rMCP is 101.4 mm from center, eMCP is 100 mm from center. Do I say this somewhere else?	27
█ There’s gotta be a better way to describe it	28
█ what’s the open area of the detector? how big is each pixel?	28
█ John says: Chapter (((2.5.3))) is very good and complete, showing you understand what is needed about photoionization. A good reason to omit 3.5 ‘photoionization as a probe’ as I said above.	29

■ Probably worth mentioning that we test this stuff offline on stable ^{41}K . But also, surely it should be mentioned in like the AC-MOT/Polarization section too.	29
■ JB: “you could reference the letter for the value of the field 150V/cm.” . . .	29
■ As a check: the camera measurements for photons from de-excitation. It’s aimed 35 degrees from vertical, with its horizontal axis the same as one of the other axes. I think it’s the TOF axis. I can check this when my computer comes back. Also, there’s an unknown additional delay between some of our DAQ channels that can’t be explained by accounting for cable lengths, so we really like having the check there.	29
■ JB says: “yes, camera x-axis is tof axis.”	29
■ Chamber walls are made from 316-L stainless steel, chosen for strength, cost, and minimal eddy currents.	31
■ Intro blurb goes here?	32
■ Ben doesn’t seem to include Runs 436 and 437 in *any* set of good runs. Is it an oversight? I think they’re perfectly legit electron runs. They’re fairly long runs...	33
■ Ben includes 448 as a ‘good’ recoil run. But I don’t. Why? Also 451, 451, 453. ...Also 467,468,469,470,471,472. Also-also, 492, 493, 494, 495, 496. .	33
■ how precise is the rMCP supposed to do? in practice, it wasn’t nearly that good.	34
■ It’s not really *every* event...	34
■ A diagram of how delay lines work would really help here, but there’s no time for that. I’ll put it in if someone asks.	34
■ Do I want the above section about how delay lines work to go in the other chapter? Maybe.	34
■ OK, I have to *actually* discuss this a bit somewhere though.	35
■ Are these things *definitely* in nanoseconds? Check!	36
■ I *think* we used an alpha source? Not sure what else we could have done, but I better check this!	38

■ It is worth mentioning that the mask calibration data was collected without the presence of the magnetic fields involved in trapping and optical pumping, but these were of course present in the online data to which it was being compared. Since a magnetic field can change the trajectory of a charged particle, one might suspect that there could be some effect on the resulting image. There are two stages at which this might occur: while the ion is accelerating through the electric field within the experimental chamber before impacting the rMCP, and while the electron shower is emerging from the back of the MCP stack before it is incident on the delay lines. ... But also, I really don't want to get into this, otherwise somebody will ask me to quantify the size of the effect. Turns out: it's tiny, but it will be really annoying to demonstrate that.	39
■ You know, I think this one is flipped relative to the previous image. Bleh. Probably this one is the correct one, but who wants to deal with that? Also did we switch MCP plates between calibration and the run? I think possibly we did! I'll have to ask the eLog.	41
■ Does this thing even have a TOF cut?	41
■ Also... does the camera data go in this section??	42
■ Trap position – Measured using the same dataset that was used to quantify the polarization. The trap drifts slightly over the course of our data collection. Describe the rMCP calibration needed to extract this info. . .	44
■ Sig figs here need work.	44
■ Parameters measured with the recoil runs, and applied on the appropriate electron runs.	44
■ Also, we noticed the trap drifting after one of the runs, because one of the batteries on one of the thingies adjusting the laser frequency (I think) was failing.	44
■ JB: "If we rejected the data with the MOT moving (indeed a battery determining the voltage controlled oscillator frequency offset between absorption in stable ^{41}K cell and the ^{37}K resonance) then that's all you need to say."	44
■ describe how you'd turn this into a physical description of the cloud, with like a temperature and a sail velocity and shit. with equations.	44

■ We now consider how to clean up our data. We make some fairly obvious, intuitive cuts, and those are described here. Later, we'll make less intuitively obvious cuts.	48
■ Point at that other conclusion-ier section.	48
■ change by 0.2% of its value vs change by 0.5% of its value, according to Ben's thesis pg 143.	49
■ Ben didn't do the 5 cycle discarding thing in his Abeta analysis, but he *did* do it in his OP analysis.	49
■ JB says: To repeat a comment, since the Appendix on analysis changes is being dispersed throughout, when you state somewhere (I think it's in Ch. 6)((5?)) make sure you state clearly that the only change for BB1 cuts is the radius cut, e.g. that you took the same T and E from the waveforms (I'm not even sure whether the waveforms are recorded anyway). You ask 'how can I state this' but there's no reason to be subtle. Just say upfront that Ben and Spencer's theses did all the groundwork on the BB1, and here you include selected details needed to understand the present analysis. If you need to include some redundant material, don't worry too much about that.	
...	
MJA: In fact, I think the BB1 radius may have been the same. The uniform energy threshold was different though. But I get the point.	
...	
Also, yes, the waveforms are absolutely recorded in the MIDAS files but they haven't been saved to modern ntuples, because they made the files huge. I think it's probably pretty easy to switch that on/off in the Analyzer though to generate a set of ntuples that has that info included.	50
Figure: Show individual beta energy spectra. ...with a variety of different cuts, perhaps?	50
■ How do I *say* that Ben was the one who did most of the DSSD calibration stuff? I maybe don't need to describe all of it here, but I *could*, and maybe it's needed in order to understand like 4 rows in my error budget.	51

█ JB: "You can describe anything you did differently or improved, but you can and should otherwise defer all details of the scintillator calibration and DSSD calibration to Ben's paper and his thesis and Spencer's. E.g. Section 5.3 "statistical agreement between BB1 X and Y detectors' energies only makes a small effect on results" does not need the technical details beyond that statement."	51
█ JB: "If you have some way of documenting the coding you used, that would be great." ... yeah, it would, wouldn't it?	51
█ I think Ben might have selected 60 keV? That's maybe something for the appendix.	51
█ Did I even mention the collimator? Like, in the previous chapter or something..?	51
█ Also-also (did I mention it already?) look for events with only *one* DSSD hit (two could indicate the beta scattered back out of the detector in another pixel, or alternately an accidental coincidence of two beta decay events. either way, no good for analysis.) Also, only one scint hit, and it has to be the on the same detector with the DSSD. (...A scintillator hit as indicated by a TDC readout, as well as a max. recorded scint energy for the "extra" scintillator at something stupidly tiny, like 10 keV. Probably *actually* 10 keV.)	51
█ After all other cuts – not before!! – we eventually use only events with scint energy between 400 - 4800 keV. High cutoff is because of the low number of events, which makes the observable—the superratio asymmetry—poorly defined and poorly behaved. Low cutoff is because it's really hard to model what's going on down there to the required level of precision. The observable depends most heavily on low beta energy events, so it is imperative that the lower energy portion of the spectra be thoroughly understood if they are to be used for analysis.	52
█ Somewhere I should list what the energy cutoff is for this spectrum. Or semi-equivalently, the Q-value.	52

█ MJA: I can describe the eMCP calibration here, even though it mostly wasn't implemented by me. It is tangentially relevant to data selection and background estimation by providing an experimental energy spectrum for shake-off electrons. It's actually a pretty neat algorithm that I basically wasn't involved with.

...

JB: eMCP. You need to describe the timing information obtained. You also need a statement of whether or not you used the position information in your cuts.

...

MJA: Wait. So have I done that yet in this section? 52

█ I described the HEX-75 somewhere in a previous chapter, right?? 52

█ I dislike how this section is organized.. should discuss the cut we *didn't* make at the end. 52

█ Do I need to describe MCPs and delay lines somewhere? Maybe not... 52

█ This pic is probably better used in an SOE section somewhere. 53

█ Wait, what? 53

█ Um. Did I for sure get the labels correct on this??? It seems really wrong. 54

█ Surely this thing goes somewhere else instead. 54

█ The LE spectra allows for us to use a more precise model of the SOE TOFs, so that's nice. 55

█ This goes in that one appendix, if I haven't already put it there. ...Also, is this even fucking true?!? 55

█ "...removing X fraction of the remaining events." 56

█ Probably need to put that figure somewhere else. 56

█ "To check the agreement of the model with reality, we compare the averaged superratio asymmetries from both, as in Fig. 4.14." ... probably goes in the other section. 56

Figure: Show SimpleMC spectra, show the supersum, show the superratio, show the superratio asymmetry. Maybe do some simple fits to show how much better the superratio asymmetry is than *not* the superratio asymmetry. 58

█ add comment about how you need G4 to do scattering/backscattering. I think I wrote a blurb like this *somewhere* already.... 58

■ because for A_β even a BSM interaction will *basically* look like a SM interaction, and I think something somewhere isn't precise enough to distinguish it.	59
■ which other corrections? coulomb and/or radiative corrections, but somehow when I say that, I'm apparently talking about a different thing than everyone else who uses those terms. also, weak magnetism. also ... ??? .	59
■ Is this true? Does it not include *any* BSM interactions?	59
■ Furthermore, although it is currently understood that the weak interaction is predominantly or perhaps entirely ‘left-handed’, the JTW treatment leaves certain phase angles unfixed, and is therefore able to accurately describe a decay which is, for example, partially ‘right-handed’ – however the latter feature is not directly relevant to the project at hand. [It’s several phase angles in JTW, but maybe it’s fundamentally only like one angle on some level? Also I think it’s not actually a “gauge freedom,” per se. No, I’m pretty sure this ‘phase angle’ description is all wrong.] Also, consider time reversal! Anyway, most of this paragraph probably goes better in Section 1.3.	59
■ Surely I describe what recoil-order corrections even *are* in some appendix somewhere, right? Or, possibly, in Section 1.3. Possibly the paragraphs above need to be moved...	59
■ Things that the G4 simulation did that I kept include: an accurate representation of the complex details of our experimental geometry. Also, the noise spectra on the DSSDs.	61
■ Reference previous section where I discuss this, maybe?	61
■ See: Some other section? Maybe?	62
■ Is it definitely 14 of them?	62
■ Obviously, from a physical standpoint, the initial beta energy E_0 must be positive, but the response function still includes several expressions of the form, $ E_0 $. This is not done by accident, but rather is an intentional adjustment used to encourage the parameters to behave well within a fit.	63
■ In these response functions, $x =?$	63
■ To evaluate Erf [] for parameter fits, root’s built-in function was used. Root also includes a built-in Landau function, but it makes everything very slow if we use it.	63

█ Also, I think for this particular part of analysis, the cutoff was like 600 keV.	65
█ Some of this content needs to go somewhere else.	65
█ We never attempt to do this, because reasons. Don't I talk about this somewhere?	65
█ ...as previously mentioned, re-introducing the energy from the BB1s invites problems with maintaining a uniform energy threshold over the entire detector.	65
█ somewhere I have to talk about the empirical noise spectrum etc. on the BB1s. Or maybe I've already mentioned it somewhere.	65
█ Needs a picture of the *full* beta energy distributions that come out of the lineshape thing. To compare with (a) data and (b) G4. Probably a superratio in there somewhere too.	67
█ Um. Which of the scattering things did I actually put in at the end? And when did I do it? Like, how did I account for (back-)scattering? I tried with/without scattering, I think? and eventually decided not to do it. for some reason. I think it breaks normalization in some way that's more subtle than you would think.	
... Do I need the angular distribution in the end? I think maybe I put in scattering later, and just used a cone for the first round. I re-did this to do the opposite thing at some point.	67
█ What even <i>is</i> the thing plotted below E_0 in the 'residuals' spot, you ask? It's 'PseudoE', which describes the difference between the original input energy, E_0 , and the energy where the output spectrum is maximal. Or something. To 'pretty good' order, it's a straight line. the 'PseudoE' plot shows what's left after you fit it to a straight line. It's fucking weird that it's negative everywhere. Like, what?	72
█ How many DOF for these things? I should put it on the picture.	75
█ Events from the trap aren't generated with the same position in G4 and comsol! ugh. ...but it's fine, because the betas are fast. Comsol gets the position right, which is where it actually matters.	76

■ A ‘timing resolution’ is *absolutely* applied to these things. Taken from the width of the prompt peak in the SOE TOF. It’s believed to come from betas that hit the eMCP then scatter into a scintillator. The phase space where this could even happen isn’t very big, but you can still see the peak. Probably not the other way around, because it’s hard to scatter out of the whole scintillator, and if it just scattered off the DSSD then you wouldn’t see it in the scintillator.	76
■ Generate a CDF for Lev and a CDF for 0eV. For events from the trap, G4 is pointlike but COMSOL has the correct cloud distribution.	76
■ For every "good" beta hit event, pick whether to use 0eV(9%) or Levinger(91%). Then, select an SOE TOF (from decay time) from the CDF. Subtract this instance of SOE TOF from this instance of beta TOF to get a thing like an experimental spectrum. Apply a detector resolution (just a gaussian) to this result. *then* we can make basically whatever spectra we like out of this. e.g., beta energy within the cut we’re using.this all happens in MakeHarderMulti(...) and also MakeHarderer(...).also, we still haven’t used the two percent branch on this.	76
■ Because there’s an offset for the data that we can’t measure directly to the precision needed, we simply recenter the whole SOE TOF spectrum to be centered on zero. In this way, we can more easily match it up to simulations. long high-energy tail. it’s actually critical to the analysis.	76
■ No, don’t reference these pictures yet – we haven’t discussed the SOE TOF.	77
■ Is this even what these events are?	80
■ Upper limit for the fraction of events generated this way can be estimated by assuming that all losses from the trap not due to radioactive decay emerge isotropically from the trap and then stick to whatever chamber wall is in its path. This upper limit is too big by a factor of 2.	81
■ Alexandre did this.	81
■ Rephrase.	82
■ Reference Section 3.7, probably.	82
■ Show the "average asymmetry" (all energies) as a function of TOF, with real data, best model normalization, and extrema of model normalizations. Show our cut. Turns out, it’s a lot of work for a really tiny correction. Oh well.	83

JB says:

A simple estimate from the collaboration that builds intuition for this result: Scatter in the SiC mirrors and DSSD actually produces an efficiency change at low beta energy. Energy loss is not minimally ionizing in these structures, and instead will have a long Landau tail that can take events below energy threshold in the scintillator. The collaboration has modelled explicitly the false asymmetry as a function of Kbeta between 600 and 1300 keV, producing roughly $(K-0.6 \text{ MeV})/(0.7 \text{ MeV})$, i.e. 50% at $K\beta=0.95 \text{ MeV}$. This efficiency degradation would be distributed roughly equally between the SiC and DSSD. If completely ignored, this would introduce by inspection a false bFierz of approximately 0.5. Scattering effects will vary between linear and $\sqrt{\text{thickness}}$, so assuming worst case of linear, the mechanical thickness uncertainty of 5 micron/300 micron and 6 micron/275 micron, an average of 2%, making a random contribution of order 0.01 each. The Be window has larger mechanical thickness uncertainty of 23micron/229 micron, but energy loss and scattering in this material is 5x smaller, so the net effect would be similar.

• • •

To minimize this systematic for future experiments, the collaboration has implemented pellicle mirrors of negligible thickness, 100 nm Au on 4 micron kapton. The collaboration is also implementing Be-windowed wire chambers in place of the DSSD.

• • •

It's actually not nearly as big as I'd originally expected. It's huge in the lineshape thing, but pretty tiny in everything else.

from John: "I used Ben's threshold when determining the uncertainty from the lineshape tail (UFTLT). If you're saying the UFTLT depends on the threshold used, ok, of course it does. But if you're claiming that UFTLT depends on the **uncertainty** of the threshold, that's manifestly smaller than the UFTLT itself, and I'm going to assert it isn't worth evaluating."

I got it out of the Sim_to_Asym directory, so that's where I have to go looking to see how I made it and/or make a new one.

85

86

86

88

■ JB: I hope the discussion is clear in your head. Any effect that relies on scattering computation in G4 should have an uncertainty on order 10% of the correction – hopefully you are keeping a distinction here between the finite geometry acceptance (which I guess is exact) scattering off the collimator.	89
■ As per JB's comment in section 3.6: "statistical agreement between BB1 X and Y detectors' energies only makes a small effect on results" does not need the technical details beyond that statement."	89
Figure: Surely this requires at *least* one image of the pixelated BB1 data. Maybe some of a few waveforms and energy distributions too.Feels like cheating to include some of that stuff, since Ben was the one who actually used it mostly.	89
■ JB on missing figure: "if you used such an image as part of your uncertainty estimate, yes [include it]"	89
■ Remember: There's noise applied to simulated BB1s, matching some spectrum.	89
■ JB: The simulations of course include it event-by-event, not just a minimally ionizing average loss.	89
■ This content got moved to Ch. 4.4.	90
■ This content got moved over *there*. (ie, Section 4.3.)	90
■ A lot of this content has gone into (Section 4.2) instead. I really need to just mention it here (Sec. 5.6) and give an indication of how good the result is. Then evaluate stuff.	90
■ JB: so it's still critical to write down more of the lineshape work.	90
■ JB: yes, brems strahlung is 'braking radiation' so gets 2 ss's. the lineshape tail in any scintillator also includes backscattered events – we are not claiming the 2-pixel cut is complete	90
■ Here is Subsection 9.5.5 "The low-energy tail uncertainty, and what it does" complete. There should be no figure. Direct quote from John follows in the next two paragraphs. Maybe I should paraphrase, but it's so nicely written!	91

■ JB: Dan and I independently discussed (((Ch. 6))) yesterday, and he has suggestions to help. So I will also schedule a meeting with Dan and you to discuss (((Ch. 6))) Results and whether the S,T part must be deleted and left to a paper. You don't have enough time, and although this should be quite straightforward, it is not your critical result and it's the only thing that can go.	94
■ John says to just skip doing the C_S and C_T stuff, for now. No time. Really, C_S is already basically done, but then that'll lead to awkward questions about C_T	94
■ Just write a blurb to qualitatively summarize a bunch of the stuff in Ch. 5. Do I want to put my error budget table here? If not, here it is! (5.1). . .	94
■ Other things to discuss here: which things are dominant error sources, and how viable it would be to improve those for future experiments.	94
■ JB says: To put your work in context, please add at the end of that minimal S,T section, or at the end of "Our Decay" section ... The best existing measurement of b_{Fierz} is in the decay of the neutron [8], $b_{\text{Fierz}} = 0.017 \pm 0.021$, consistent with the Standard Model prediction of zero. Our measurement is strongly related, yet complementary. In terms on non-Standard Model Lorentz current structures, to lowest order in the non-SM currents the same equation applies: $b_{\text{Fierz}} = \pm (C_S + C'_S + (C_T - C'_T)\lambda^2)/(1 + \lambda^2)$ (the plus is for β^- decay and the - for β^+ decay) [6]. [to be continued...]	95

■ [...continued from prev.]

In our ^{37}K case, $\lambda^2 = |M_{\text{GT}}|^2/|M_F|^2$ is close to $3/5$ (the expected value $j/(j+1)$ for a single $j=3/2$ d $3/2$ nucleon) [11], while for the neutron λ^2 is close to 3 (the expected value for an $(j+1)/j$ $j=1/2$ s $1/2$ nucleon). $|M_F|$, the Fermi matrix element, is nearly the same for both of these isospin = $1/2$ decays (the largest correction is the larger isospin mixing of ~ 0.01 in ^{37}K). So our observable is relatively less sensitive to Lorentz tensor currents, and will predominantly constrain or discover Lorentz scalar currents.

...

Full considerations would require a weighted fit of b_{Fierz} experiments and similar observables [12], and are beyond the scope of this thesis. The info from this thesis, values of A_β and b_{Fierz} with their uncertainties, can together with the known fT value (lifetime and branching ratio) allow the community and/or the collaboration to include the results in a future constraint or discovery of scalar and tensor Lorentz currents contributing to β decay.

96

■ Probably shouldn't get a clearpage in the end. It's for my sanity during writing.	102
■ John says the whole R_{slow} thing should go in here somewhere.	102
■ Appendix I keep, it's excellent. It should be moved as is to Conclusions under "Future Experiment for the collaboration"! so people know you worked so hard on it!!	102
■ The citation format I'm using is really stupid. You must force yourself to ignore this right now, Melissa!	109
■ JB says Appendix A should all go in the analysis section, and not in an appendix at all.	110
■ JB says: Appendix A (ie, *this appendix*) is very important, and should at least be a subsection in the Analysis chapter.	

...

You could condense the Appendix into a set of bullet points at the end of the intro to the Analysis section (which you still need, badly!), and then its content could be interleaved in the Analysis chapter. E.g. you already have redundancy in the LE and TE discussion vs. the Appendix, and the discussion is more complete in the Analysis chapter, which is good. . . .

110

■ I really want this appendix to stay here. I'll make sure to mention everything in the body of the thesis though, since it *is* important. But at some point, somebody is going to really want to have this info written into a short summary.	110
■ Somebody will surely ask for a justification for why I did this differently, and I don't have one beyond "this seemed more reasonable to me", which is of course nobody will ever accept as a reason.	111
■ John says to keep this appendix, because it's great now.	112
■ We have already specialized to β^+ decay.	112
■ Also, $\xi = G_v^2 \cos \theta_C f_1(E)$	114
■ There was something wrong with this assumption. Something circular. I forget. Blah.	116
■ Somewhere I have to define q^2 and Δ are.	116
■ Should I just list the values of things that I inherited from Ian Towner's personal communication that one time?	117
■ and also, I think something like that the weak charge is the same distribution as the electric charge	117
■ What is less clear, given the context in the paper, is whether or not when Holstein writes out his simplified expressions for $\Delta F_x(E_\beta, u, v, s)$ he actually means $F_\mp(Z, E_\beta) \Delta F_i(E_\beta, u, v, s)$. These terms are pretty small, so it probably doesn't *really* matter, but it would still be really nice to *know*, damn it.	117
■ Also, pretty sure one of those never gets used. Which one was it? idk. . .	119
■ Note: It's not the case that $ \vec{J} == J$. It's actually super fucking infuriating notation.	119
■ I see some stuff in my old Appendix D that needs to be moved (in here? Or maybe in Old Appendix E) before it goes away forever.	120
■ JB: Appendix C has some redundancies with B. You will have to sort that out. (n.b.: from context, it's less clear which appendices he's actually talking about, but whatever, there's certainly redundancies all around. . .	120

■ Appendix KLM you have to pick what you want– I hope that's Appendix K (that's this one!) – and remove the rest as you say they're "old". Appendix K could be moved to the end of Experimental Methods because it's absolutely critical and helpful!! but if you want to reference it there and leave it as an Appendix, it's up to you.	130
■ Does this even agree with whatever I wrote about the geometry in the other section?	131
■ Not quite true. Some strips are missing.	131
■ This is only true if we neglect (back-)scatter. This is not actually a good approximation. But we have pretty good simulations to give us the real numbers, anyway.	131
■ Is that definitely true, or is it only true to lowest order?	132

Chapter 1

Background

The nuclear weak force is one of four fundamental forces described within physics. It mediates the process of beta decay, which is of particular interest to us here. Although beta decay is generally well understood, it presents a unique opportunity for precision measurements to search for physics beyond the Standard Model within the Weak coupling. By observing the kinematics and angular correlations involved in the decay process, one gains access to a wealth of information about the form of the operators mediating the decay.

1.1 Beta Decay within the Standard Model

A nucleus undergoing beta decay converts one of its protons (neutrons) into a neutron (proton), and simultaneously emits a lepton and anti-lepton. The daughter nucleon remains bound in place of its parent, and the overall electric charge of the nucleus is changed by -1 (+1), with the extra charge being carried away by the anti-lepton (lepton). In particular, at the nucleon level, three beta decay processes are possible:

$$p \rightarrow n + e^+ + \bar{\nu}_e \tag{1.1}$$

$$n \rightarrow p + e^- + \nu_e, \tag{1.2}$$

$$p + e^- \rightarrow n + \nu_e \tag{1.3}$$

where the processes described in Eqs. 1.1 and 1.3 are energetically disallowed for an unbound proton, however there is no similar requirement for Eq. 1.2.

Limiting the focus of this discussion to Eq. 1.1, we note that this expression provides no information at all about the momenta or spin of the outgoing daughter particles. This behaviour is governed by the form of the Weak coupling that mediates the decay.

Within the field of nuclear physics, it is common to classify beta decay processes as being either “Allowed” or “Forbidden” (sometimes with an associated number to describe the extent to which it is Forbidden), where Forbidden processes are generally suppressed but not truly forbidden. In an Allowed transition, the positron and anti-neutrino are treated as being created at the nuclear centre, and as a result they may not carry away any *orbital* angular momentum. However, since the outgoing leptons both have spin $S = 1/2$, it is still possible for the total nuclear angular momentum, J , to be changed in an Allowed decay. This implies that an Allowed transition must *always* change the total nuclear angular momentum by either 0 or ± 1 .

The Allowed decays traditionally are further separated into a “Fermi” singlet in which the two leptons have anti-parallel spins and there is no change to nuclear angular momentum ($\Delta J = 0$), and a “Gamow-Teller” triplet, where the two lepton spins are aligned in parallel to one another and so the *projection* of the nuclear angular momentum is changed by ± 1 . This implies that the total nuclear angular momentum is changed by $\Delta J = \{0, \pm 1\}$ during a Gamow-Teller transition. A mixed transition is also possible, however we note that the $J_i = J_f = 0$ decays must always be pure Fermi transitions, because there is no way to produce this result from two outgoing leptons with parallel spins. [13] [15] [14].

Given the differing behaviour within the angular momenta of the daughters in Fermi and Gamow-Teller transitions, it is perhaps not surprising that that the *linear* momenta of the outgoing particles should also follow a different set of distributions in these two cases. At the level of the Weak coupling, Fermi- and Gamow-Teller transitions are governed by different operators, with the Fermi interaction mediated by a so-called “vector” (V) coupling, and the Gamow-Teller interaction mediated by an “axial-vector” (A) coupling.

1.2 A Generalized Description of the Weak Interaction

According to the predictions of the Standard Model (SM), the Weak force involves only vector (V) and axial-vector (A) couplings, where a relative sign within the quark-lepton Lagrangian produces the left-handed “($V - A$)” form of the interaction in maximal violation of parity. In terms of physical behaviour, one consequence of this model is that “regular matter” leptons emerge from a Weak interaction with left-handed chirality, while antimatter leptons emerge with right-handed chirality. Any deviation from this behavior would be indicative of “new” or “exotic” (i.e., not previously discovered) physics.

There exists an extensive body of experimental evidence to demonstrate that the above model is overall a very good description of the beta decay process [3]. Despite the success of the ($V - A$) model, there are still certain lingering questions that must be addressed by precision measurements. Any deviation from maximal parity violation (i.e., a “($V + A$)” contribution to the Weak force) would be of great interest to the community, as would the presence of certain other exotic couplings, such as the so-called Scalar (S) and Tensor (T) interactions. Any such behaviour beyond the Standard Model (BSM) would represent a non-dominant contribution to the interaction, however the possibility cannot be entirely ruled out.

The generalized nucleon-level Lagrangian to describe the Weak interaction including BSM behaviour is given by:

$$\begin{aligned} \mathcal{L} = & -\bar{p}\gamma^\mu n \left(C_V^+ \bar{e} \gamma_\mu \nu_L + C_V^- \bar{e} \gamma_\mu \nu_R \right) - \bar{p}\gamma^\mu \gamma_5 n \left(C_A^+ \bar{e} \gamma_\mu \nu_L - C_A^- \bar{e} \gamma_\mu \nu_R \right) \\ & - \bar{p}n \left(C_S^+ \bar{e} \nu_L + C_S^- \bar{e} \nu_R \right) - \frac{1}{2} \bar{p}\sigma^{\mu\nu} n \left(C_T^+ \bar{e} \sigma_{\mu\nu} \nu_L + C_T^- \bar{e} \sigma_{\mu\nu} \nu_R \right) \\ & + \bar{p}\gamma_5 n \left(C_P^+ \bar{e} \nu_L - C_P^- \bar{e} \nu_R \right) + \text{H.C.}, \end{aligned} \quad (1.4)$$

where the coupling constants C_X^\pm (with $X = \{V, A, S, T, P\}$) are written in such a way as to separate out the left-handed (C_X^+) and right-handed (C_X^-) components from one another, and the neutrino fields $\nu_{L,R}$ are given a similar treatment. A simple variable transform relates Eq. 1.4 to expressions that are potentially more familiar from the older literature, much of which was written before it had been determined that the

Weak force is primarily or entirely left-handed:

$$\nu_L = \frac{1}{2}\nu(1 + \gamma_5) \quad (1.5)$$

$$\nu_R = \frac{1}{2}\nu(1 - \gamma_5) \quad (1.6)$$

$$C_X = \frac{1}{2}(C_X^+ + C_X^-) \quad (1.7)$$

$$C'_X = \frac{1}{2}(C_X^+ - C_X^-) \quad (1.8)$$

It can be seen from the form of the Lagrangian that the V, A, S, T, P couplings within are described as such because they *behave* as vectors, axial-vectors, scalars, tensors, and pseudoscalars (respectively) under a Lorentz transform, where the Lagrangian itself must be a scalar both before and after a Lorentz transform [4] [12].

Seriously, this section needs some citations. Notably, C.S. Wu [3] (done) and Lee+Yang [4] (done). Perhaps also Hong+Sternberg+Garcia [5]. Probably a bunch more people too though.

Write a paragraph about what we're looking for with this experiment.

JB on intuitive concepts that are missing:

The SM couples to left-handed neutrinos and right-handed antineutrinos. Since the neutrinos only have weak interactions, there are no right-handed nu's nor left-handed antinu's in nature. The neutrino asymmetry B_ν is a number with no energy dependence.

Similarly, the SM weak interaction only couples to right-handed positrons and left-handed electrons. Since these are massive particles, the average helicity of positrons is not 1, but instead v/c. One can always boost to a frame where the positron keeps its circulation but is moving in the opposite direction. This is why the beta asymmetry is A v/c, not just A.

The Fierz term's additional energy dependence of m/E also comes from helicity arguments, stemming from the fact that it still is coupling to SM nu's and antinu's only, so the beta's are generated with wrong handedness.

The details are built at 4th-year undergrad level in Garcia's paper with his student and post-doc [5].

1.3 Mathematical Formalism

In a beta decay event, conservation of energy and momentum are of course required, but those conditions alone cannot provide a full description of the kinematics of emitted particles. The distribution of energy and momenta is probabilistic rather than deterministic with three bodies involved, and the full probability distribution

for the momenta of outgoing particles cannot be written in closed form.

Because the nucleus is significantly more massive than either of the other two outgoing particles, the great majority of the released kinetic energy is distributed between the leptons, while the nucleus receives only a tiny fraction of the total. This feature lends itself to an approximation in which the energy of the recoiling nucleus (the “recoil”) is neglected entirely, and the decay may be described only in terms of the momenta of the outgoing positron(electron) and neutrino(anti-neutrino), as in the description from Jackson, Treiman, and Wylde (JTW) [6] [16]. The terms that have been neglected in this treatment are sometimes called ‘recoil-order corrections’.

In order to proceed with a measurement, we must find an equation to describe the probability of beta decay events with any given distribution of energy and momenta among the daughter particles, as a function of the strength of the specific couplings of interest to us. To do this, two sets of formalisms are combined – the older formalism of JTW, which describes the effects of all types of Standard Model and exotic couplings of interest to us here, but which truncates its expression at first order in the (small) parameter of transferred nuclear recoil energy, and a newer formalism from Holstein [17], which includes terms up to several orders higher in recoil energy, but which does not include any description of the exotic couplings of particular interest to us. We note that because any exotic couplings present in nature have already been determined to be either small or nonexistent, it is sufficient to describe these parameters with expressions truncated at first order, despite the fact that it is still necessary to describe the larger Standard Model couplings with higher-order terms.

Unfortunately, the outgoing (anti)-neutrino is very difficult to detect directly, and we make no attempt to do so in this experiment. Instead, we might look for coincidences between an outgoing beta and a recoiling nucleus, and use that information to reconstruct the kinematics of the neutrino.

The procedure for combining the two formalisms is described in detail in Appendix B. Integrating the JTW expression over neutrino direction, we find:

$$\begin{aligned} d^3\Gamma dE_\beta d^3\hat{\Omega}_\beta &= \frac{2}{(2\pi)^4} F_{\mp}(Z, E_\beta) p_\beta E_\beta (E_0 - E_\beta)^2 dE_\beta d^3\hat{\Omega}_\beta \xi \\ &\times \left[1 + b_{\text{Fierz}} \frac{m_e c^2}{E_\beta} + A_\beta \left(\frac{\vec{J}}{J} \cdot \frac{\vec{p}_\beta}{E_\beta} \right) \right], \end{aligned} \quad (1.9)$$

Do it! Do the master equation!

JB: cut "so we will simply provide the combined master equation here"
Don't. The equation you have is all you need.

where a comparison with Holstein's treatment yields the relation,

$$\xi = G_v^2 \cos \theta_C f_1(E). \quad (1.10)$$

JB on intuitive concepts that are missing:

The beta asymmetry dependence on the Fierz term only comes through the normalization of $W(\theta) = 1 + b_{\text{Fierz}} m/E + A_\beta \cos(\theta)$.

i.e.:

$W'(\theta) = 1 + A_\beta/(1 + b_{\text{Fierz}} m/E) \cos(\theta)$. (the angular distribution must be unity where $\cos(\theta)$ vanishes, by definition).

1.4 Our Decay

Here, we will focus on the decay,



which is extremely well suited to the type of experiment to be discussed in this thesis. The parent, ^{37}K , is an isotope of potassium—an alkali. Though this fact may initially seem unremarkable, it is their ‘hydrogen-like’ single valence electron which allows alkalis to be readily trapped within a magneto-optical trap, a critical component of our experimental design (see Chapter 2).

A potential concern in any experiment concerned with the angular correlations resulting from one particular decay branch is the background from competing decay branches. As can be seen in Fig. 1.1, the decay of ^{37}K is dominated by a single branch which contributes nearly 98% of ^{37}K decay events, and the remaining events nearly all arise from a single branch contributing around 2% of the decay events. The other branches combined account for only around 0.04% of decays. Taken all together, this means that the background events which must be accounted for are both infrequent and well understood.

As in any decay, the angular correlations between the emerging daughter particles provide a rich source of information about the type of interaction that produced the decay. This particular decay involves a set of ‘mirror’ nuclei, meaning that the nuclear wavefunctions of the parent and daughter are identical up to their isospin quantum number and corresponding electrical charge. Because the two wavefunctions

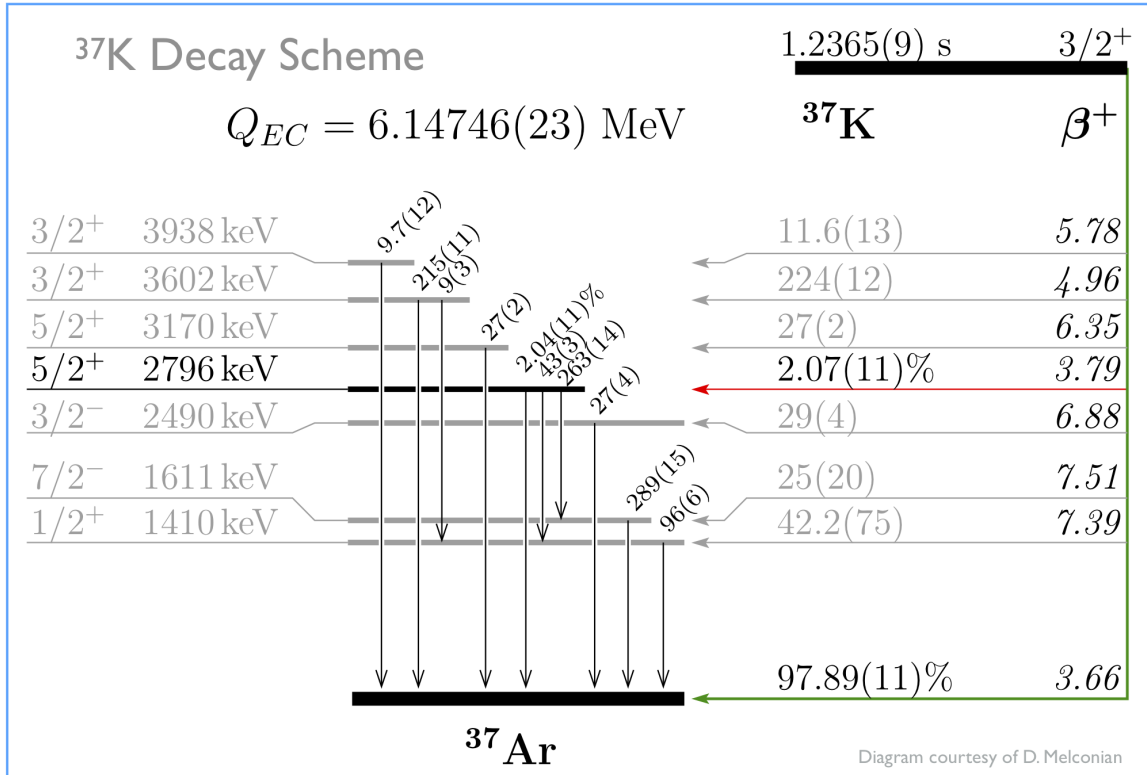


Figure 1.1: A level diagram for the decay of ^{37}K .

are so similar, effects to the decay from nuclear structure corrections can be kept to a minimum, and it is therefore possible to place especially strong constraints on the size of the theoretical uncertainties associated with the decay.

Also, ^{37}K is a really nice isotope for this, because its big A_β value means we have a big thing to multiply any b_{Fierz} value there might be when we construct the superratio asymmetry to eliminate systematics.

Is it definitely true that the nuclear structure corrections are *smaller*? Or is it just that they're better understood?

1.5 The Shake-off Electron Spectrum

Although the beta decay process is primarily concerned with the emission of beta particles (electrons or positrons) from a Weak interaction that occurs within the nucleus, it is common for one or more *orbital* electrons to also be lost in the process. Although beta particles are emitted over a continuous energy spectrum, they commonly carry several MeV of kinetic energy. By contrast, an atomic electron that becomes unbound in this process is likely to only carry a few eV of kinetic energy,

and we say that they are ‘shaken’ off.

We will amend Eq. 1.11 to reflect the presence of N such ‘shake-off electrons’ (SOEs) within each decay event, as



where it is clear that, since the parent ${}^{37}\text{K}$ atom was electrically neutral before its decay by β^+ emission, the daughter ${}^{37}\text{Ar}$ will initially have an ‘extra’ orbital electron (and therefore a negative net charge) if no electrons are shaken off. We also note that it is common for multiple SOEs to be created in a given decay event.

Do I want to re-assign N somehow so the notation works better?

A further consideration is that the outer electron in an ${}^{37}\text{Ar}^-$ ion is *not bound*, and in an electric field such as is present within our experimental chamber, this outer electron is removed immediately to be accelerated through the field, leaving behind a neutral ${}^{37}\text{Ar}$ atom. Although this is in principle a different physical loss mechanism, we will refer to unbound electrons resulting from either process as SOEs.

cite someone!! I don't know who.

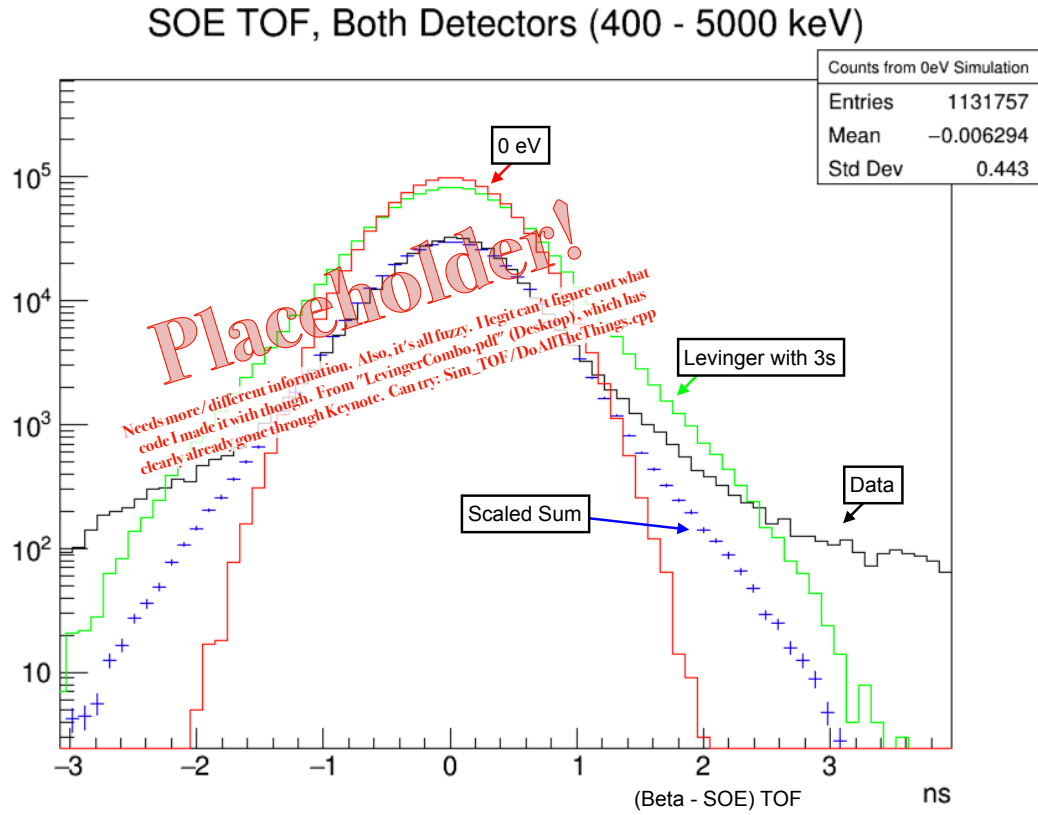
It is useful to consider the energy spectrum of these shake-off electrons. The most straightforward component of the SOE energy spectrum arises from the electrons that are lost immediately following decay, and we take these to initially have 0eV in kinetic energy.

For the shake-off electrons arising from the Weak process itself, the initial energy spectra for SOEs originating in a particular orbital shell can be estimated according to the procedure outlined by Levinger [10]. The strategy is to assume that the sudden approximation holds, and simply calculate the overlap in electron wavefunctions between the initial and final states, where the final state may be either an outgoing electron or one bound within the atom. Analytic expressions can be obtained if the atom is treated as being hydrogenic – an excellent approximation here, as ${}^{37}\text{K}$ is an alkali.

Unfortunately, this treatment cannot determine the fractional contribution of each orbital to the total, nor can it determine the *number* of electrons likely to be removed in a single decay event. The implications of the SOE energy spectrum to the present experiment are discussed further in Section 4.4

In the end, we used $(0.09) * (0\text{eV}) + (0.91) * (0.85 * (4S) + 0.15 * (3P))$. But I say that in the other section. Also, John used Eq.20 for the 4S, and Eq.24 for the 3P.

Comment on how well this matches our data? Somehow?



Maybe just kill this picture? At least reference it in the text somewhere.

Figure 1.2: Shake-off electron TOF (w.r.t. beta TOA) spectrum, showing how the spectrum is different if one includes different sets of initial electrons to be shaken off. I forget why some of them have 0 eV. Maybe those are the ones from the $^{37}\text{Ar}^+$ Levinger TOF spectra for some different sets of SOE initial orbitals before shake-off. (At least that's what it's supposed to be, after I fix the picture). It's reconstructed event-by-event with beta times-of-flight that would pass some basic 'good event' cuts. Anyway, it turns out, it doesn't much matter what orbitals you lose SOEs from. That's nice. In the end, I used 85+15. (Need to re-plot this.)

1.6 Fierz Interference – The Physical Signature

The physical effects resulting from the presence of scalar or tensor couplings include a small perturbation to the energy spectrum of betas produced by radioactive decay.

JB on that missing figure that I've now put in: "A dependence of A_{β} on beta energy is also introduced.

UCNA fits energy spectrum and $A_{\beta}[E_{\beta}]$ simultaneously now."

The point is, the presence of either scalar or tensor interactions will produce a b_{Fierz} term in the decay PDF. It has other effects on the PDF, but those come in at higher-order in the tiny scalar and tensor couplings. So, the Fierz term would be by far the biggest thing that changes in the PDF. The PDF describes the energy and momentum of the outgoing beta w.r.t. a variety of other things. Notably, we can write an elegant-ish description of beta momentum w.r.t. nuclear polarization direction, and ignore the neutrino completely after integrating over it. We have a PDF in beta *direction* (w.r.t. polarization), and beta *energy*. To lowest order (and lowest order is best order) the distribution w.r.t. polarization direction doesn't change, but the distribution w.r.t. energy does change. Or ... something? The point is, it makes a change in the beta energy spectrum. This change is most pronounced at low energies, because the Fierz term is scaled by $(1/E_{\beta})$. However, the asymmetry is also a function of E_{β} . A different function of E_{β} . In fact, it is scaled by (p_{β}/E_{β}) within the PDF, which is distinctly different than b_{Fierz} . So, one might ask what effect a b_{Fierz} term would produce on a constructed asymmetry spectrum.This explanation has gone way off track.

Here's a reference to the picture that shows the result of a non-zero b_{Fierz} term. It's Fig. 1.3.

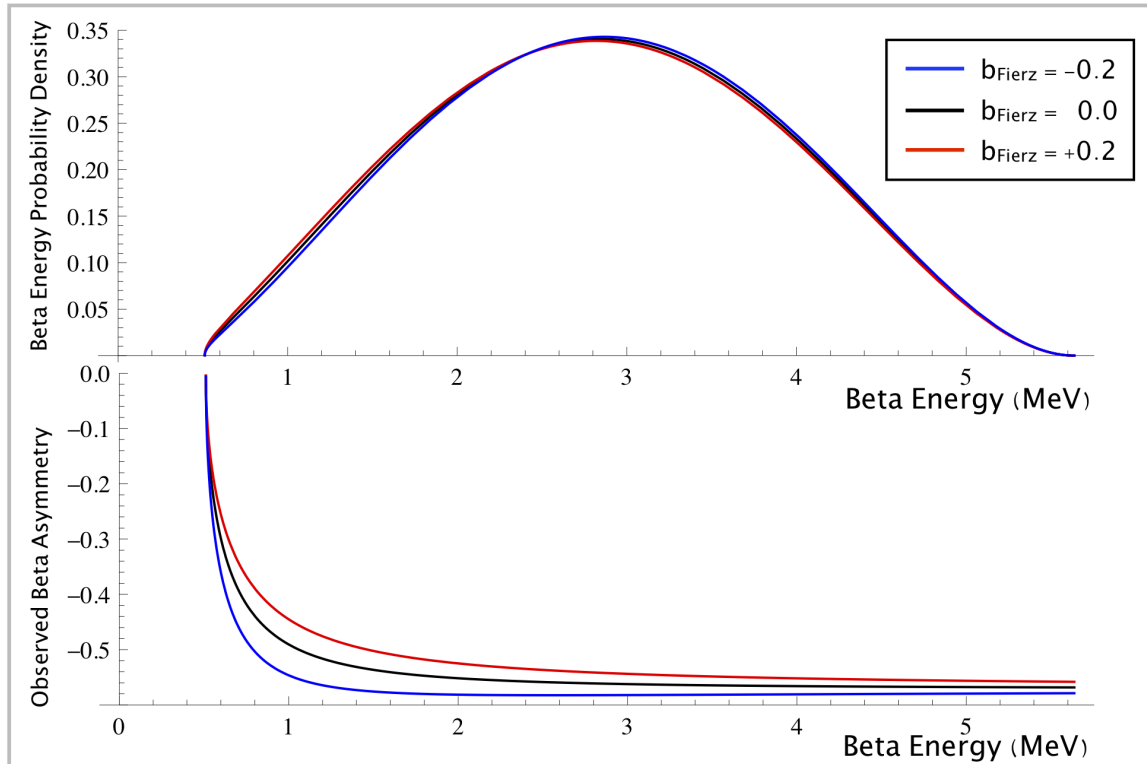


Figure 1.3: Here's why it's better to extract b_{Fierz} from an asymmetry, in this case.

1.7 On the Superratio, the Supersum, and the Constructed Asymmetry

JB: You need to at some point say that the supersum is the beta energy spectrum. There are experiments trying to do this method better, but they are very difficult. UCNA published a combined energy spectrum and Abeta[EBeta] analysis on the neutron in March 2020 [7].

...

MJA: I can't help but also notice the follow-up article from September 2020 [8]. Ugh.

The data can be combined into a superratio asymmetry. This has the benefit of causing many systematics to cancel themselves out at leading order. It also will increase the fractional size of the effects we're looking for. This can be shown by using math.

Not all systematics effects are eliminated. We'll want to be careful to propagate through any effects that are relevant. Using the superratio asymmetry as our physical observable makes this process a bit messier for the things that don't cancel out, but it's all just math. Some other groups have performed similar measurements using the supersum as the physical observable. There are pros and cons to both methods. I can show, using a back-of-the-envelope calculation, that for this particular dataset, the superratio asymmetry method produces a better result.

Chapter 2

Considerations and Implementation of Atomic Techniques

2.1 An Overview of Magneto-Optical Traps

I need to organize the sections/subsections in this chapter/section better, and generally just de-Frankenstein it.

Since its initial description by Raab et. al. in 1987 [18], the magneto-optical trap (MOT) has become a widely used technique in many atomic physics laboratories. The MOT produces confined samples of cold, electrically neutral and isotopically pure atoms confined within a small spatial region. It is these properties that make the MOT a valuable tool not only in atomic physics, but for precision measurements in nuclear physics as well, and the TRIUMF Neutral Atom Trap (TRINAT) collaboration has adopted the technique wholeheartedly.

The technique is used predominantly with alkalis due to their simple orbital electron structure, and once set up it is quite robust. The MOT's trapping force is specific to the isotope for which the trap has been tuned. This feature makes it ideal for use in precision radioactive decay experiments, since the daughters are unaffected by the trapping forces keeping the parent confined.

A typical MOT can be created from relatively simple components: a quadrupole-shaped magnetic field, typically generated by two current-carrying coils of wire, and a circularly polarized laser tuned to match one or more atomic transitions in the isotope of interest. Because a MOT is easily disrupted by interactions with untrapped atoms,

the trap must be created within a vacuum system. Finally, a source of atoms to be trapped is required. [See Fig. 2.1.]

In order to understand the mechanism by which a MOT is able to confine atoms, we must first introduce the Zeeman effect (Section 2.1.1) and a description of an optical molasses (Section 2.1.2). A functional MOT combines the forces resulting from these two physical effects to trap and cool atoms.

2.1.1 Zeeman Splitting

In the presence of an external magnetic field \vec{B} , the Hamiltonian associated with an atom's orbital electrons will acquire an additional "Zeeman Shift" term, given by [19]

$$H_{\text{Zeeman}} = -\vec{\mu} \cdot \vec{B}, \quad (2.1)$$

where $\vec{\mu}$ is the magnetic moment associated with the orbital under consideration. In the limit where the magnetic field is too weak to significantly disrupt the coupling between the electron's spin- and orbital angular momenta, $\vec{\mu}$ may be treated as being fixed with respect to changes in the magnetic field. It is this weak field regime which will be primarily of interest to us in work with magneto-optical traps.

With $\vec{\mu}$ fixed, it is clear that the magnitude of the energy shift must scale linearly with the strength of the magnetic field. In considering the perturbation to the energy of a particular *transition*, the perturbations to the initial and final states must of course be subtracted:

$$\Delta E_{\text{transition}} = -(\vec{\mu}_f - \vec{\mu}_i) \cdot \vec{B}. \quad (2.2)$$

Needs a level diagram. Maybe.

When this is combined with a circularly polarized laser beam, the effect is to move the atomic resonance closer to- or farther from- the frequency of the laser. The circular polarization, combined with some selection rules, means a circularly polarized laser will only couple to one particular transition, w.r.t. angular momentum. ie, for a σ_+ polarized laser, the atom's overall angular momentum projection (along some axis) will be incremented by +1. The Zeeman shift means that in a magnetic field, this transition ($M+=1$) not be the same as the $M=1$ transition. So, if you have a magnetic field that changes linearly across space, you can make it so that in $+B_z$ regions, the laser beam with one certain polarization is closer to resonance and therefore more likely to be absorbed – and similarly, in $-B_z$ regions, a different laser with the opposite polarization will be more likely to be absorbed. Again, if the B-field is linear in space, you can do it so that as the atoms get further and further from the ‘centre’ region, the effect gets progressively stronger. So, if you’ve done this right, you can make it so that the atoms get a stronger “push” back towards the center the farther away they’ve drifted.

They still get the optical molasses cooling effect for free.

2.1.2 Doppler Cooling

We now consider a somewhat more general case in which a cloud of two-level atoms lies along the path of two counter-propagating laser beams, both detuned slightly to the red of resonance. For simplicity, this cloud will be treated as being constrained in the other two dimensions such that it must within the laser’s path. With two counter-propagating laser beams of equal intensity and detuning, the “push” from interaction with one beam is exactly counteracted by the push from the opposite-propagating beam, and there is no net velocity transfer to the cloud.

Detuning the laser from resonance will of course decrease absorption upon interacting with an atom at rest – however the atoms within the cloud are not at rest, but rather are undergoing thermal motion. As such, within the rest frame of each individual atom, the two laser beams will appear to be Doppler shifted in opposite directions, with the sign dependent on atomic motion. In particular, atoms moving against a laser’s direction of propagation will see that laser beam as being blueshifted. Since the laser has been red-detuned within the lab frame, the blueshift moves the laser frequency as seen by the atom back toward resonance, and makes its photons more likely to be absorbed. Similarly, for an atom moving in the same direction as a red-detuned laser beam, this laser will be seen as further red-shifted, and absorption likelihood is decreased. Because of the difference in absorption, such an atom becomes more likely to receive a push back against its (lab frame) direction of motion, slowing

...and opposite polarization. Or something. I have to talk about the selection rules somewhere else.

it down, and less likely to receive a push to increase its lab frame speed.

Optical molasses
equation? Maybe?

The overall effect on a one-dimensional cloud of atoms in the path of two counter-propagating red-detuned lasers is that the atoms will be slowed and cooled. Such a setup is sometimes referred to as a one-dimensional “optical molasses” due to the viscous drag force induced on atomic motion. It is straightforward to extend this model to three dimensions. Although this setup will decrease atomic velocity, it does not include a confining force, so the atoms are still free to move out of the lasers’ path, albeit at a decreased speed.

“...This will slow the atom down, at least up to a limit related to the linewidth of the atomic transition and/or the laser. There’s something to look up.”

Removed ‘Angular Momentum and Selection Rules’ section. Because it was super wrong.

2.1.3 Atom Trapping with a MOT

The laser, which must be circularly polarized in the appropriate directions and tuned slightly to the red of an atomic resonance, is split into three perpendicular retroreflected beams, doppler cooling the atoms and (with the appropriate magnetic field) confining them in all three dimensions (see Figure 2.1).

JB: on 3.3 (now 2.3) “Atom Trapping with a MOT” ((that’s here!)):

The content and scope are ok, but the informal phrasing is going to confuse people. You have to pay some attention and rephrase these sections.

Do I *have* an equation I can put here? Surely there must be one somewhere, but I really don’t want to dig it up, and I don’t think it’s really necessary.

Needs work.

Really, at the end of the previous section, I described the MOT’s trapping mechanism. That’s literally what it is. You just need to do it in 3 dimensions, rather than only one. Fortunately, an anti-helmholz(sp?) coil gives us a quadrupole-shaped magnetic field, which *actually* has a magnetic field that changes linearly along any axis in the region near the center.

Optical molasses + zeeman splitting = magneto-optical trap. Anyway, see Fig. 2.1.

Upon decay, atoms literally aren’t trapped anymore by the trap. No trapping forces, no slowing forces, because it’s all isotope-specific. This is super useful for us.

Ignore the repumper.

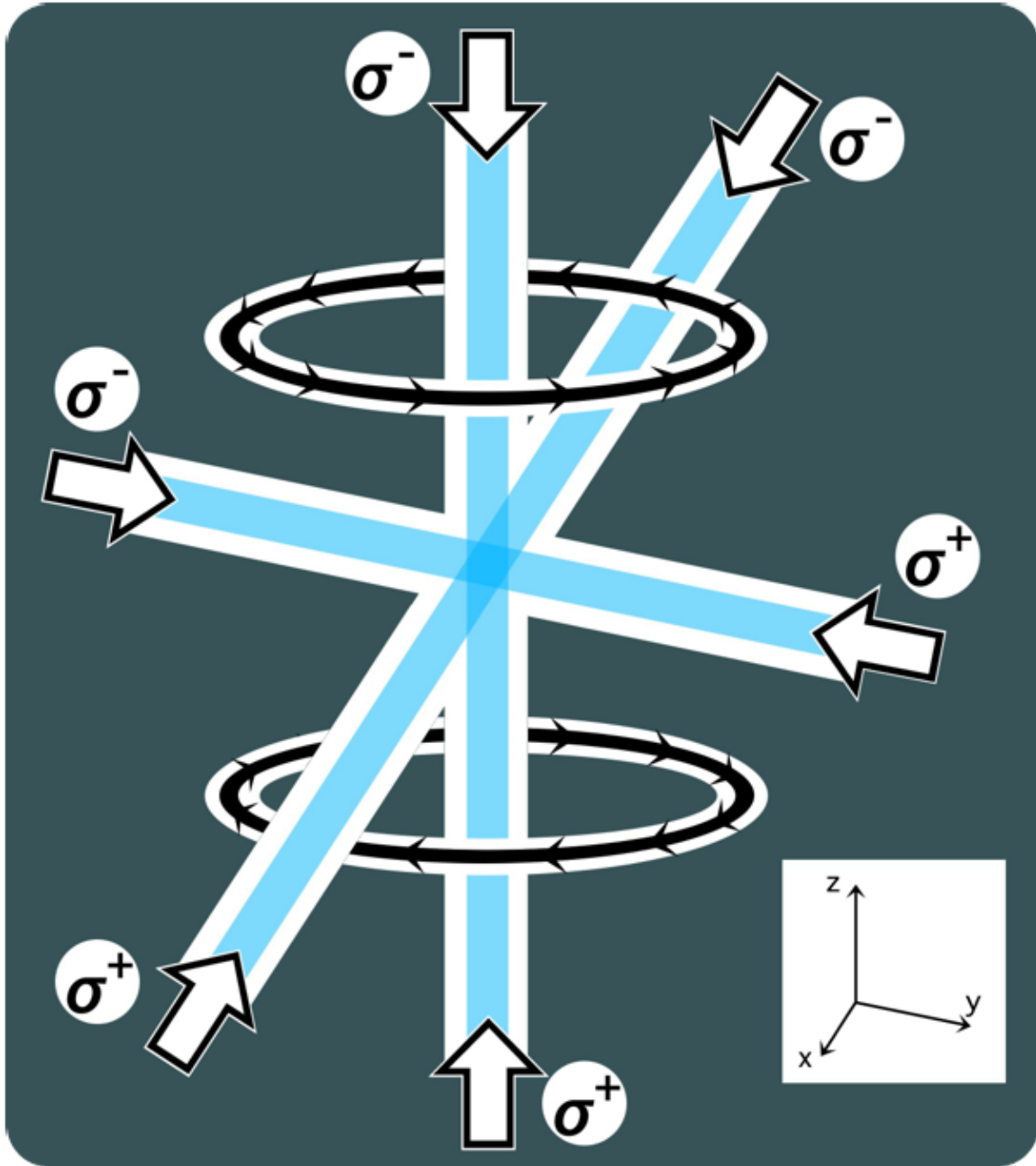


Figure 2.1: Components of a magneto-optical trap, including current-carrying magnetic field coils and counterpropagating circularly polarized laser beams. Diagram taken from [1]

Removed ‘Photoionization as a Probe’ section from the ‘Intro to Atomic Physics’ section, because John says it’s horribly wrong anyhow. Plus, it’s redundant with the ‘Photoionization Laser’ section (2.5.3).

2.2 Optical Pumping

Direct quote from John follows below:

The optical pumping process is described in detail in our collaboration's Ref. [2]. The main detail described here is that the optical pumping is disturbed by any component of magnetic field not along the quantization axis. (Ours is the vertical axis, defined by the direction of the optical pumping light, and along which the detectors are placed.) This required sophistication with an AC MOT described below.

End quote from John. But also!:

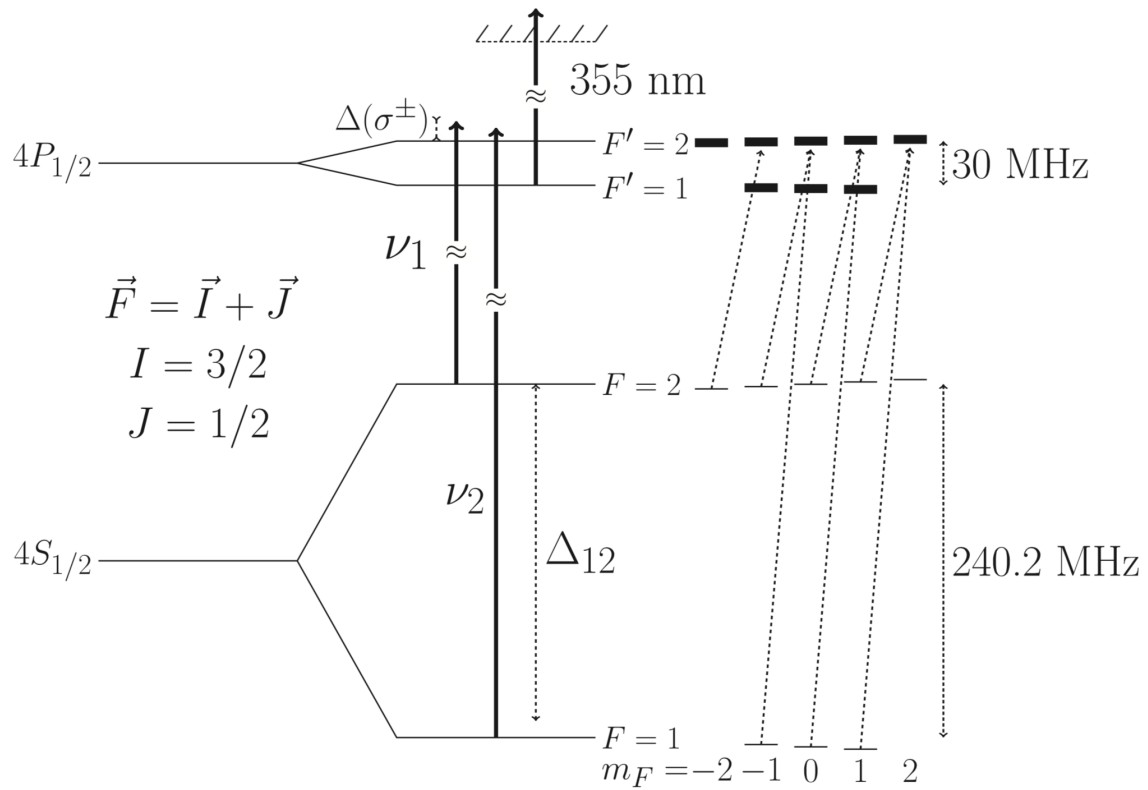
“...Then you can refer to that (ie, John's red quoted mini-blurb about optical pumping, (which I may relocate to Sec. 2.5.3? Or not?) in section 3.4 (now 2.4, about the AC-MOT – ie, Sec. 2.4, (even though I might remove that section entirely and put all its content into Sec. 2.4)), where you're trying to now but the phrasing is poor.”

“Until recently, one limitation of such samples was the necessity for the presence of a relatively large magnetic field, which is expected to partially destroy atomic polarization, limiting the precision of many types of measurements. Here we discuss the construction of a newer type of MOT, the AC-MOT, which minimizes residual magnetic fields. The guys in [9] came up with the idea of the AC-MOT. They made it work and did some stuff with it. Good for them.”

Need a nice, uniform, constant magnetic field for your polarization to larmor precess around. Then, however depolarized (from the axis of the magnetic field) you were to start out, you don't like precess in a way that changes the projection you care about.

But also, I should actually describe the optical pumping, too. And point at Ben's OP paper that we did [2].

JB says: “I would say you don't need an atomic level diagram. You could just describe in words the semiclassical picture of atoms absorbing photons until they are nearly fully polarized, then they stop absorbing. The optical pumping + photoionization is then an in situ probe of the polarization. ... You would need to add in words that quantum mechanical corrections to this picture are in the optical Bloch equation approach in B. Fenker et al. The depolarized states still have high nuclear polarization (1/2 for $F = 2, M_F = 1$, 5/6 for $F = 1, M_F = 1$) and determining the ratio of those two populations provides most of the info we need – we model with the O.B.E, measure the optical pumping light polarization, and float an average transverse magnetic field. This is adequate to determine the depolarized fraction to 10% accuracy, which is all that is needed.”



Describe what's going on here! Alternately, cut the whole image. It's from that paper anyway.

Figure 2.2: An atomic level diagram for the optical pumping of ^{37}K , taken from [2].

2.3 An Overview of the Double MOT System and Duty Cycle

put this in! "...and is designed to operate at ultra-high vacuum (UHV) to minimize trap losses from collisions." Also, I think it helps prevent sparking?

JB: ...You could call the first half of such a chapter "General considerations of Atomic techniques used" and the 2nd half "Experimental Implementation of Atomic Techniques used"

Supersection: Experimental Implementation of Atomic Techniques Used

Remember the pulser LED! To evaluate the stability of the scintillator gain!

JB says: chapter (((this section))) is really good, and in good shape for the committee

We obtain a sample of neutral, cold, nuclear spin-polarized ^{37}K atoms with a known spatial position, via the TRIUMF accelerator facility, by intermittently running a magneto-optical trap (MOT) to confine and cool the atoms, then cycling the trap off to polarize the atoms. With β detectors placed opposite each other along the axis of polarization, we are able to directly observe the momenta of β^+ particles emitted into 1.4% of the total solid angle nearest this axis. We also are able to extract a great deal of information about the momentum of the recoiling ^{37}Ar daughters by measuring their times of flight and hit positions on a microchannel plate detector with a delay line. Because the nuclear polarization is known to within $< 0.1\%$ [2], and we are able to account for many systematic effects by periodically reversing the polarization and by collecting unpolarized decay data while the atoms are trapped within the MOT, we expect to be well equipped to implement a test of ‘handedness’ within the nuclear weak force.

The experimental subject matter of this thesis was conducted at TRIUMF using the apparatus of the TRIUMF Neutral Atom Trap (TRINAT) collaboration. The TRINAT laboratory offers an experimental set-up which is uniquely suited to precision tests of Standard Model beta decay physics, by virtue of its ability to produce highly localized samples of cold, isotopically pure atoms within an open detector geometry. Although the discussion in this chapter will focus on the methodologies used to collect one particular dataset, taken over approximately 7 days of beamtime in June 2014, the full apparatus and the techniques used are fairly versatile, and can be (and have been) applied to several related experiments using other isotopes.

Cite a bunch of papers here.

Surely most of this paragraph goes in an intro chapter somewhere.

The TRINAT lab accepts radioactive ions delivered by the ISAC beamline at TRIUMF. These ions are collected on the surface of a hot zirconium foil where they are electrically neutralized, and subsequently escape from the foil into the first of two experimental chambers (the “collection chamber”). Further details on the neutralization process are presented in a previous publication [20]. Within the collection chamber, atoms of one specific isotope – for the purposes of this thesis, ^{37}K – are continuously collected into a magneto-optical trap from the tail end of the thermal distribution. Although this procedure preferentially traps only the slowest atoms, once trapped, atoms will be cooled further as a side-effect of the MOT’s trapping mechanism. The result is a small ($\sim 1 \text{ mm diameter}$), cold ($\sim 1 \text{ mK}$) cloud of atoms of a particular isotope.

made possible by UHV!

These properties of the atomic cloud allow for a relatively clean transfer of linear momentum from an appropriately tuned laser beam to the atoms within the cloud, and we use this mechanism to “push” the atoms out of the collection MOT and into

TRINAT DOUBLE MOT TRAPPING SYSTEM

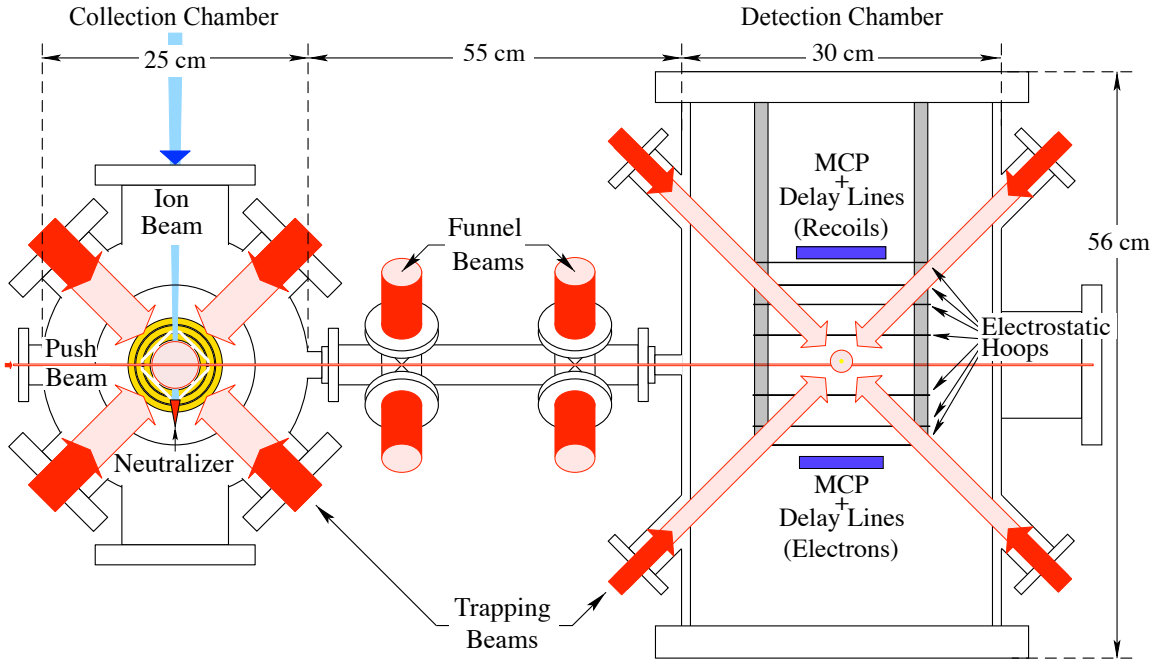


Figure 2.3: The TRINAT experimental set-up, viewed from above. The two MOT system reduces background in the detection chamber. Funnel beams along the atom transfer path keep the atoms focused.

Figure was originally created by Alexandre, modified by ... someone else? Or Alexandre? And I got it from ... probably an experimental proposal? I should figure out how to cite a proposal...

the “detection chamber”, where they are loaded into a second MOT (see Fig. 2.3). During regular operation, atoms are transferred approximately once per second.

There is no need to release previously trapped atoms in the second MOT when a new group of atoms is loaded. Although the trap loses atoms over time as a result of a variety of physical processes, during typical operation the majority of atoms loaded in a given transfer will still be trapped at the time the next set of atoms is loaded, and after several transfer cycles, something like a steady state is obtained.

discussed ... idk,
somewhere else.

Because the transfer and trapping mechanisms rely on tuning laser frequencies to specific atomic resonances, these mechanisms act on only a single isotope, and all others remain unaffected. The result is a significant reduction of background contaminants within the detection chamber relative to initial beamline output. The transfer methodology is discussed in some detail within another publication [21].

We now turn our attention to what happens to the atom cloud in the detection

chamber between loading phases (see Fig. 2.4). One of the goals for the 2014 ^{37}K beamtime required that the atom cloud must be spin-polarized, as well as being cold and spatially confined. Although the MOT makes it straightforward to produce a cold and well confined cloud of atoms, it is fundamentally incompatible with techniques to polarize these atoms. The physical reasons behind this are discussed in Section 2.4.

I *do* discuss this, right?? Right??

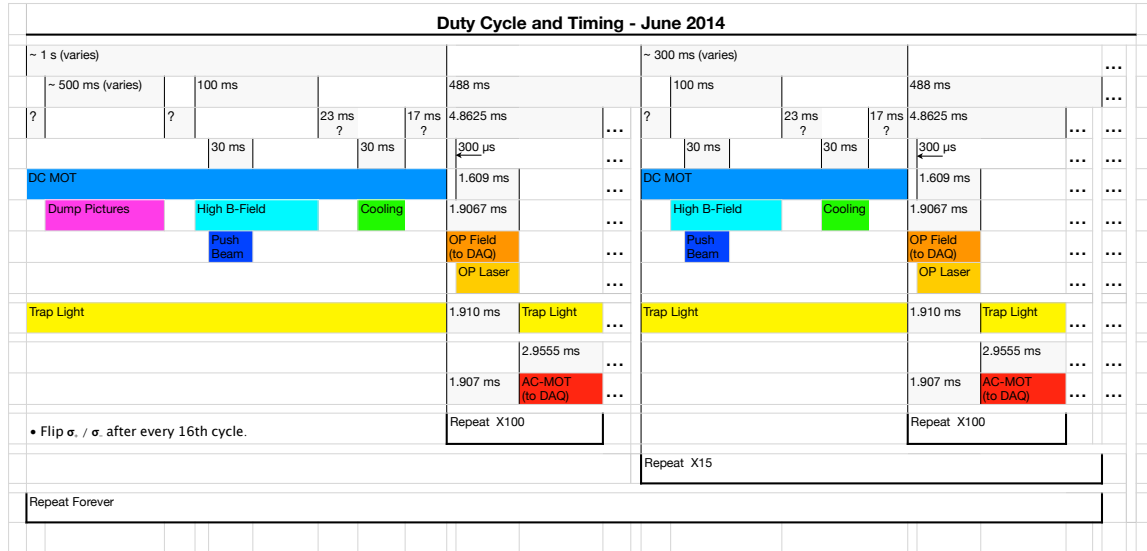


Figure 2.4: The duty cycle used for transferring, cooling, trapping, and optically pumping ^{37}K during the June 2014 experiment. Not drawn to scale. Question marks indicate timings that varied either as a result of electronic jitter or as a result of variable times to execute the control code. Atoms are transferred during operation of the DC-MOT. Though the push beam laser itself is only on for 30 ms, the bulk of the DC-MOT's operation time afterwards is needed to collect and cool the transferred atoms. After 100 on/off cycles of optical pumping and the AC-MOT, the DC-MOT resumes and the next group of atoms is transferred in. After 16 atom transfers, the polarization of the optical pumping laser is flipped to spin-polarize the atoms in the opposite direction, in order to minimize systematic errors.

Once the newly transferred set of ^{37}K atoms has been collected into the cloud, the entire MOT apparatus cycles 100 times between a state where it is ‘on’ and actively confining atoms, and a state where it is ‘off’ and instead the atoms are spin-polarized by optical pumping while the atom cloud expands ballistically before being re-trapped. These 100 on/off cycles take a combined total of 488 ms. The laser components of the trap are straightforward to cycle on and off on these timescales, but the magnetic field is much more challenging to cycle in this manner.

Immediately following each set of 100 optical pumping cycles, another set of atoms is transferred in from the collection chamber to the detection chamber, joining the atoms that remain in the trap (see Fig. 2.4). The details of the trapping and optical pumping cycles are described further in Section 2.4, and the optical pumping technique and its results for this beamtime are the subject of a recent publication [2].

2.4 The AC-MOT and Polarization Setup

JB on Ch. 3.4 (now 2.4) ((now Ch. 2.4)) “The AC-MOT” (that’s this section!): The content and scope are ok, but the informal phrasing is going to confuse people. You have to pay some attention and rephrase these sections.

John suggests that maybe I should just refer directly to his red, quoted OP blurb in the chapter about the AC-MOT.

This content *came from* that other section, and needs to go in here somewhere: “Many laser ports to make the MOT functional, and for optical pumping. Fancy mirror geometry to combine optical pumping and trapping light along the vertical axis. Water-cooled (anti-)Helmholz coils within the chamber for the AC-MOT, fast switching to produce an optical pumping field.”

Citation for Harvey and Murray goes here [9]. Also, myself [1].

“...where you’re trying to now but the phrasing is poor.”

Here’s a diagram of our AC-MOT running one AC-MOT/OP cycle, in Fig. 2.5.

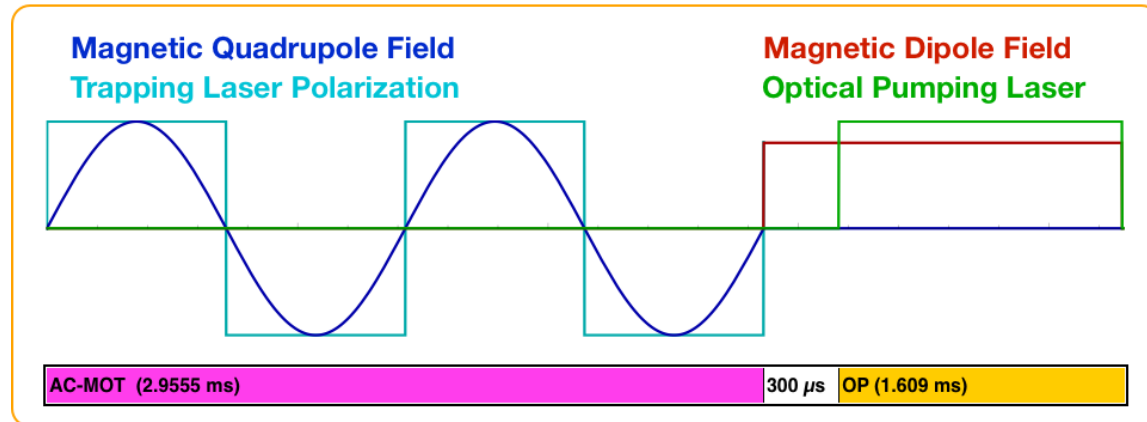


Figure 2.5: One cycle of trapping with the AC-MOT, followed by optical pumping to spin-polarize the atoms. After atoms are transferred into the science chamber, this cycle is repeated 100 times before the next transfer. The magnetic dipole field is created by running parallel (rather than anti-parallel as is needed for the MOT) currents through the two coils.

Normal MOTs are DC-MOTs. They just sort-of go. It's continuous. We used an AC-MOT though! The point of an AC-MOT is to shut off the magnetic field as quickly as possible. With a well-controlled and uniform magnetic field, we can optically pump the atoms, which I think I'm going to describe in the upcoming section (2.2).

Sadly, this also removes our trapping mechanism. We could keep the optical molasses after the field is off if we wanted to, but we don't, because we wouldn't be able to optically pump the atoms then. But at least the atoms are cold-ish (we can measure! I think it's done indirectly in that one table, or for realsies in Ben's thesis), so we can let them just chill for a little while before we have to re-trap them. Don't lose too much.

Anyway, the idea of the AC-MOT is to run a sinusoidal current through your anti-Helmholtz coils. You'll get eddy currents in your nearby metal *stuff* when you have a changing current, and those will *also* make a magnetic field. So, the idea with an AC-MOT is that with a sinusoid, you have clear control over what the eddy currents are actually doing, and you can just shut the current off when the eddy currents are zero (current in the anti-Helmholtz coils will be close to zero at this time too, depending on frequency of the sinusoid...), so you can reduce the size of the eddy currents by like an order of magnitude. Eddy currents in general take a while to die away, so it's good to make them as small as possible. ...Also, eddy currents making a magnetic field will screw up your optical pumping, because um, reasons? I think it's not just the detuning, it's also something about the Larmor precession.

How much do we lose? Have we quantified that somewhere? Probably.

begin content of the historical other AC-MOT+Polarization section.

Probably document things about the waveform and frequency used for the beamtime, since I don't think it's in my MSc.

John objects to the phrasing of the following paragraph, because you fundamentally need polarized atoms to measure b_{Fierz} .

As alluded to in the previous section (2.3), the measurement in question required a spin-polarized sample of atoms, and a precise knowledge of what that polarization was. This was primarily needed in order to facilitate a measurement of A_β that was performed on the same data that is the subject of discussion here. [22] While this is arguably less critical to a measurement of b_{Fierz} , it can still be an asset for eliminating systematic effects. We use only the polarized portion of the duty cycle in order to minimize other systematic errors, such as the scintillator energy calibration and overall trap position. It also makes for a more straightforward interpretation of

Plus, it barely makes sense to talk about measuring b_{Fierz} if you don't know A_β .

the relationship of the measured values of A_β and b_{Fierz} when the systematic effects are the same for both measurements. Finally, using only polarized data allows us to make use of the ‘superratio’ construction in data analysis, a powerful tool for reducing (many) systematic errors at the expense of statistical precision (see Chapter 1.6).

End paragraph that John hates.

The TRINAT science chamber includes 6 ‘viewports’ specifically designed to be used for the trapping laser (see Fig. 2.7.).

JB says: “Since you worked hard on the logic triggers, a photoion spectrum with duty cycle would be appropriate if you want.”

A MOT also requires a quadrupolar magnetic field, which we generate with two current-carrying anti-Helmholtz coils located within the vacuum chamber itself. The coils themselves are hollow, and are cooled continuously by pumping temperature-controlled water through them.

One feature which makes our MOT unusual has been developed as a result of our need to rapidly cycle the MOT on and off – that is, it is an “AC-MOT”. Rather than running the trap with one particular magnetic field and one set of laser polarizations to match, we run a sinusoidal AC current in the magnetic field coils, and so the sign and magnitude of the magnetic field alternate smoothly between two extrema, and the trapping laser polarizations are rapidly swapped to remain in sync with the field [9][1]. See Figure 2.5.

Note that because the atoms within a MOT can be treated as following a thermal distribution, some fraction of the fastest atoms continuously escape from the trap’s potential well. Even with the most carefully-tuned apparatus, the AC-MOT cannot quite match a similar standard MOT in terms of retaining atoms. The TRINAT AC-MOT has a ‘trapping half-life’ of around 6 seconds, and although that may not be particularly impressive by the standards of other MOTs, it is more than adequate for our purposes. ^{37}K itself has a radioactive half-life of only 1.6 seconds (cite someone), so our dominant loss mechanism is radioactive decay rather than thermal escape.

We spin-polarize ^{37}K atoms within the trapping region by optical pumping [2]. A circularly polarized laser is tuned to match the relevant atomic resonances, and is directed through the trapping region along the vertical axis in both directions. When a photon is absorbed by an atom, the atom transitions to an excited state and its total angular momentum (electron spin + orbital + nuclear spin) along the vertical axis is incremented by one unit. When the atom is de-excited a photon is emitted

isotropically, so it follows that if there are available states of higher and lower angular momentum, the *average* change in the angular momentum projection is zero. If the atom is not yet spin-polarized, it can absorb and re-emit another photon, following a biased random walk towards complete polarization.

In order to optimally polarize a sample of atoms by this method, it is necessary to have precise control over the magnetic field. This is because absent other forces, a spin will undergo Larmor precession about the magnetic field lines. In particular, the magnetic field must be aligned along the polarization axis (otherwise the tendency will be to actually depolarize the atoms), and it must be uniform in magnitude over the region of interest (otherwise its divergencelessness will result in the field also having a non-uniform direction, which results in a spatially-dependent depolarization mechanism). Note that this type of magnetic field is not compatible with the MOT, which requires a linear magnetic field gradient in all directions (characteristic of a quadrupolar field shape), and has necessitated our use of the AC-MOT as described in (Sub-)Section 2.4.

At some point I have to decide if that's going to be a section or a subsection.

2.5 Measurement Geometry and Detectors

The TRINAT detection chamber operates at ultra-high vacuum (UHV) and provides not only the apparatus necessary to intermittently confine and then spin-polarize atoms, but also the variety of detectors and implements required to quantify their position, temperature, and polarization. The detection chamber further boasts an array of electrostatic hoops to collect both positively and negatively charged low energy particles into two opposing microchannel plate (MCP) detectors, each backed by a set of delay lines to measure hit position, and a further set of two beta detectors positioned across from each other along the polarization axis, each of which consists of a 40x40 pixel double-sided silicon strip detector (DSSD) and a scintillator coupled to a photomultiplier tube (PMT) (see Fig. 2.6).

2.5.1 Microchannel Plates and Electrostatic Hoops

Two stacks of microchannel plates (MCPs) have been placed on opposing sides of the chamber, and perpendicular to the axis of polarization. Each stack of MCPs is a relatively large detector backed by a series of delay lines for position sensitivity.

These two MCP detectors are designed to operate in conjunction with a series of seven electrostatic ‘hoops’ positioned within the chamber and connected to a series of high voltage power supplies. The hoops are designed in such a way as to maintain a constant and (roughly) uniform electric field across the space between the two MCP detectors, without blocking either the path of particles originating from the central cloud, or necessary laser beams. The resulting electric field acts to pull positively charged ions towards one MCP detector and negatively charged electrons towards the other (see Figs. 2.6 and 2.7).

The detector intended to collect the negatively charged electrons (the “eMCP”) has an active area of 75.0 mm, and is positioned 100.0 mm from the chamber centre. It features a Z-stack configuration of three plates, and it is backed by a set of three separate delay lines in a “hexagonal” arrangement for redundant position sensitivity (the “HEX75”). The detector used to collect positively charged ions (the “iMCP,” or equivalently the “rMCP” since many of the ions collected are recoils from decay) is 80.0 mm in diameter and positioned 101.4 mm from the chamber centre. It features only two plates arranged in a chevron configuration, and it is backed by a set of two separate delay lines (the “DLD80”) for position sensitivity. In the context of the present work, the rMCP data is used primarily in conjunction with the photoionization laser to characterize the atom cloud (Section 2.5.3), while the eMCP data is used, together with the beta detectors, as a ‘tag’ for decay events originating from the cloud.

Due to an unfortunate interaction between the two MCP detectors, during the 2014 beamtime it was not possible to run both the eMCP and the rMCP simultaneously without producing a large background on at least one detector (there seemed to be no consistency as to which detector was most affected at a given time). As a result, data was instead collected with only one MCP detector biased at a time, and the active detector was alternated every few hours to spend approximately equal time collecting data with the eMCP and rMCP. [Online scientific data has been collected](#) with the eMCP at electric field strengths of 66.7 V/cm and 150. V/cm, while rMCP data has been collected at 395. V/cm, 415. V/cm, and 535. V/cm. Note that these field strengths are all too low to significantly perturb any but the least energetic of the (positively charged) betas originating from decay, and those betas already lack the energy that would be needed to travel through the SiC mirror and Be foil vacuum seal into a beta detector.

Do I talk about how this works somewhere? Probably in that section on cuts.

Reference that one table.

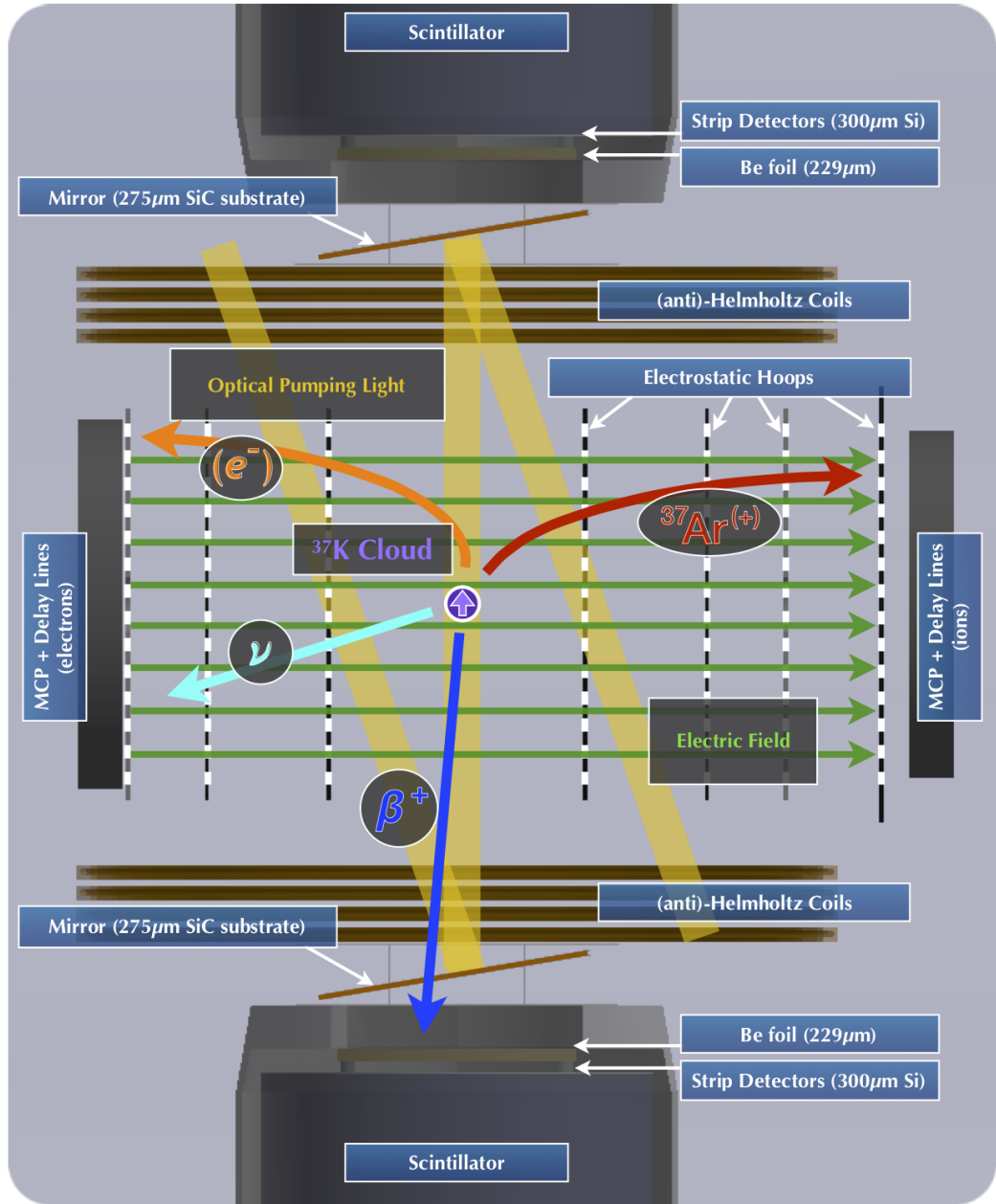


Figure 2.6: A scale diagram of the interior of the TRINAT detection chamber, shown edge-on with a decay event. After a decay, the daughter will be unaffected by forces from the MOT. Positively charged recoils and negatively charged shake-off electrons are pulled towards detectors in opposite directions. Although the β^+ is charged, it is also highly relativistic and escapes the electric field with minimal perturbation.

rMCP is 101.4 mm from center, eMCP is 100 mm from center. Do I say this somewhere else?

2.5.2 Beta Detectors

The beta detectors, located above and below the atom cloud along the axis of polarization (Fig. 2.6), are each the combination of a plastic scintillator and a set of silicon strip detectors. Using all of the available information, these detectors are able to reconstruct the energy of an incident beta, as well as its hit position, and provide a timestamp for the hit's arrival. Together the upper and lower beta detectors subtend approximately 1.4% of the total solid angle as measured with respect to the cloud position.

The two sets of beta detectors were positioned directly along the axis of polarization. Each beta detector consists of a plastic scintillator and photo-multiplier tube (PMT) placed directly behind a 40×40 -pixel double-sided silicon strip detector (DSSD). The scintillator is used to measure the overall energy of the incoming particles, as well as to assign a timestamp to these events, while the DSSD is used both to localize the hit position to one (or in some cases, two) individual pixel(s), and also to discriminate between different types of incoming particles. In particular, though the scintillator will measure the energy of an incoming beta or an incoming gamma with similar efficiency, the beta will lose a portion of its kinetic energy as it passes through the DSSD into the scintillator. By contrast, an incident gamma will deposit only a very small amount of energy in the DSSD layer, making it possible to reject events with insufficient energy deposited in the DSSD as likely gamma ray events. Given that the decay of interest to us emits positrons, we expect a persistent background 511 keV gamma rays that are not of interest to us, so it is extremely important that we are able to clean these background events from our spectrum.

It must be noted that the path between the cloud of trapped atoms and either beta detector is blocked by two objects: a $275\text{ }\mu\text{m}$ silicon carbide mirror (necessary for both trapping and optical pumping), and a $229\text{ }\mu\text{m}$ beryllium foil (separating the UHV vacuum within the chamber from the outside world). In order to minimize beta scattering and energy attenuation, these objects have had their materials selected to use the lightest nuclei with the desired material properties, and have been manufactured to be as thin as possible without compromising the experiment. As the $^{37}\text{K} \rightarrow ^{37}\text{Ar} + \beta^+ + \nu_e$ decay process releases $Q = 5.125\text{ MeV}$ of kinetic energy [23], the great majority of betas are energetic enough to punch through both obstacles without significant energy loss before being collected by the beta detectors.

There's gotta be a better way to describe it

what's the open area of the detector? how big is each pixel?

2.5.3 The Photoionization Laser

John says: Chapter (((2.5.3))) is very good and complete, showing you understand what is-needed about photoionization. A good reason to omit 3.5 ‘photoionization as a aprobe’ as I said above.

In order to measure properties of the trapped ^{37}K cloud, a 10 kHz pulsed laser at 355 nm is directed towards the cloud. These photons have sufficient energy to photoionize neutral ^{37}K from its excited atomic state, which is populated by the trapping laser when the MOT is active, releasing 0.77 eV of kinetic energy, but do not interact with ground state ^{37}K atoms. The laser is of sufficiently low intensity that only $\sim 1\%$ of excited state atoms are photoionized, so the technique is only very minimally destructive.

Probably worth mentioning that we test this stuff offline on stable ^{41}K . But also, surely it should be mentioned in like the AC-MOT/Polarization section too.

Because an electric field has been applied within this region (Section 2.5.1) the $^{37}\text{K}^+$ ions are immediately pulled into the detector on one side of the chamber, while the freed e^- is pulled towards the detector on the opposite side of the chamber. Because $^{37}\text{K}^+$ is quite heavy relative to its initial energy, it can be treated as moving in a straight line directly to the detector, where its hit position on the microchannel plate is taken as a 2D projection of its position within the cloud. Similarly, given a sufficient understanding of the electric field, the time difference between the laser pulse and the microchannel plate hit allows for a calculation of the ion’s initial position along the third axis.

JB: “you could reference the letter for the value of the field 150V/cm.”

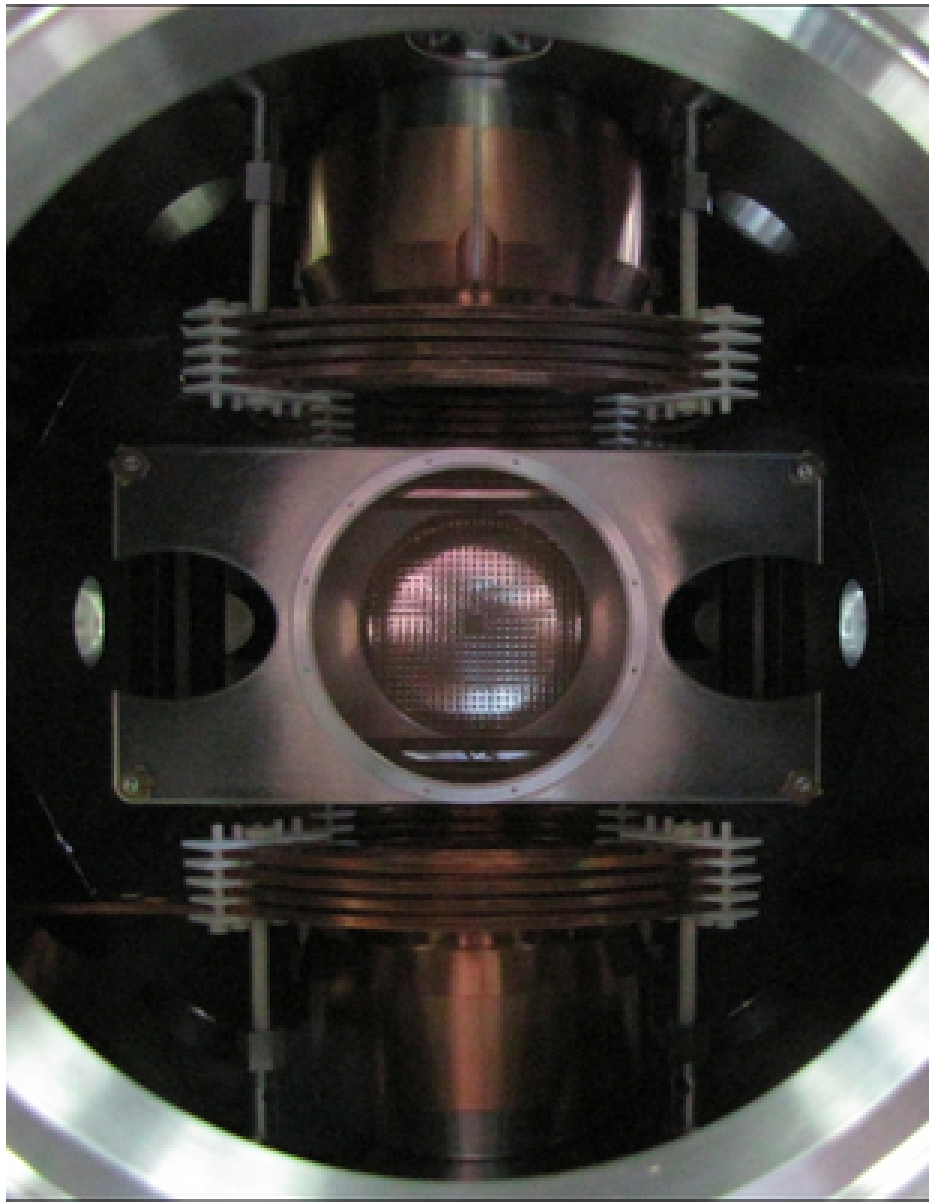
As a check: the camera measurements for photons from de-excitation. It’s aimed 35 degrees from vertical, with its horizontal axis the same as one of the other axes. I think it’s the TOF axis. I can check this when my computer comes back. Also, there’s an unknown additional delay between some of our DAQ channels that can’t be explained by accounting for cable lengths, so we really like having the check there.

JB says: “yes, camera x-axis is tof axis.”

With this procedure, it is possible to produce a precise map of the cloud’s position and size, both of which are necessary for the precision measurements of angular correlation parameters that are of interest to us here. However, it also allows us to extract a third measurement: the cloud’s polarization.

The key to the polarization measurement is that only atoms in the excited atomic state can be photoionized via the 355 nm laser. While the MOT runs, atoms are

constantly being pushed around and excited by the trapping lasers, so this period of time provides a lot of information for characterizing the trap size and position. When the MOT is shut off, the atoms quickly return to their ground states and are no longer photoionized until the optical pumping laser is turned on. As described in Section 2.2, and in greater detail in [2], the optical pumping process involves repeatedly exciting atoms from their ground states until the atoms finally cannot absorb any further angular momentum and remain in their fully-polarized (ground) state until they are perturbed. Therefore, there is a sharp spike in excited-state atoms (and therefore photoions) when the optical pumping begins, and none if the cloud has been fully polarized. The number of photoion events that occur once the sample has been maximally polarized, in comparison with the size and shape of the initial spike of photoions, provides a very precise characterization of the cloud's final polarization [2].



Chamber walls are made from 316-L stainless steel, chosen for strength, cost, and minimal eddy currents.

Figure 2.7: Inside the TRINAT science chamber. This photo is taken from the vantage point of one of the microchannel plates, looking into the chamber towards the second microchannel plate. The current-carrying copper Helmholtz coils and two beta telescopes are visible at the top and bottom. The metallic piece in the foreground is one of the electrostatic hoops used to generate an electric field within the chamber. The hoop's central circular hole allows access to the microchannel plate, and the two elongated holes on the sides allow the MOT's trapping lasers to pass unimpeded at an angle of 45 degrees 'out of the page'.

Chapter 3

Calibrations and Data Selection

Intro blurb goes here?

3.1 An Overview of Available Data

Although the detection chamber was designed to feature two MCP detectors on opposing sides of an applied electric field intended for simultaneous use (see Section 2.5.1), in practice the two detectors produced quite a bit of feedback when operated at the same time. In order to salvage usable data from the beamtime, it was necessary to run only one detector at a time, but switched which detector was in use every few hours, collecting approximately the same amount of data with each detector (see Tables 3.1 and 3.2). Thus, the runs are sorted into ‘electron’ and ‘recoil’ runs, depending on what the detector in use was intended to detect. The data is further split up into several runsets based on when certain settings were adjusted, and the individual runsets have been treated separately for nearly all parts of the analysis.

While the beta asymmetry and Fierz interference are best evaluated using the electron runs, the polarization (a dominant uncertainty in the beta asymmetry measurement) and cloud position are best evaluated with recoil runs. The polarization measurement is the subject of a recent publication (see [2]), and the evaluation of cloud position is discussed in Section 3.4. The recoil runs may also be analyzed in the future as part of a search for right-handed Weak interactions (described further in Chapter 6.4).

In considering Tables 3.1 and 3.2, we note that Runsets EA and RA were neglected

Electron Runs

	OP Delay	Events	Electric Field	Runs
Runset EA	$300\ \mu s$	0	66.67 V/cm	314, 362, 363, 383-386, 393.
Runset EB	$300\ \mu s$	173,640	150.0 V/cm	428-437, 440-445.
Runset EC	$700\ \mu s$	18,129	150.0 V/cm	476, 477.
Runset ED	$400\ \mu s$	207,596	150.0 V/cm	478-489, 502-505, 510, 513.

Ben doesn't seem to include Runs 436 and 437 in *any* set of good runs. Is it an oversight? I think they're perfectly legit electron runs. They're fairly long runs...

Table 3.1: A list of 2014 online electron runs with potentially usable data. The “Events” column includes only the number of events that passed all cuts.

Recoil Runs

	OP Delay	Electric Field	Runs
Runset RA	$300\ \mu s$	395.0 V/cm	303, 308-313, 318, 326, 327, 328, 340, 342, 343, 376, 377, 378, 394, 395, 396, 398-402.
Runset RB	$300\ \mu s$	535.0 V/cm	409-419, 421-426, 446, 447, 449.
Runset RC	$700\ \mu s$	395.0 V/cm	450, 454, 455.
Runset RD	$700\ \mu s$	415.0 V/cm	460-466, 473, 474.
Runset RE	$400\ \mu s$	415.0 V/cm	491, 497, 498, 499, 509.

Ben includes 448 as a ‘good’ recoil run. But I don’t. Why? Also 451, 451, 453. ...Also 467,468,469,470,471,472. Also-also, 492, 493, 494, 495, 496.

Table 3.2: A list of 2014 online recoil runs and associated parameters. A count of good events that pass all cuts is not included because different cuts must be used for polarization and trap position data.

completely during analysis after it was determined that one scintillator had an improperly set hardware threshold such that lower energy betas weren’t being detected at all. Additionally, there was a QDC module failure before Run 450, resulting in an abrupt change in calibration for the two scintillators. The electric field is larger during recoil runs in an attempt to maximize the fraction of nuclear recoils collected, as well as the separation in TOF between different charge states. For electron runs, although not all SOEs were collected, the lower electric fields were preferred in order to decrease background events and the sparking incidents. Although the final analysis uses only the eMCP runs directly, the result could not have been obtained with the

same degree of precision had the rMCP data not been present.

3.2 Preliminary Data Selection with the rMCP

As described in Chapter 2.5.3, the primary function of the rMCP within the context of this experiment is as a probe of the atom cloud, and it provided a critical check of the cloud's position, size, and polarization state over the course of the beamtime. The process of cleaning, calibrating, and analyzing this data is described here.

The two delay lines located just behind the rMCP provide information about hit position. The principle behind a delay line's operation is relatively straightforward. The delay line itself is made from a thin wire wound into a flattened coil that covers the area of the microchannel plate. The second delay line is oriented perpendicular to the first and immediately behind it, but also covers the full area of the microchannel plate. When a charged particle is incident on the stack of microchannel plates, an electron shower is initiated. The shower gains strength as it propagates through the MCPs' microchannels, and emerges on the back side of the stack after having been greatly amplified. This electron shower is then incident on a delay line, generating an electrical pulse that propagates from the hit point towards both ends of the wire. Although the wire is conductive, the propagation speed is finite, and this fact is key to extracting the hit position. The time of arrival for the electrical pulse is recorded at each end of the delay line wire, and it is the difference between the two times that tells where along the wire the original hit occurred. In general, a single delay line is only precise enough to determine the hit position as projected along the direction perpendicular to its coil's wires. The electron shower continues past the first delay line to hit the delay line immediately behind, which again creates an electrical pulse that propagates towards the ends of that wire, and a similar procedure can be used to evaluate the hit position in the perpendicular direction. Therefore, for an event in which the rMCP is hit and an electron shower is triggered, we expect to have five timestamps associated with that hit – one associated with the MCP stack itself, and two from each delay line.

how precise is the rMCP supposed to do? in practice, it wasn't nearly that good.

It's not really *every* event....

A diagram of how delay lines work would really help here, but there's no time for that. I'll put it in if someone asks.

Do I want the above section about how delay lines work to go in the other chapter? Maybe.

This understanding of how delay lines work informs the initial stages of data

processing for rMCP events. To obtain the cleanest possible rMCP data, the first step is to simply throw out every event which doesn't have a complete set of five timestamps associated with it – even though it would still be possible to make good use of many events which have only partial data. Even though many “real” rMCP hit events came in under threshold in one or more channels, detector noise was plentiful, and that noise varied in both quality and quantity over the course of the beamtime. Therefore, it was decided to be more important for the rMCP data to be as clean as possible, despite the fact that its statistical power would be reduced. (Note that this step is *not* done on the eMCP side – more on that in Section 3.7)

The next stage of rMCP data cleaning is to discard events with an aberrant set of timestamps. A delay line is essentially just a long wire, and the time it takes to propagate a signal from one end of the wire to the other is fixed. This means that no matter where along the delay line a pulse is generated, if one adds rather than subtracts the timestamps at which the pulse arrives at each of the two ends, that sum should be constant after accounting for the time of the original hit – which we can determine from the timestamp associated with the MCP. To that end, we construct delay line sums for the “x” and “z” delay lines,

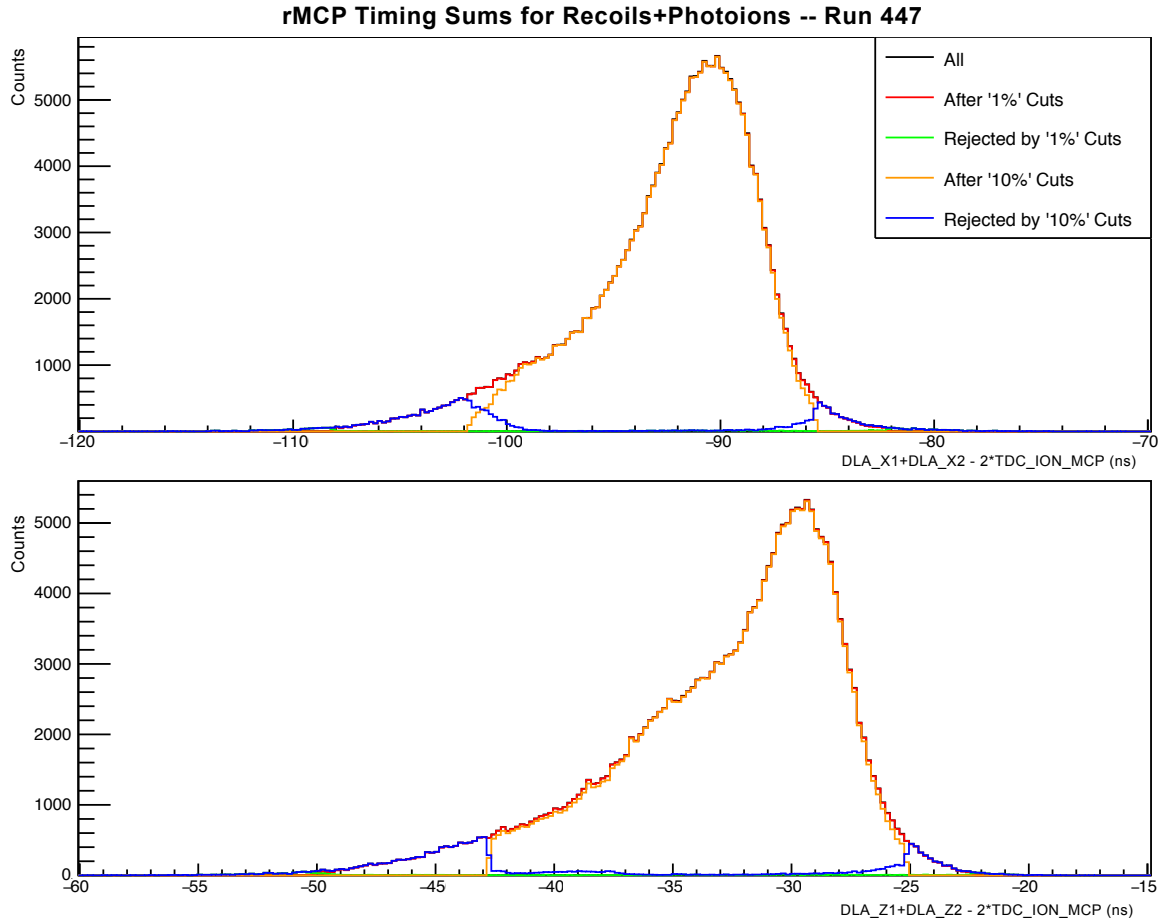
$$\text{DLA_XSUM} = (\text{TDC_DL_X1}) + (\text{TDC_DL_X2}) - 2(\text{TDC_ION_MCP}) \quad (3.1)$$

$$\text{DLA_ZSUM} = (\text{TDC_DL_Z1}) + (\text{TDC_DL_Z2}) - 2(\text{TDC_ION_MCP}). \quad (3.2)$$

OK, I have to *actually* discuss this a bit somewhere though.

For a perfectly operating detector, one would expect for a collection of many measurements of DLA_XSUM and DLA_ZSUM to each look like an isolated delta spike. In practice however, our distributions had a more complex set of features. The shapes, widths, and even positions of these distributions changed from run to run, and not all of these changes could be attributed to a known cause (e.g. a change in detector settings). Distributions from a single run are shown in Fig. 3.1.

Because the characteristics of these timing sum distributions varied from run to run, it didn't make sense to aggregate all the data before taking cuts, so any cuts had to be chosen on a run-by-run basis. Because of the asymmetry and occasional bimodality of the distributions, it also didn't make sense to try to fit the distributions to a function such as a gaussian and then cut away some number of sigma from the fit function. The algorithm that was used in the end was to determine the peak's maximum, then discard events from the portion of the distribution in which the distribution's height is less than 10% of the maximum. Fig. 3.2 shows the effect of



Are these things **definitely** in nanoseconds? Check!

Figure 3.1: Timing sums and associated cuts for the rMCP detector, run 447. The ‘10%’ cuts shown simply eliminate events in which the distribution’s height at that value is less than ‘10%’ of that distribution’s maximum, and the ‘1%’ cuts are performed in a similar manner. Note that this is *not* the equivalent of eliminating 10% (1%) of events. The above distributions each show the results within their own distribution after cuts are taken on the *other* distribution. Only a single run is shown here to avoid washing out features – because the characteristics of these spectra varied significantly over the course of the beamtime, and not all of the changes can be attributed to a change in settings.

these cuts on the measured cloud position within a single run.

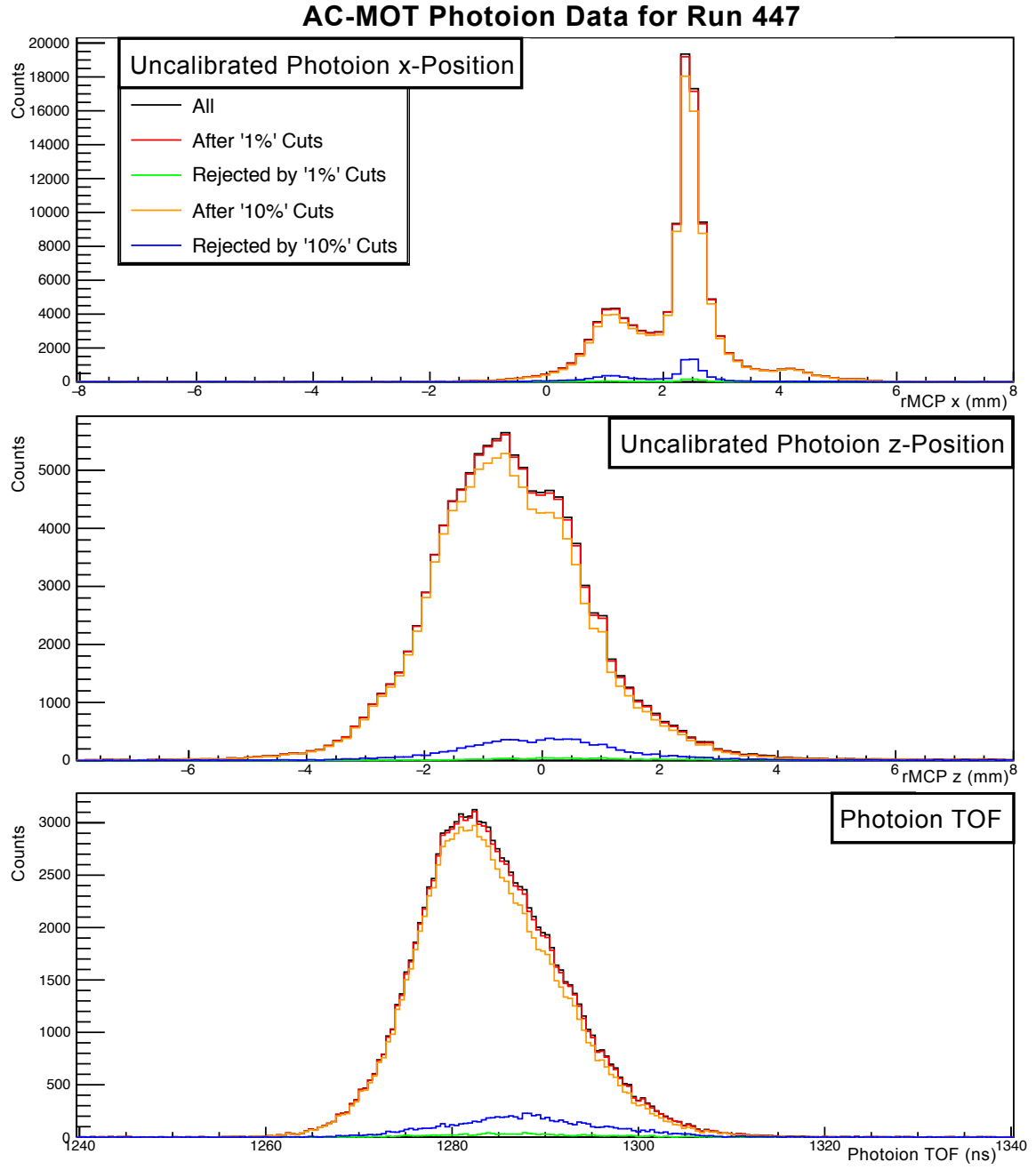


Figure 3.2: Cloud Position for run 447 for rMCP timing sum cuts as shown in Fig. 3.1.

3.3 Calibrations with the rMCP

A calibration mask was created for the rMCP, to eliminate any nonlinearities in the images produced. Several months before the ^{37}K beamtime was to occur, the

mask was attached in front of the rMCP, and a test of the delay lines' ability to produce an image was performed using an alpha source to illuminate the full surface of the detector. The mask was later removed in advance of the beamtime, in order to preserve the highest possible surface area, and calibrations were performed using the older mask data and subsequently applied to the online ^{37}K data.

I *think* we used an alpha source? Not sure what else we could have done, but I better check this!

The calibration to the offline data with a visible mask was performed over a number of steps. The data was given a preliminary rough calibration, performed on each delay line separately, which simply involved taking the difference in pulse arrival times between each end of the delay line, scaling the result by a factor chosen to get the image to be the approximate correct size, and then subtracting an offset to center the image.

With the preliminary calibration providing a visible image to work with, the '10%' cuts as described in Section 3.2 were applied, significantly sharpening the visual mask lines and overall image border. Next, a small rotation was applied, followed by a more precise centering algorithm. Following this, a linear stretching algorithm was applied to adjust the height and width of each row and column individually, while aligning the grid lines to their known position on the detector. Finally, an additional radial stretch was applied to only the outer areas of the image. This last adjustment can be justified by noting that it's expected for the outer parts of the detector to produce a more distorted image, and that appeared to be the case here. See Fig. 3.3.

When the online rMCP data was eventually collected, it was found that the rMCP image appeared offset by several centimeters relative to the previous calibration, which necessarily affected the location of the timing sum peaks (similar to those shown in Fig. 3.1). The most likely cause for this is a change in cable lengths between the readout and data acquisition in the months between the calibration and online data collection, but it meant a new set of '10%' cuts needed to be established for the online data, and also cast some doubt on the validity of the established calibrations. In the end, these cuts were established on a run-by-run basis due to the varying shape of the timing sum peaks.

Our ability to confidently accurately apply the old offline calibration to the new online data depended on our ability to center the image correctly, as different parts of the image are stretched and squeezed differently. The appearance of the plate edge—the only remaining indicator of the quality of the centering or overall calibration—changed shape slightly from run to run. Despite this, images from the online data

were all summed together after applying run-by-run cuts, and the resulting image was centered by eye.

The centering was performed iteratively, because the subsequent steps in the calibration will distort the image differently depending on how accurately it was centered beforehand. These subsequent steps in which the image is stretched and squished will also change the apparent centering of the overall image. Calibrated and uncalibrated images are shown in Fig. 3.3 for both offline and online data.

The lower plots in Fig. 3.3 show an unfortunate pattern of vertical stripes across the full surface of the rMCP. These stripes persisted over many (but not all) of the online runs. They can still be clearly seen in Fig. 3.4, which is a sum of all Runset RB's photoion events. The cause for these stripes could not be determined, and they could not be removed in post-processing analysis.

It is worth mentioning that the mask calibration data was collected without the presence of the magnetic fields involved in trapping and optical pumping, but these were of course present in the online data to which it was being compared. Since a magnetic field can change the trajectory of a charged particle, one might suspect that there could be some effect on the resulting image. There are two stages at which this might occur: while the ion is accelerating through the electric field within the experimental chamber before impacting the rMCP, and while the electron shower is emerging from the back of the MCP stack before it is incident on the delay lines. ... But also, I really don't want to get into this, otherwise somebody will ask me to quantify the size of the effect. Turns out: it's tiny, but it will be really annoying to demonstrate that.

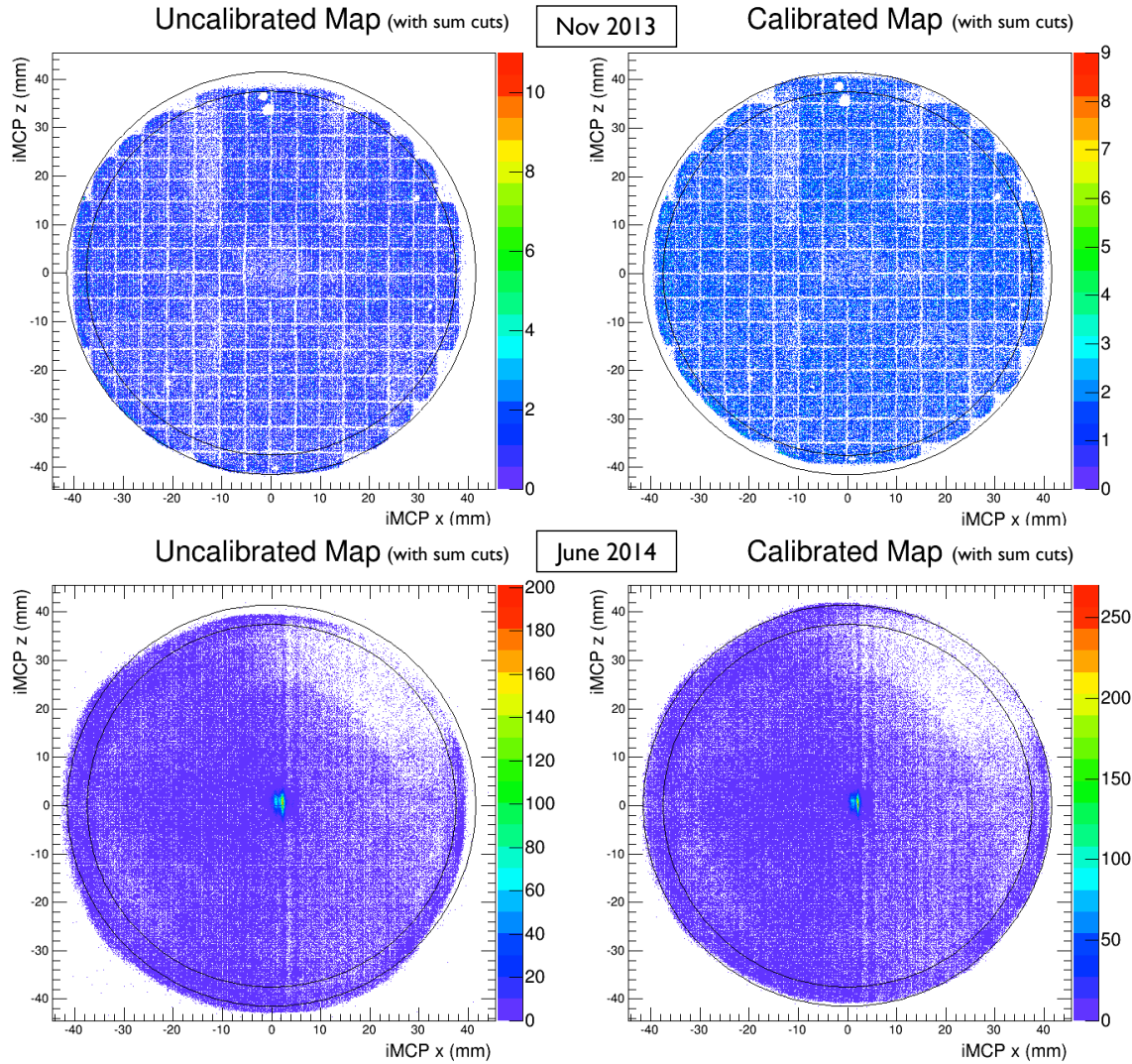
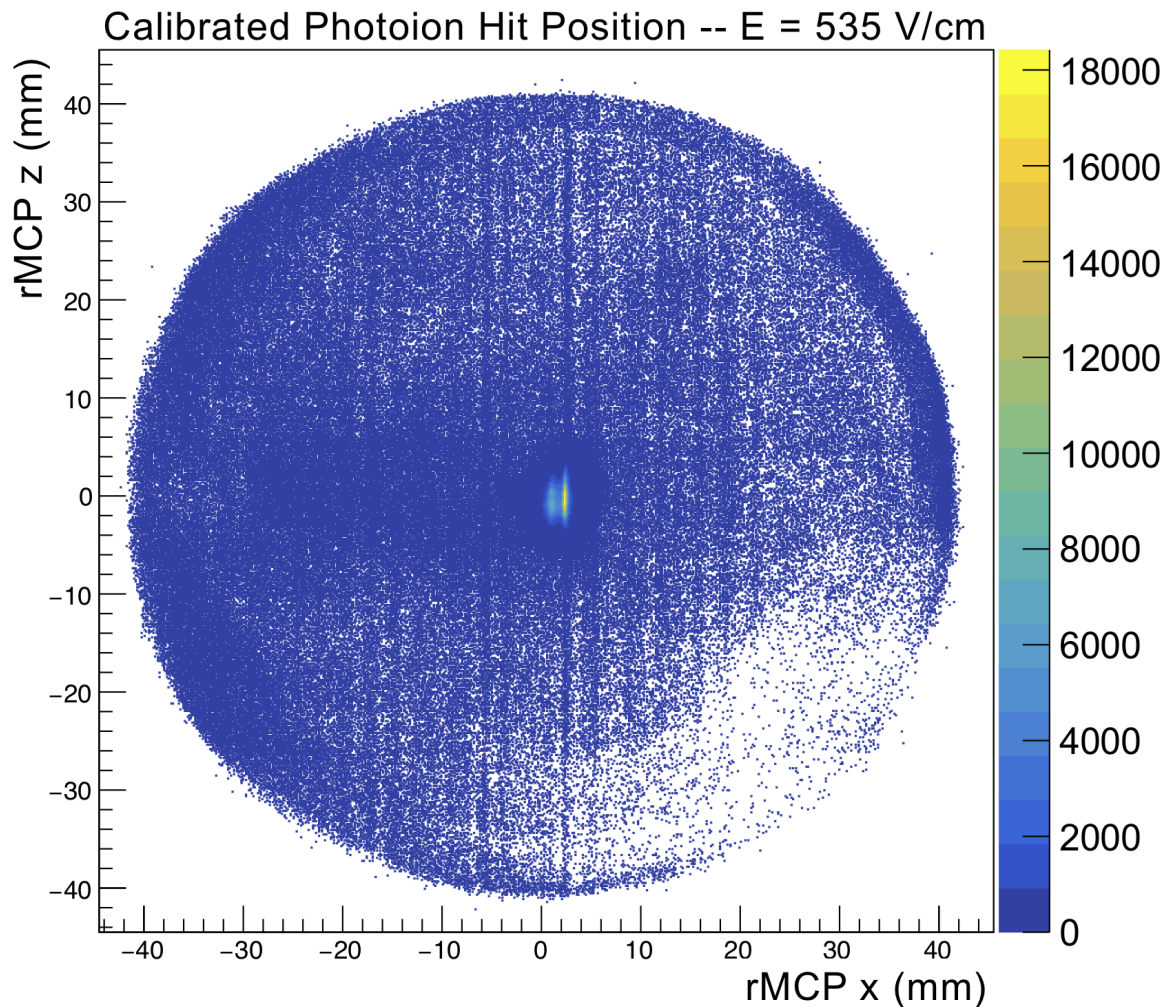


Figure 3.3: rMCP Calibration. The left images show the rMCP hit map with only a basic preliminary calibration; the images on the right are filled with the same hit data, but after the calibration has been performed. The upper two images are from data collected offline in advance of the 2014 beamtime using an alpha source; the shadow from a calibration mask is clearly visible. The lower images show rMCP data taken from a single online run, and includes both photoion and nuclear recoil data, collected over both the polarized and AC-MOT times. The photoion image of the atom cloud visible in the centre of the lower plots.



You know, I think this one is flipped relative to the previous image. Bleh. Probably this one is the correct one, but who wants to deal with that? Also did we switch MCP plates between calibration and the run? I think possibly we did! I'll have to ask the eLog.

Does this thing even have a TOF cut?

Figure 3.4: Photoion Hit Positions in 2D. This is the entirety of the good photoion data taken at 535 V/cm. The central bright spot is an image of the atom cloud arising from photoionization events of unpolarized atoms; the rest is background. Vertical stripes of indeterminate cause can be seen across the face of the image – it has not been possible to eliminate them in analysis.

3.4 Measurements of the Atom Cloud

With the rMCP detector calibrated (Section 3.3), several types of data may be extracted. It is possible to extract the hit positions and times-of-flight for the incident nuclear recoils, and an analysis of such data could be used to perform a test of right-handed currents within the nuclear weak force, as discussed in Chapter 6.4. However, we will focus here on what may be learned about the *atom cloud* from rMCP events in coincidence with the photoionization laser.

This class of data (events with both an rMCP hit and a photoionization laser hit in coincidence) can be used to measure cloud polarization, and the methodology and results of that process as it applies to this particular experiment are discussed in a recent publication [2]. We are also interested in the cloud’s position and size during the periods of time where decay data is collected, since this represents a potential systematic effect that must be accounted for within our models. The latter will be the primary focus of this section.

Also... does the camera data go in this section??

The first step in such a measurement is to try to eliminate as much background as possible. We have already required that every event considered here must include both an rMCP hit and a photoionization laser pulse. As we are interested in measurements of trap position, it makes sense to also require a *complete* set of position data recorded on the rMCP’s delay lines. This is further trimmed by a ‘10% cut’ on the timing sums, as described in Sec. 3.2. Any event including a scintillator hit is rejected, as these events have an increased likelihood for a recoiling ion to be detected on the rMCP instead of- or in addition to the photoion we expect (It is at this stage of the process that Fig. 3.4 is created.). Finally, some fairly loose cuts are applied about the central x- and z-positions, as well as the ion’s time of flight (measured with respect to the arrival of a photoionization laser pulse).

With these basic cuts performed, the cloud position and size must be measured. In particular, we are interested in measurements of the cloud *during the time when it is considered to be polarized* – however the great majority of photoionization events occur when the cloud is *not* polarized. We plot the projection of the cloud’s position on the x- and z-axes, and its TOF (indicative of position along the y-axis) as a function of ‘AC-MOT Time’ in Fig. 3.5.

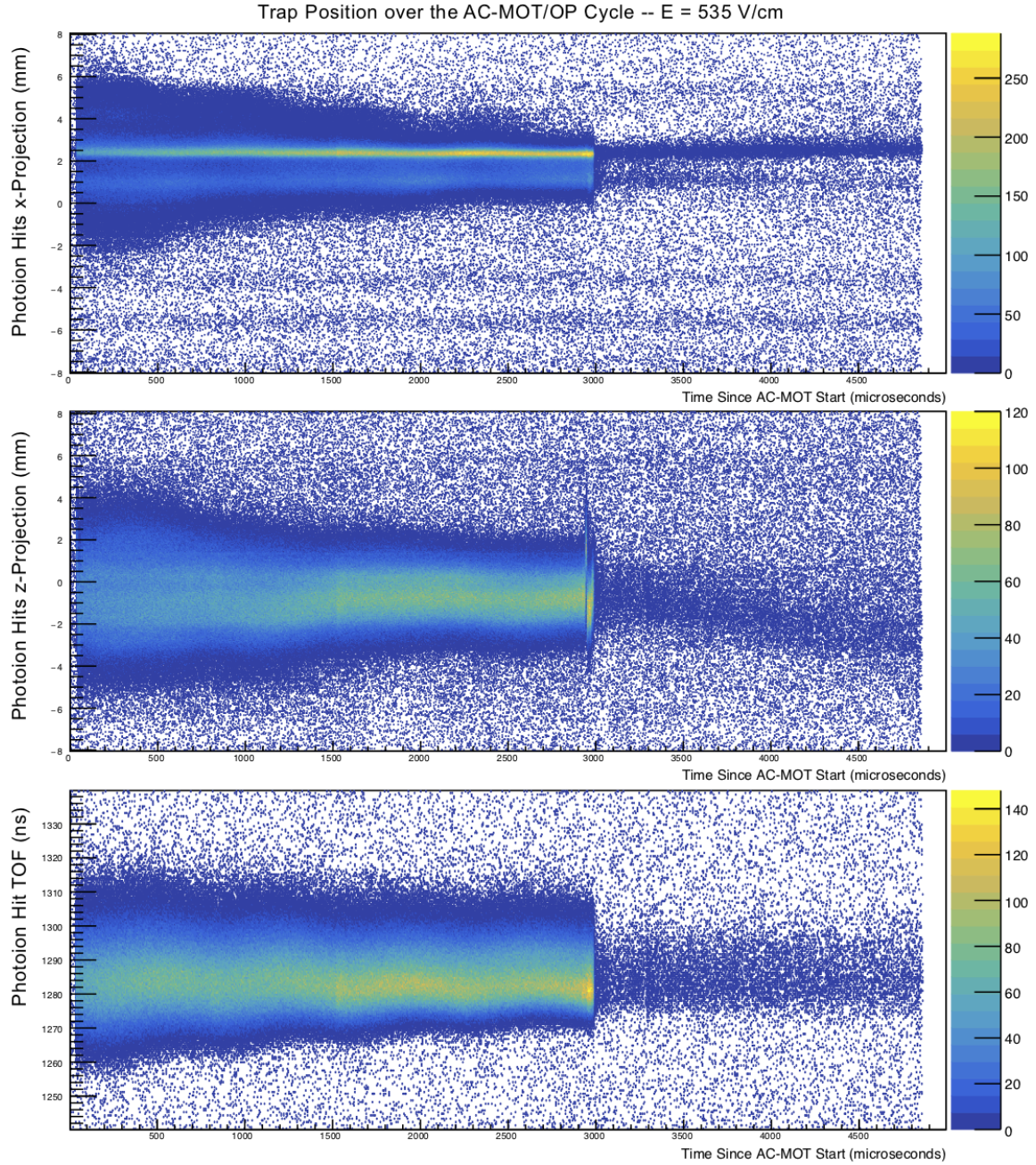


Figure 3.5: Projections of Photoion x- and z- Hit Positions and TOF at 535 V/cm, as a function of time since the start of the last AC-MOT cycle. The photoionization laser only acts on excited atomic states, which are readily available during the operation of the MOT. When the MOT is shut off, the atoms quickly de-excite. At the start of optical pumping 300 μ s later, there is a short burst of photoions due to the atoms being temporarily placed into an excited state as part of the optical pumping process. The photoion burst falls away rapidly as atoms are optically pumped into the stretched state and can no longer be excited by the optical pumping laser.

Trap position – Measured using the same dataset that was used to quantify the polarization. The trap drifts slightly over the course of our data collection. Describe the rMCP calibration needed to extract this info.

Runsets		Initial Position	Final Position	Initial Size	Final Size
EB \leftarrow RB	x	1.77 \pm 0.03	2.06 \pm 0.08	0.601 \pm 0.013	1.504 \pm 0.047
	y	-3.51 \pm 0.04	-3.33 \pm 0.05	1.009 \pm 0.013	1.551 \pm 0.018
	z	-0.661 \pm 0.005	-0.551 \pm 0.021	0.891 \pm 0.004	1.707 \pm 0.015
EC \leftarrow RD	x	2.22 \pm 0.05	2.33 \pm 0.11	1.18 \pm 0.04	1.538 \pm 0.087
	y	-3.68 \pm 0.04	-3.31 \pm 0.06	0.965 \pm 0.012	1.460 \pm 0.030
	z	-0.437 \pm 0.09	-0.346 \pm 0.037	0.927 \pm 0.007	1.797 \pm 0.026
ED \leftarrow RE	x	2.274 \pm 0.012	2.46 \pm 0.06	0.386 \pm 0.016	1.382 \pm 0.046
	y	-4.54 \pm 0.04	-4.28 \pm 0.04	0.986 \pm 0.08	1.502 \pm 0.013
	z	-0.587 \pm 0.04	-0.481 \pm 0.018	0.969 \pm 0.003	1.861 \pm 0.013

Sig figs here need work.

Parameters measured with the recoil runs, and applied on the appropriate electron runs.

Table 3.3: Cloud Positions and Sizes – Measured immediately before and immediately following the optical pumping phase of the trapping cycle. All entries are expressed in units of mm, and the “size” parameters describe the gaussian width.

Also, we noticed the trap drifting after one of the runs, because one of the batteries on one of the thingies adjusting the laser frequency (I think) was failing.

JB: “If we rejected the data with the MOT moving (indeed a battery determining the voltage controlled oscillator frequency offset between absorption in stable ^{41}K cell and the ^{37}K resonance) then that’s all you need to say.”

describe how you’d turn this into a physical description of the cloud, with like a temperature and a sail velocity and shit. with equations.

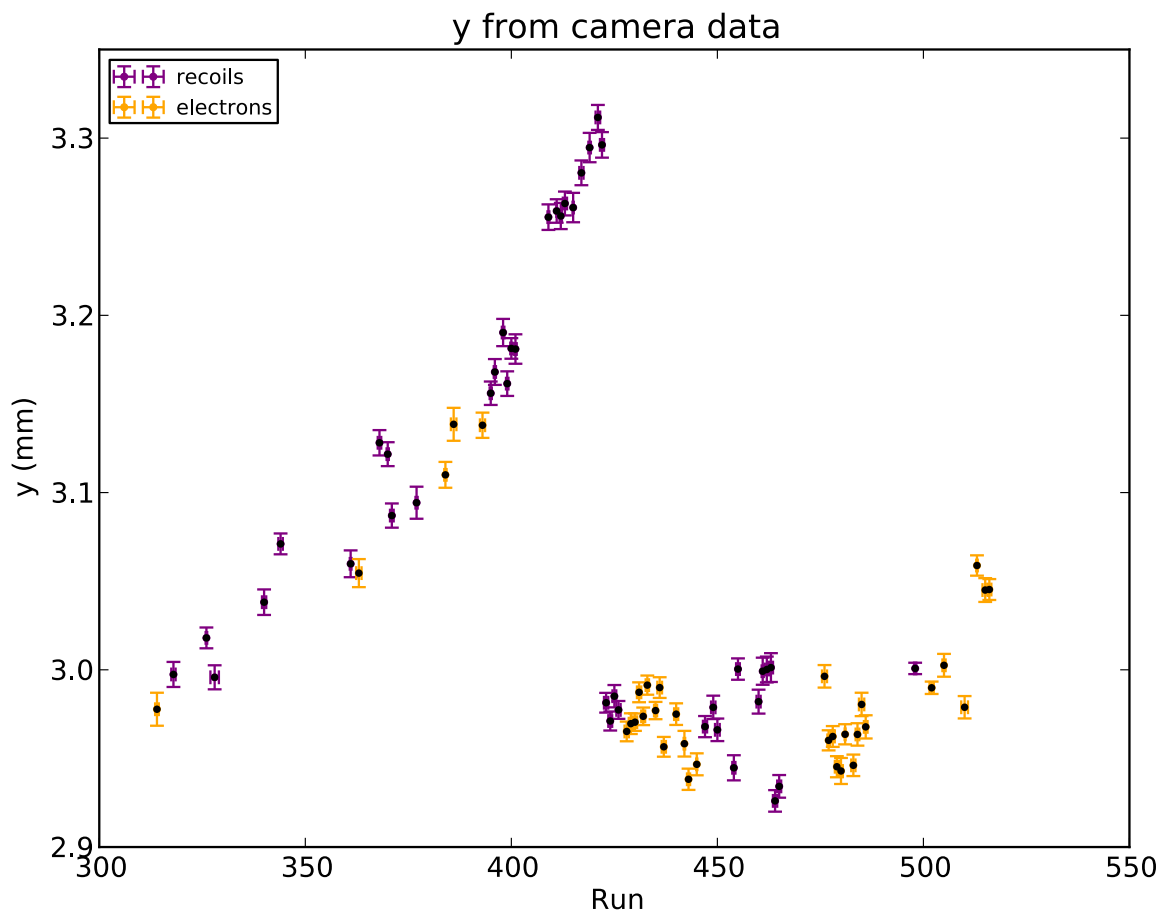


Figure 3.6: Trap Position along the “Time-of-Flight” Axis. Electron runs and recoil runs plotted by run number. (I should probably re-plot this. Maybe combine info with Fig. (3.7).)

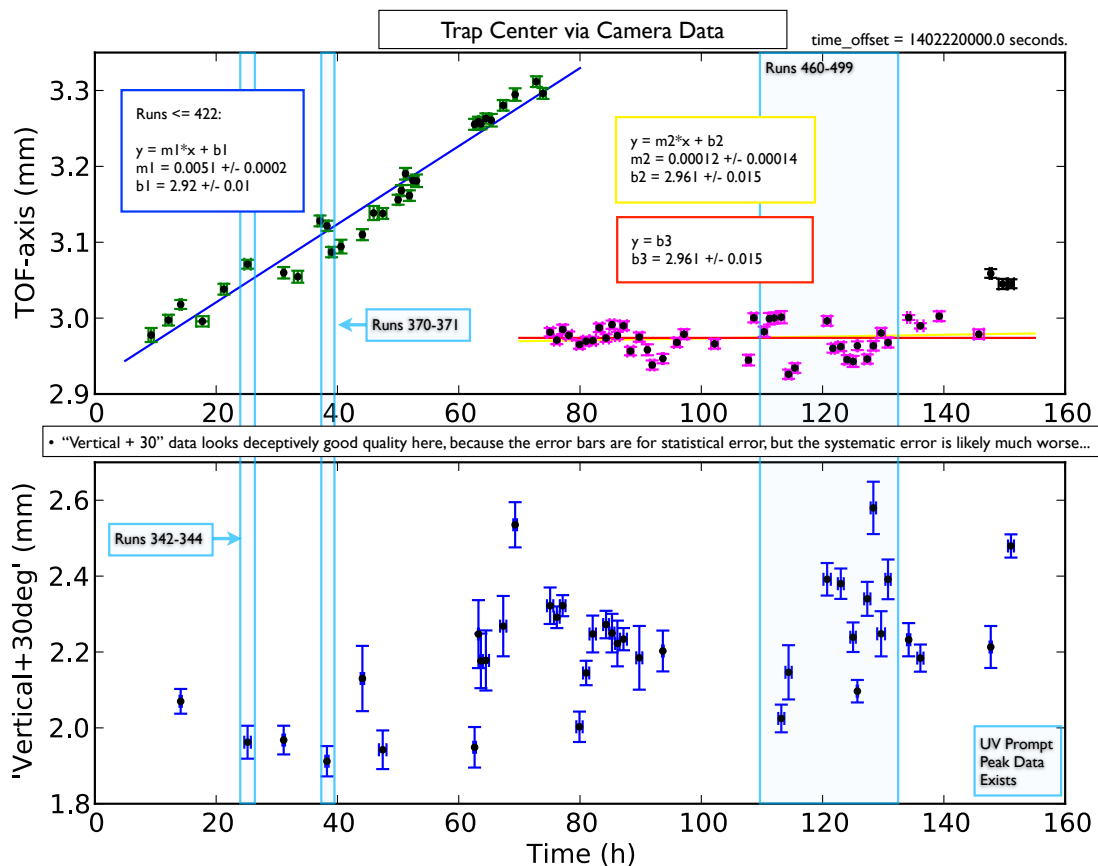


Figure 3.7: Trap Position along the “Time-of-Flight” Axis and the “Vertical+30” Axis. All runs plotted by time of run. (Need to re-plot this.)

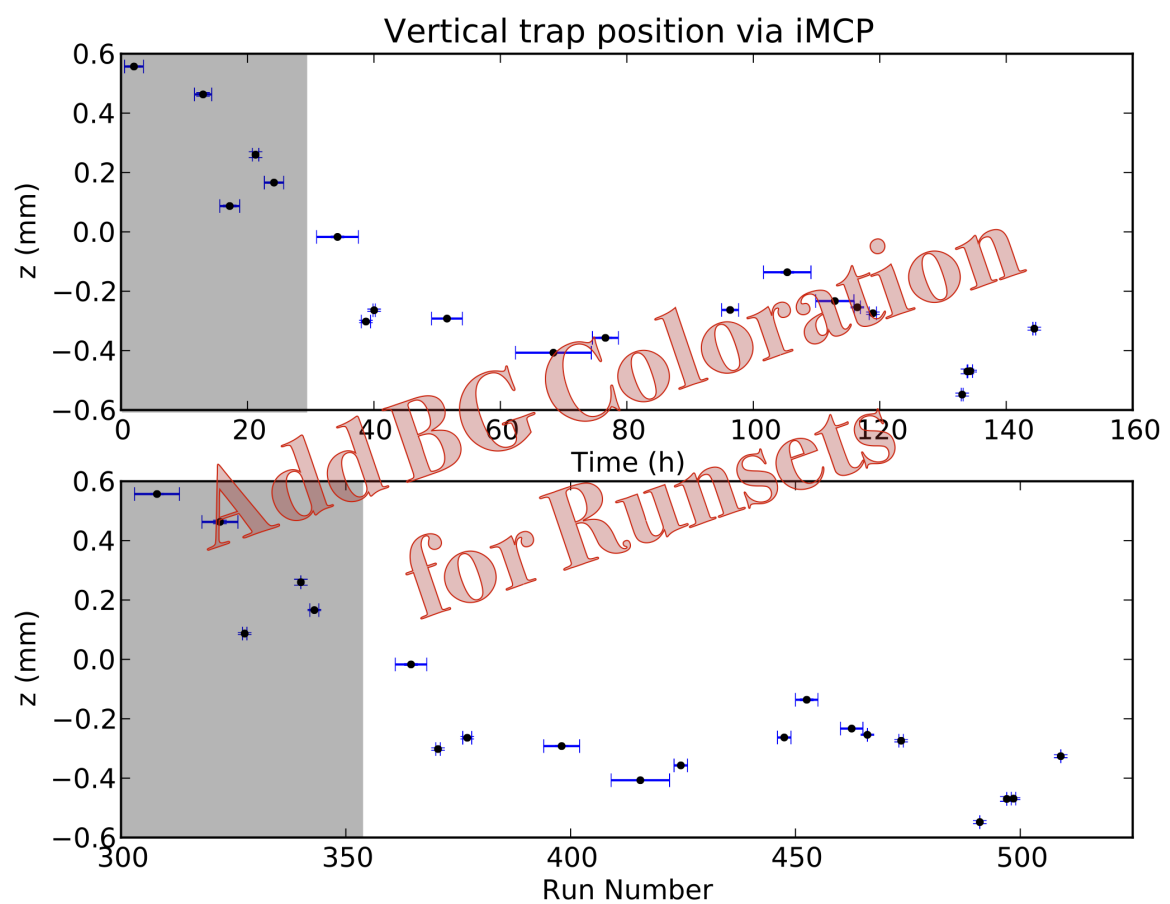


Figure 3.8: Trap Position along the Vertical Axis, plotted as a function of time of run (top) and run number (bottom).

3.5 Electron Run Data Selection and Preliminary Cuts

We now consider how to clean up our data. We make some fairly obvious, intuitive cuts, and those are described here. Later, we'll make less intuitively obvious cuts.

Before proceeding further, several basic cuts are performed on the data. For the Electron Runs which are to be processed directly into a physical measurement, we consider only events in which there was a recorded hit *both* on the eMCP *and* on exactly one of the scintillators. The required scintillator hit, of course, is potentially a beta, and so it is obvious why this must be present. Events in which both scintillators record a hit are discarded, as they fall into two categories: an accidental coincidence, where we are seeing two different decays that, by chance, both occurred within the time window allocated to a single event (a few μs before and after the first recorded scintillator hit), a backscatter event in which a beta was incident on one scintillator before being scattered out into the opposite scintillator. Although it would be possible to process the former event type into usable information if we could be certain that it was truly an accidental coincidence, contamination from the latter event type would serve to increase the systematic uncertainty arising from beta scattering—already a dominant source of error.

The eMCP is used primarily to record incident shake-off electrons. As described in Section 1.5, every beta decay event will produce one or more SOEs. Most (but not all) SOEs originating from the atom cloud will be incident on the eMCP, however not all incident SOEs on the eMCP will produce a recorded hit. The electric field is such that SOEs originating elsewhere within the chamber may or may not be incident on the eMCP. Therefore, while imposing an eMCP hit requirement will eliminate some ‘good’ events originating from the cloud, it also eliminates a much larger fraction of background events originating from other surfaces within the chamber. This ability to ‘tag’ good events originating in the cloud is absolutely essential to any analysis involving angular correlations within this geometry.

In later sections, we will consider how to evaluate a further cut to be imposed on the time difference between scintillator and eMCP hits (Section 3.7), and some subtleties within analysis relating to this choice (Sections 4.3 and 4.4).

It is also necessary to remove from direct consideration any event which is coincident with a pulse from the photoionization laser. When photoionization occurs within

Point at that other conclusion-ier section.

the atom cloud, an orbital electron is removed from the atom and will be accelerated by the electric field into the eMCP, just as a shake-off electron from a decay would be. If, by chance, this photoelectron arrives in coincidence with a scintillator hit, it would be interpreted as a decay event from the trap – unless we preemptively discard it.

Over the course of the runtime, there were several instances where we noted an apparent electrical discharge within the experimental chamber, producing enormous backgrounds for a short time. The detectors typically recovered quickly afterward, so it was neither necessary nor useful to stop an entire run to wait for the system to recover. Instead, the time when the discharge occurred was recorded, and events within approximately one minute of the spark time were discarded.

We use only the “fully polarized” events for which we have a detailed understanding of the nuclear polarization (described in more detail in [2]). This means we must use *only* events from the “optical pumping” portion of the duty cycle (see Fig. 2.4), and discard events when the DC- or AC-MOT is active. After the AC-MOT is shut off, there is a short delay before optical pumping begins (see Tables 3.1 and 3.2) to allow the magnetic field to decay, and it is only after $100\ \mu s$ of optical pumping that we consider the atoms to be fully polarized. Furthermore, because the magnetic field from the DC-MOT is slow to decay (relative to the field from the AC-MOT), all events from the first five AC/OP cycles after every atom transfer are discarded. A further benefit of our insistence on considering only polarized data is that the scintillators’ gains are more stable in the presence of only the (small, stable) magnetic field used for optical pumping than they are in the presence of a larger oscillating magnetic field used for trapping [24].

change by 0.2% of its value vs change by 0.5% of its value, according to Ben’s thesis pg 143.

Ben didn’t do the 5 cycle discarding thing in his Abeta analysis, but he *did* do it in his OP analysis.

Finally, because this analysis depends heavily on energy measurements from the two scintillators as a proxy for beta energy, it is necessary to remove events in which the pulser LED fired. Although the pulser LED is useful for evaluating the stability of the scintillators, in the case where an LED pulse occurs together with a true beta hit in the scintillator, it may change the measured energy. Therefore, we discard all events that include an LED pulse.

3.6 Further Cuts Using the DSSD

JB says: To repeat a comment, since the Appendix on analysis changes is being dispersed throughout, when you state somewhere (I think it's in Ch. 6)((5?)) make sure you state clearly that the only change for BB1 cuts is the radius cut, e.g. that you took the same T and E from the waveforms (I'm not even sure whether the waveforms are recorded anyway). You ask 'how can I state this' but there's no reason to be subtle. Just say upfront that Ben and Spencer's theses did all the groundwork on the BB1, and here you include selected details needed to understand the present analysis. If you need to include some redundant material, don't worry too much about that.

...

MJA: In fact, I think the BB1 radius may have been the same. The uniform energy threshold was different though. But I get the point.

...

Also, yes, the waveforms are absolutely recorded in the MIDAS files but they haven't been saved to modern ntuples, because they made the files huge. I think it's probably pretty easy to switch that on/off in the Analyzer though to generate a set of ntuples that has that info included.

Missing
figure

Show individual beta energy spectra. ...with a variety of different cuts, perhaps?

Although it was not possible to use the DSSD in real-time analysis or event triggering, the DSSDs may be used, after the data has been collected, to distinguish between different types of particles incident on the detector, as more energy will be deposited by heavier particles. When a scintillator hit is triggered by a particle originating within the experimental chamber, that particle will typically have passed through the DSSD before arriving at the scintillator.

In the present experiment, the two primary particles that will concern us are β^+ particles originating from the decay of ^{37}K , and γ rays, which may be produced through a variety of processes, e.g. directly from the 2% decay branch, through annihilation of β^+ particles upon their interaction with regular-matter electrons, or bremsstrahlung radiation from emitted β s.

We would like to look specifically at events involving β^+ particles arriving direct

from a decay within the atom cloud, and the DSSD may be used to eliminate events in which the scintillator is triggered by a γ . An incident β will typically deposit some portion of its energy in the DSSD as it passes through, however an incident γ will deposit significantly less energy; for this setup the energy deposited by a γ is generally indistinguishable from background on the DSSDs. Therefore, we require that a ‘good’ event must include a ‘good’ hit to the DSSD as well as a hit to the associated scintillator.

In order to proceed at this point, and because the DSSD readout records so much information, it is necessary to develop some criteria to determine whether or not we will accept any given DSSD readout as a β hit.

How do I *say* that Ben was the one who did most of the DSSD calibration stuff? I maybe don’t need to describe all of it here, but I *could*, and maybe it’s needed in order to understand like 4 rows in my error budget.

JB: “You can describe anything you did differently or improved, but you can and should otherwise defer all details of the scintillator calibration and DSSD calibration to Ben’s paper and his thesis and Spencer’s. E.g. Section 5.3 “statistical agreement between BB1 X and Y detectors’ energies only makes a small effect on results” does not need the technical details beyond that statement.”

JB: “If you have some way of documenting the coding you used, that would be great.” ... yeah, it would, wouldn’t it?

We read out the full waveform for every strip at each event with a scintillator hit, but in post-processing take *only* the ‘time’ and ‘energy’ from the peak waveform height and the time in the waveform at which that occurs. Each strip will have its own noise spectrum and energy calibration. To classify an event as a good DSSD hit, we require at least one ‘x’ strip and one ‘y’ strip record an energy above the noise threshold. We require that the x strip and the y strip agree (to within some number of standard deviations) in amount of energy deposited, and in the time at which that hit occurred. In order to avoid problems resulting from the strips’ non-uniform noise thresholds, we further require that the energy deposited be greater than some lower-end cutoff which is selected so as to be higher than every individual strip’s noise threshold. In this case, the DSSD’s lower energy uniform threshold was set at 50 keV.

I think Ben might have selected 60 keV? That’s maybe something for the appendix.

We also elect to use only events where a beta hit the DSSD within a 15.5 mm radius of the center of the detector, so as to avoid scattering effects from the collimator walls.

Did I even mention the collimator? Like, in the previous chapter or something..?

Also-also (did I mention it already?) look for events with only *one* DSSD hit (two could indicate the beta scattered back out of the detector in another pixel, or alternately an accidental coincidence of two beta decay events. either way, no good for analysis.) Also, only one scint hit, and it has to be the on the same detector with the DSSD. (...A scintillator hit as indicated by a TDC readout, as well as a max. recorded scint energy for the “extra” scintillator at something stupidly tiny, like 10 keV. Probably *actually* 10 keV.)

After all other cuts – not before!! – we eventually use only events with scint energy between 400 - 4800 keV. High cutoff is because of the low number of events, which makes the observable—the superratio asymmetry—poorly defined and poorly behaved. Low cutoff is because it’s really hard to model what’s going on down there to the required level of precision. The observable depends most heavily on low beta energy events, so it is imperative that the lower energy portion of the spectra be thoroughly understood if they are to be used for analysis.

Somewhere I should list what the energy cutoff is for this spectrum. Or semi-equivalently, the Q-value.

3.7 Timing Improvements with the Leading Edge and Scintillator Walk Correction

MJA: I can describe the eMCP calibration here, even though it mostly wasn’t implemented by me. It is tangentially relevant to data selection and background estimation by providing an experimental energy spectrum for shake-off electrons. It’s actually a pretty neat algorithm that I basically wasn’t involved with.

...

JB: eMCP. You need to describe the timing information obtained. You also need a statement of whether or not you used the position information in your cuts.

...

MJA: Wait. So have I done that yet in this section?

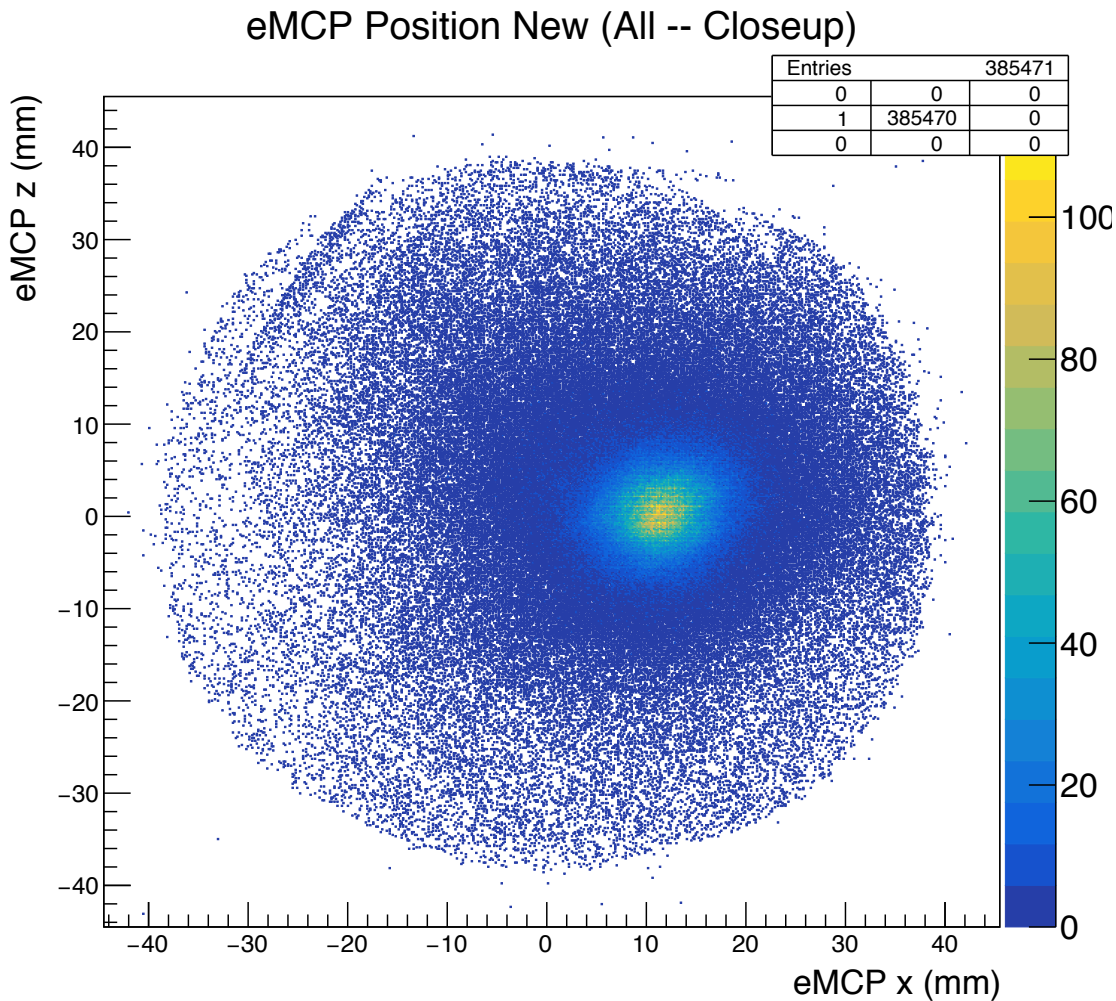
I described the HEX-75 somewhere in a previous chapter, right??

I dislike how this section is organized.. should discuss the cut we *didn’t* make at the end.

The eMCP features a set of three delay lines, intended to be used to record the position of a hit, as in Fig. 3.9. Though only two delay lines is sufficient to determine the position within the plane of the MCP if they are both hit, the presence of a third delay line allows for some redundancy. In practice, however, a large fraction of otherwise ‘good’ events include a hit on the eMCP, but have insufficient information recorded on the delay line channels to reconstruct a position.

Because a SOE from the trap is most likely to land in the centre of the plate, while

Do I need to describe MCPs and delay lines somewhere? Maybe not...



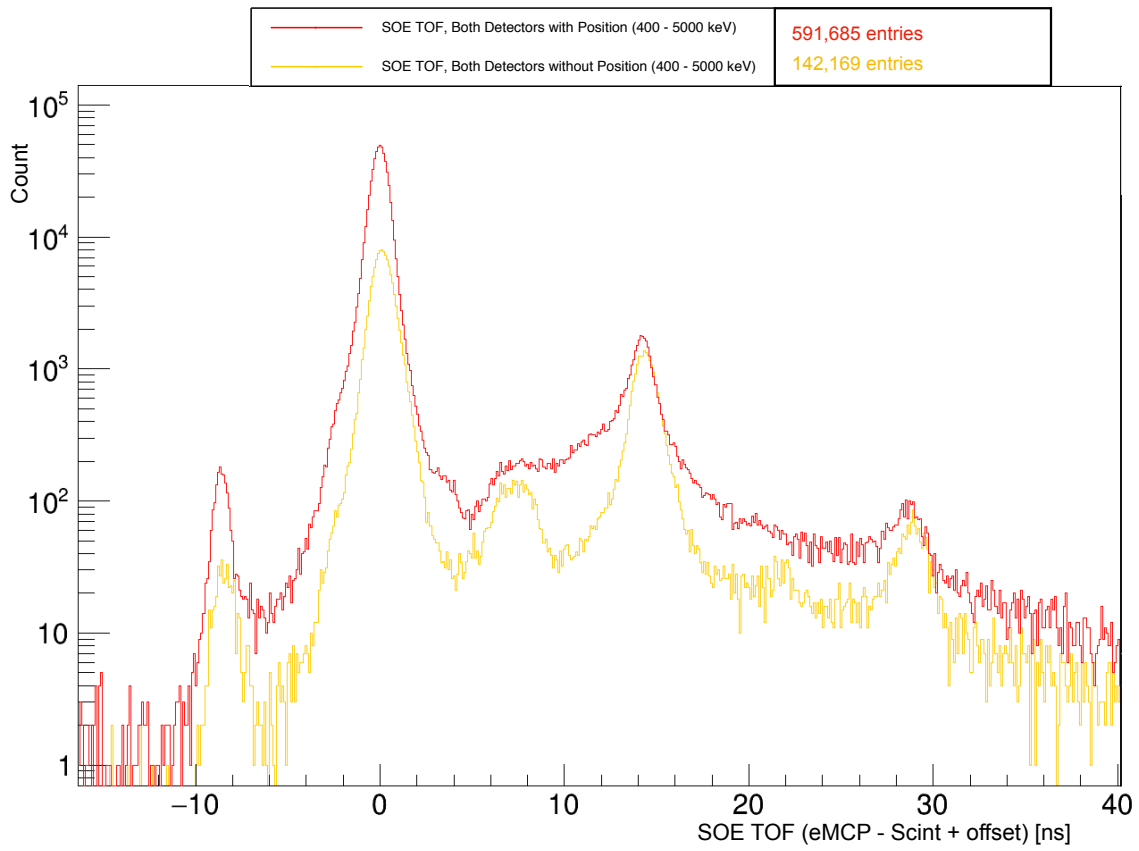
This pic is probably better used in an SOE section somewhere.

Figure 3.9: Position as measured on the eMCP, after some data cleaning.

the background from other sources is roughly constant across the plate, it might make sense to accept only events where the eMCP hit is within some radius of the central peak. This methodology was seriously considered because the remaining data has a much lower fraction of background events polluting it – however this results in a loss of around half of the events even for the most generous eMCP radius cuts (see Fig. 3.10). Therefore, it was decided that no position cuts on the eMCP would be made in the final analysis.

Wait, what?

Several years after the data was initially collected, a problem was discovered with



Um. Did I for sure get the labels correct on this??? It seems really wrong.

Surely this thing goes somewhere else instead.

Figure 3.10: Beta-electron TOF, for events with and without eMCP hit position information. A cut will eventually be taken to accept only events sufficiently near the largest peak – in this case the number of events is ‘only’ decreased by a factor of 2.

our low-level analyzer software, which we had been using to convert large and unwieldy MIDAS data sets into somewhat smaller and more manageable ROOT data sets. In particular, for every timestamp recorded, our raw MIDAS data actually included both a timestamp for the leading edge (LE) of the pulse, and a timestamp for the trailing edge (TE). The analyzer had—for years—been reporting the timestamp associated with the trailing edge of the pulse. Initially it was unclear if there might have been a reason behind this choice, but a closer examination of the data showed that the LE data included less timing jitter and noise, as well as a sharper peak for timing pulses across the board (as in Fig. 3.11), with some channels showing a larger effect than

others. This was corrected, and the entirety of this analysis has been performed now using the cleaner LE spectra.

The LE spectra allows for us to use a more precise model of the SOE TOFs, so that's nice.

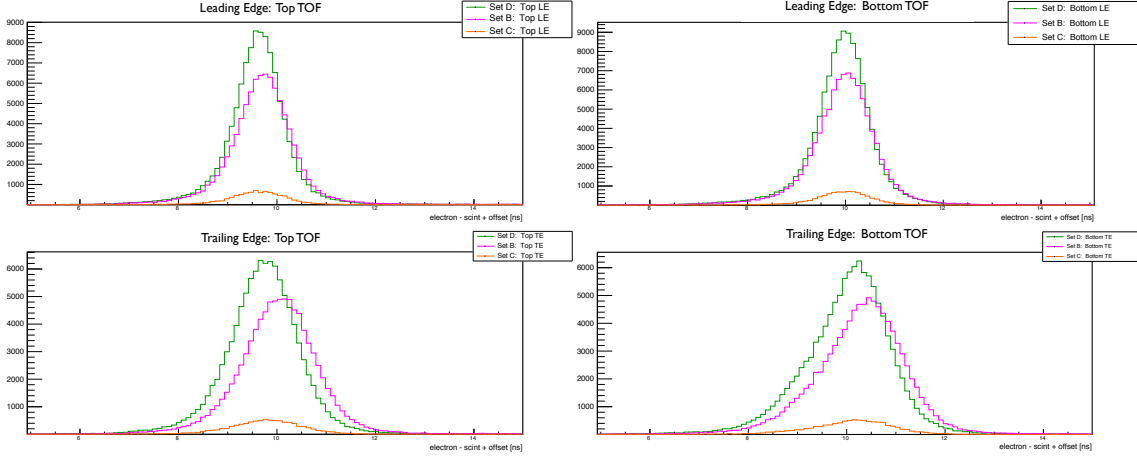


Figure 3.11: SOE TOF peaks (eMPC - Scintillator), using the leading edge (LE) and using the trailing edge (TE). Data is sorted according to runset. For each individual runset, the TE peak is broader than the LE peak. The centroid of each runset is also more variable in the TE plots.

The place where this change between the TE and LE timestamps had the biggest impact on the analysis is in the shake-off electron time-of-flight spectra, on which a cut must eventually be taken. Although this problem was not discovered in time to be used in the previous measurement of A_β using this same data [22], it likely would have had a negligible effect on the final result, because the SOE TOF cut that was used there was comparatively loose, and the evaluation of the background that remained was not a dominant systematic effect.

With the data reprocessed using the leading edge for timestamps, I wanted to eliminate as much background as possible from the SOE TOF spectrum. With this goal in mind, the next step was to correct the scintillator timing for its low energy ‘walk’ (see Fig. 3.12). A quartic polynomial was fit to each of the 2D timing vs energy spectra (the top and bottom detectors were treated separately), and the result was used to produce a ‘straightened’ SOE TOF spectrum with respect to measured scintillator energy, and as expected, the resulting SOE TOF spectrum was a bit more sharply peaked.

With the SOE TOF spectra cleaned up, a cut can be taken to reduce the fraction

This goes in that one appendix, if I haven't already put it there.
...Also, is this even fucking true?!?

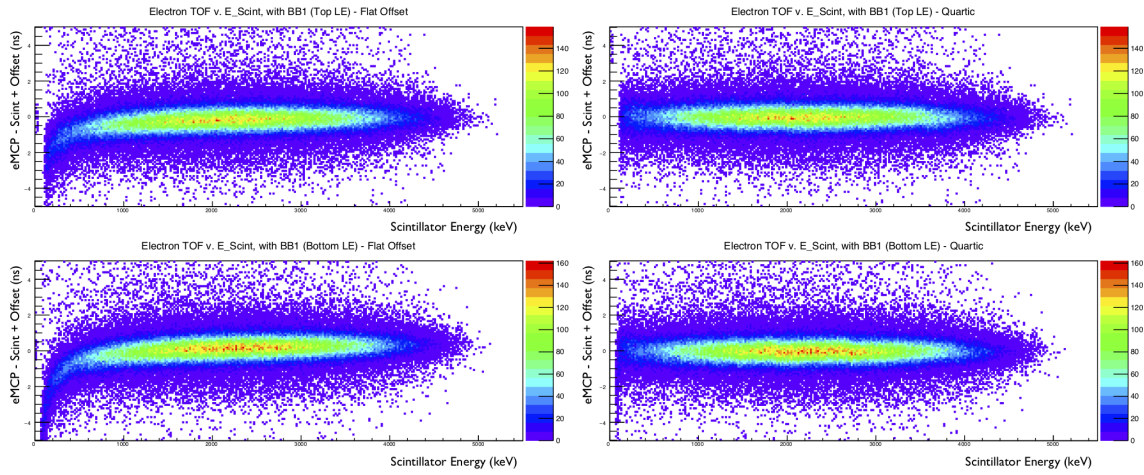


Figure 3.12: SOE TOF walk, before (left) and after (right) applying a quartic adjustment to straighten out the effective TOF.

of background events. Informed by the model of background spectra described in Section 4.4, a was made to include only a 2.344 ns window around the primary peak in further analysis . (see Fig. 4.13).

Probably need to put that figure somewhere else.

“...removing X fraction of the remaining events.”

“To check the agreement of the model with reality, we compare the averaged superratio asymmetries from both, as in Fig. 4.14.” probably goes in the other section.

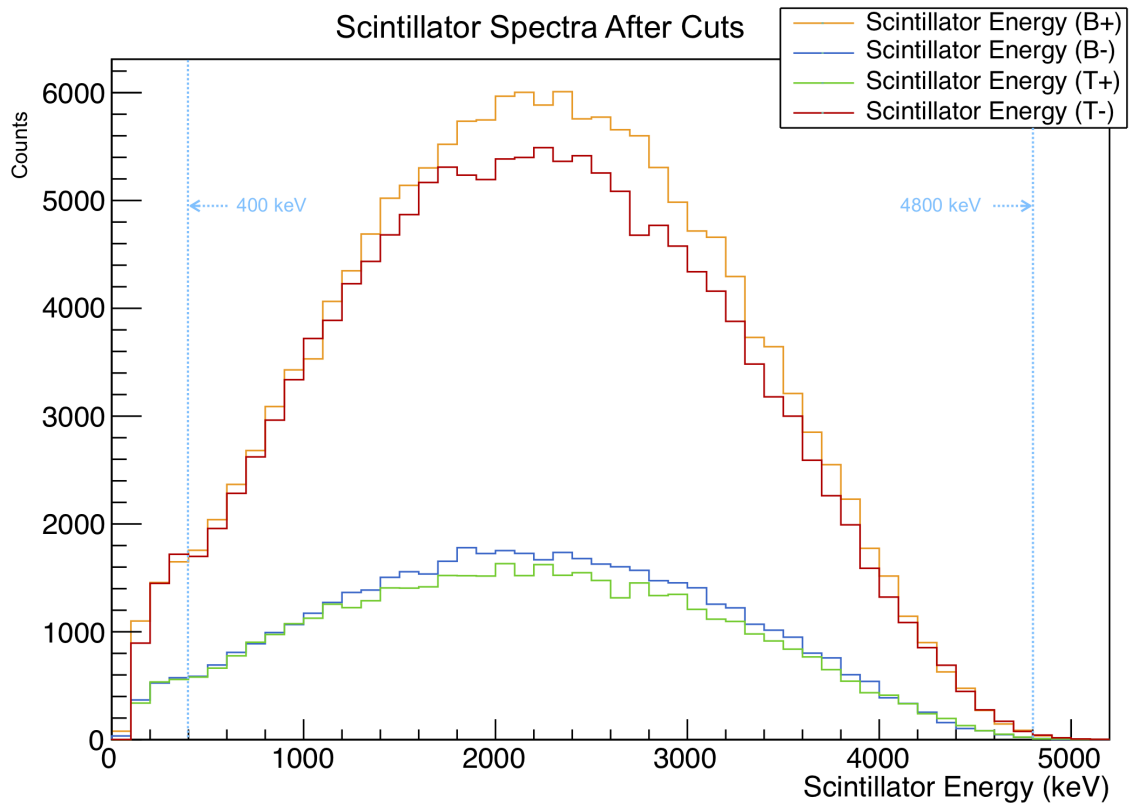
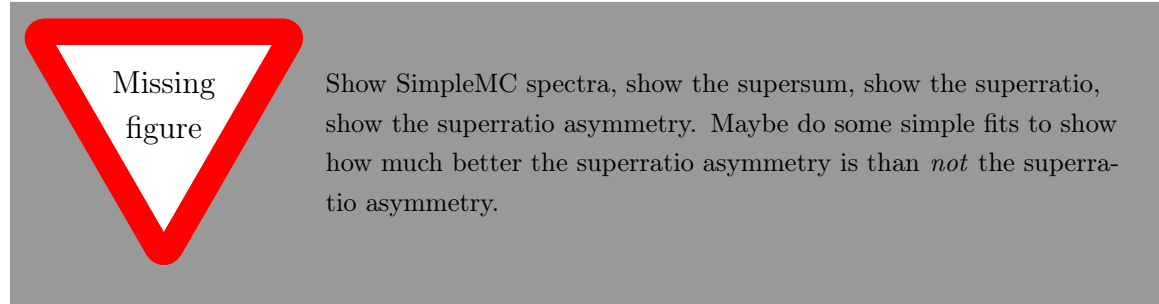


Figure 3.13: Experimental Scintillator Spectra, for both detectors in both polarization states. These spectra are what remain after all cuts have been taken. All runsets are included.

Chapter 4

Simulations



The TRINAT collaboration has created a Geant4 (G4) simulation which models the geometry and materials within the experimental chamber, and uses a monte carlo algorithm to describe generalized physical processes such as particle scattering and energy loss, within the geometry specific to the experiment. This software library has been maintained and updated over several generations of graduate students [24] [25].

add comment about how you need G4 to do scattering/backscattering. I think I wrote a blurb like this *somewhere* already....

4.1 Considerations for Software Upgrade Implementation

Prior to the simulations required for this particular experiment, two different sets of changes to the G4 code were needed – the first to enable multithreading, and the second to introduce certain BSM interactions to the decay distribution.

Enabling multithreading allows for a single instance of the Geant4 simulation to run on several processors at once, effectively speeding up the overall simulation by a factor of the number of processors used. In the years since the simulation was originally created, the Geant4 collaboration had created libraries intended specifically to support multithread usage, and since the running G4 simulations had historically been very time consuming for the TRINAT collaboration, the decision was made to implement multithreading within our own monte carlo software, on the hopes that this would enable faster progress in analysis.

Enabling multithreading support turned out to be quite time consuming, and in the end it might have been faster to have spent those months running simulations one processor at a time. Perhaps the improvement will prove valuable for use in future TRINAT experiments.

The TRINAT G4 monte carlo package had never been used to directly model interactions beyond the standard model within the decay physics. It had previously been set up by the collaboration to use a probability density function (PDF) including most of the terms from Holstein's Eq. (51) [17], which describes both electron and neutrino momenta from polarized beta decay. This treatment is quite robust, and includes corrections at recoil-order, as well as certain other corrections of similar size.

Unfortunately, terms arising from interactions beyond the standard model are not included in Holstein's description of the decay process. To understand the kinematic results of the exotic interactions of interest to us here, we turn to the classic JTW treatment of beta decay [6] [16]. In addition to the (expected) vector and axial interactions, JTW also describes the interaction in terms of (exotic) scalar and tensor interactions, should such be present.

Furthermore, although it is currently understood that the weak interaction is predominantly or perhaps entirely ‘left-handed’, the JTW treatment leaves certain phase angles unfixed, and is therefore able to accurately describe a decay which is, for example, partially ‘right-handed’ – however the latter feature is not directly relevant to the project at hand. [It’s several phase angles in JTW, but maybe it’s fundamentally only like one angle on some level? Also I think it’s not actually a “gauge freedom,” per se. No, I’m pretty sure this ‘phase angle’ description is all wrong.] Also, consider time reversal! Anyway, most of this paragraph probably goes better in Section 1.3.

because for A_β even a BSM interaction will *basically* look like a SM interaction, and I think something somewhere isn't precise enough to distinguish it.

which other corrections? coulomb and/or radiative corrections, but somehow when I say that, I'm apparently talking about a different thing than everyone else who uses those terms. also, weak magnetism. also ... ???

Is this true? Does it not include *any* BSM interactions?

Despite JTW’s broad ability to describe beta decay under a variety of physical models, this treatment includes only the leading-order terms, and smaller terms, such as recoil-order corrections, are neglected entirely.

Surely I describe what recoil-order corrections even *are* in some appendix somewhere, right?
Or, possibly, in Section 1.3. Possibly the paragraphs above need to be moved...

Because the present project is a precision measurement of the Fierz interference, a term which arises from scalar and tensor couplings, it was imperative to create an event generator for our G4 simulations that could account for these exotic interactions while also including in its PDF the higher-order effects which, in some cases, can mimic the effects of a scalar or tensor current.

While it might have been possible to directly combine JTW’s result with Holstein’s Eq. (51), it should be noted that JTW’s expression is not compatible in general with the principle of conservation of momentum; as recoil momentum is neglected entirely, the description is only of two leptons emerging from a nucleus in directions that do not directly oppose one another. Therefore, the prospect of combining these two slightly incompatible expressions directly might be enough to give one pause. On an experimental level, the mathematical description of an emerging neutrino is only of interest to us to the extent we can reconstruct it based on detecting both a beta and the recoiling nucleus from a single decay event, and within the present experiment we do not have simultaneous access to both a beta detector and a recoil detector.

In light of the above considerations, it was decided that an entirely new event generator must be created, based instead on Holstein’s Eq. (52), in which neutrino momentum has been integrated over and is therefore no longer an explicit part of the PDF [17]. As one might guess, Holstein’s Eq. (52) is greatly simplified in comparison to Holstein’s Eq. (51). A similar integration over all possible neutrino momenta can also be performed on the JTW PDF, causing several terms to vanish. The result in both the Holstein and JTW cases is a PDF over only beta energy and direction as measured with respect to nuclear polarization, and the two expressions can be combined in a straightforward manner by comparing similar terms.

It is this combined Holstein+JTW expression that forms the basis of the new G4 event generator. It must be noted that although the largest effect from any present scalar or tensor interactions would likely (depending on certain phase angles) be in a non-zero value of b_{Fierz} , these interactions can also introduce a perturbation to A_β at a higher order. In order for any precision experimental measurement of b_{Fierz} to be generalized to limits on the parameter space of scalar and tensor currents, it is important to incorporate an accurate representation of the results of such exotic

interactions on *all* available observables, and the new G4 event generator does this.

Things that the G4 simulation did that I kept include: an accurate representation of the complex details of our experimental geometry. Also, the noise spectra on the DSSDs.

4.2 The Simple Monte Carlo and Response Function

Scattering (both forward scattering and backscattering) is an important effect to consider within this experiment, and it must be evaluated through extensive and time consuming monte carlo simulations – in this case, using Geant4. However, there are a number of other systematic uncertainties that must also be evaluated, and it is computationally prohibitive (even after multithreading support was implemented) to evaluate all of them via the same sort of high statistics, scattering included, full monte carlo that we use for scattering effects. Luckily, the systematic effects arising from scattering are largely decoupled from other effects, and this section describes the framework that has been implemented in order to evaluate certain other systematic effects separately.

To this end, a fast-running Simple Monte Carlo (SMC) was developed together with an empirical “response function” similar to the one described by Clifford et al [26] to describe probabilistic beta energy loss before its detection in a scintillator. In the end, the lineshape description became quite involved, and it is unclear whether, in the end, any time was saved this way.

The purpose of the SMC was to *quickly* generate initial particle kinematics probabilistically for beta decay events, and it uses the very same event generator based on Holstein’s Eq. (52) [17] that was developed for use with the more sophisticated Geant4 simulations. However, unlike in a G4 simulation, the SMC makes no attempt to track particles through the chamber, and instead simply calculates detector hits based on initial particle momentum. This procedure obviously neglects scattering effects, which can (in differing regimes) both *increase* and *decrease* the number of beta particles incident on a detector. Furthermore, this procedure also neglects any energy absorption in materials through which the beta passes before hitting a scintillator – and the beta *must* pass through several such materials (see Fig. 2.6).

Reference previous
section where I discuss
this, maybe?

To make the best use of the SMC for evaluating systematic errors, the energy lost before a beta hits a scintillator must be accounted for somehow in order to ensure all relevant physical effects are propagated through. In particular, before hit-

ting a scintillator, a beta must pass through a $275\ \mu m$ thick silicon carbide mirror, a $229\ \mu m$ thick beryllium foil, and finally a set of $300\ \mu m$ thick double-sided silicon strip detectors (DSSDs), before finally having its remaining energy absorbed within a scintillator. Although the DSSDs are themselves detectors with the ability to record the amount of energy deposited by an incident particle, there are some known problems in achieving a uniform level of precision across the full surface of the DSSDs, so adding the DSSD energy back to the scintillator energy to produce a better estimate of the original beta energy has the potential to create some problems for the analysis. Furthermore, given the presence of the mirror, an object with a similar thickness and scattering properties to the DSSDs, re-adding the energy lost in the DSSDs would not eliminate the need to estimate probabilistic energy loss in similar materials.

See: Some other section? Maybe?

In order to create a quantitative description of the effective response function, which varies with initial beta energy, an analytic function of 14 parameters has been created to model scintillator output for decays from the central cloud for each of the two polarization states in use. In other words, although the form of the model is always the same, the 14 individual parameters will take different values for each of the four detector and polarization combinations. The full response function model is given by the expression,

Is it definitely 14 of them?

$$R(E_0, \text{Detector}, \text{Polarization}) = p_{\text{norm}} (f_{\text{moyal}} + f_1 + f_2 + f_3 + f_4 + f_5) + f_{511}, \quad (4.1)$$

where p_{norm} is one parameter, and the other terms within the expression are themselves functions of multiple parameters and are given by,

$$\begin{aligned} f_{\text{moyal}} &= (1 - p_{\text{gfrac}}) \left(1 + \frac{-p_\alpha - p_\beta}{|E_0|} - \frac{p_\Delta}{p_\gamma p_W} - p_\gamma p_W \right) \\ &\times \left(\frac{e^{\left(\frac{x - (E_0 - \frac{1}{2}p_{\text{dE}0})}{p_{\text{lres}} |E_0 - \frac{1}{2}p_{\text{dE}0}|} \right)} e^{\left(-\frac{1}{2} e^{\left(\frac{x - (E_0 - \frac{1}{2}p_{\text{dE}0})}{p_{\text{lres}} |E_0 - \frac{1}{2}p_{\text{dE}0}|} \right)} \right)}}}{\sqrt{2\pi p_{\text{lres}} |E_0 - \frac{1}{2}p_{\text{dE}0}|}} \right), \quad (4.2) \end{aligned}$$

Obviously, from a physical standpoint, the initial beta energy E_0 must be positive, but the response function still includes several expressions of the form, $|E_0|$. This is not done by accident, but rather is an intentional adjustment used to encourage the parameters to behave well within a fit.

$$f_1 = p_{\text{gfrac}} \left(1 + \frac{-p_\alpha - p_\beta}{|E_0|} - \frac{p_\Delta}{p_\gamma p_W} - p_\gamma p_W \right) \left(\frac{e^{\left(-\frac{(x - (E_0 + \frac{1}{2} p_{\text{dE0}}))^2}{2 p_{\text{toeres}} |E_0 + \frac{1}{2} p_{\text{dE0}}|} \right)}}{\sqrt{2\pi p_{\text{toeres}} |E_0 + \frac{1}{2} p_{\text{dE0}}|}} \right), \quad (4.3)$$

$$f_2 = \frac{p_\alpha}{|E_0|} \left(\frac{1 - \text{Erf} \left[\frac{(x - |E_0|)}{\sqrt{2 p_{\text{toeres}} |E_0|}} \right]}{2 |E_0|} \right), \quad (4.4)$$

In these response functions, $x = ?$

$$f_3 = \frac{p_\beta}{|E_0|} \left(\frac{e^{\frac{p_k * (x - E_0)}{|E_0|}} * e^{\frac{p_{\text{toeres}} p_k^2}{2|E_0|}}}{2(1 - e^{-p_k})} \right) \left(1 - \text{Erf} \left[\frac{(x - E_0 + p_{\text{toeres}} p_k)}{\sqrt{2 p_{\text{toeres}} |E_0|}} \right] \right), \quad (4.5)$$

$$f_4 = \frac{p_\gamma}{2} \left(\text{Erf} \left[\frac{x - E_0}{\sqrt{(2 p_{\text{toeres}} |E_0|)}} \right] - \text{Erf} \left[\frac{x - E_0 - p_W}{\sqrt{2 p_{\text{toeres}} |E_0 + p_W|}} \right] \right), \quad (4.6)$$

To evaluate $\text{Erf} []$ for parameter fits, root's built-in function was used. Root also includes a built-in Landau function, but it makes everything very slow if we use it.

$$\begin{aligned}
f_5 = & \frac{p_\Delta}{2 p_\gamma p_W^3} \left[(x - E_0) \left(\operatorname{Erf} \left[\frac{(x - E_0)}{\sqrt{2 p_{\text{toeres}} |E_0|}} \right] - 2 \operatorname{Erf} \left[\frac{(x - E_0 - p_W)}{\sqrt{2 p_{\text{toeres}} |E_0 + p_W|}} \right] \right. \right. \\
& + \operatorname{Erf} \left[\frac{(x - E_0 - 2p_W)}{\sqrt{2 p_{\text{toeres}} |E_0 + 2p_W|}} \right] \Big) + (2 p_W) \left(\operatorname{Erf} \left[\frac{(x - E_0 - p_W)}{\sqrt{2 p_{\text{toeres}} |E_0 + p_W|}} \right] \right. \\
& \left. \left. - \operatorname{Erf} \left[\frac{(x - E_0 - 2p_W)}{\sqrt{2 p_{\text{toeres}} |E_0 + 2p_W|}} \right] \right) + (2 p_{\text{toeres}} |E_0|) \left(\left(\frac{e^{\left(\frac{-(x-E_0)^2}{(4 p_{\text{toeres}} |E_0|)} \right)}}{\sqrt{2\pi p_{\text{toeres}} |E_0|}} \right) \right. \\
& \left. + \left(\frac{-2e^{\left(\frac{-(x-E_0-p_W)^2}{(4 p_{\text{toeres}} |E_0+p_W|)} \right)}}{(\sqrt{2\pi p_{\text{toeres}} |E_0 + p_W|})} \right) + \left(\frac{e^{\left(\frac{-(x-E_0-2p_W)^2}{(4 p_{\text{toeres}} |E_0+2p_W|)} \right)}}{\sqrt{2\pi p_{\text{toeres}} |E_0 + 2p_W|}} \right) \right) \right], \quad (4.7)
\end{aligned}$$

and

$$\begin{aligned}
f_{511} = & |p_{\text{scale}}| \left[\left(\frac{195}{17} \sqrt{\frac{2}{\pi}} e^{\left(\frac{-(x-308)^2}{578} \right)} \right) + \left(40 + \frac{(x-210)^2}{900} \right) \left(1 - \operatorname{Erf} \left[\frac{x-334}{30} \right] \right) \right. \\
& \left. + \left(\frac{(x-505)^2}{1440} \right) \left(1 - \operatorname{Erf} \left[\frac{x-505}{30} \right] \right) \left(1 + \operatorname{Erf} \left[\frac{x-334}{30} \right] \right) \right], \quad (4.8)
\end{aligned}$$

where a p with any subscript is taken to be a variable parameter that must be evaluated. The expressions f_1 , f_2 , f_3 , f_4 , and f_5 are motivated by or taken directly from expressions of the same name within Clifford's description, and the individual parameters p_α , p_β , p_γ , p_Δ , p_W , and p_k are closely related to their counterparts of similar name [26]. The expressions f_{moyal} and f_{511} represent a departure from the published treatment, however, and arise from physical behaviours within this experiment which are not described within Clifford's treatment.

In particular, f_{511} is a rather inelegant representation of the annihilation radiation compton edge within our geometry. Although the DSSD provides an effective veto for the overwhelming majority of these events—and indeed within Clifford's treatment this veto is treated as being perfect in its discernment—it is clear both from experimental spectra and the Geant4 simulations intended to represent them that there exist a small number of such events within our scintillator spectra that cannot be vetoed in this manner. These events must be understood and adequately accounted for.

It should be noted that no attempt is made to derive the expression for f_{511} from first principles; the expression was chosen only because of its visual similarity to the spectrum's fit residuals before its inclusion. This expression's contribution to the overall function is negligible at all but the lowest initial beta energies (Eq. 4.8's p_{scale} parameter, showing the absolute normalization of f_{511} , is plotted in the top right of Fig. 4.7.), and is always negligible at scintillator energies above ~ 500 keV, as can be seen in Fig. 4.5. We note that within the final analysis, all scintillator spectra will be given a low energy cutoff at 400 keV, so the only the higher energy tail of f_{511} will make any contribution.

The expression f_{moyal} arises from the beta particles' energy loss within materials (i.e. the mirror, the beryllium foil, and the DSSD itself, as in Fig. 2.7) before its eventual absorption within the scintillator. Although Clifford's treatment does include a ΔE detector (our DSSD would be the equivalent), the energy absorbed in this detector is added back in to the total before Clifford's final spectra are modeled. Although it would be possible to do something similar with our DSSD spectra, we would still be left with the problem of accounting for the similarly-shaped energy loss within the mirror and foil.

The distribution for energy deposition within a thin material by an energetic charged particle, first described by Lev Landau in 1944 [27], is now known as a Landau distribution. This distribution has a variety of properties that make it challenging to work with – notably its mean, variance, and all higher moments are undefined, and the distribution itself cannot be written in closed form. Its primary redeeming mathematical feature, however, is the fact that the convolution of a Landau distribution with another Landau distribution is, itself, a Landau distribution, and this means that we can represent the sum total of energy absorption within three successive thin materials as a single Landau distribution.

Within the present context, an expression for energy absorption that can be evaluated and re-evaluated quickly by computer with adjusted parameters is needed, as this must be used within a fit function. To this end, we employ a so-called 'Moyal function', which was developed in 1955 to be used as a closed form approximation to the Landau distribution [28]. Indeed, Eq. 4.2 is little more than a Moyal function.

...as previously mentioned, re-introducing the energy from the BB1s invites problems with maintaining a uniform energy threshold over the entire detector.

Also, I think for this particular part of analysis, the cutoff was like 600 keV.

Some of this content needs to go somewhere else.

We never attempt to do this, because reasons. Don't I talk about this somewhere?

somewhere I have to talk about the empirical noise spectrum etc. on the BB1s. Or maybe I've already mentioned it somewhere.

The values of these parameters are allowed to vary with initial beta energy, and must be determined empirically by a series of fits to simulated spectra. To effect this result, the TRINAT Geant4 simulation is used to generate a series of ‘mono-energetic’ spectra. That is, for each energy value under consideration (with discrete values selected to span the energy range of betas in our decay), events are generated in which every outgoing beta initially has the same amount of kinetic energy, and the angular distribution of these betas is physically appropriate for the polarization and beta energy under consideration. These mono-energetic betas are propagated through the experimental geometry via Geant4, and the resulting scintillator spectra are recorded. Each polarization state must be considered separately, but spectra for both detectors are generated simultaneously, as it is necessary to generate events into a full 4π steradians in order to fully account for betas scattered into- or away from the detectors. Cuts identical to those imposed on the experimental data are applied (see Chapter 3). Several such spectra are shown for the Bottom Detector in the ‘-’ polarization state, with their best fit response functions, components thereof, and residuals of the fit, in Figs. 4.1, 4.2, 4.3, 4.4, and 4.5.

The values of the individual parameters contributing to the fit functions in, eg, Figs. 4.1, 4.2, 4.3, 4.4, and 4.5 are allowed to vary with initial beta energy, and the energy dependence of each parameter must be modeled in order to extrapolate the shape of the response function to intermediate initial beta kinetic energy values that are not explicitly modeled. For each parameter, the energy dependence is modeled by an analytic function selected to have similar characteristics. Each of these analytic functions is itself a function of several parameters which can be adjusted to optimize its fit to the true best-fit energy dependence of the parameter it models. Because some parameters are only weakly independent, it is necessary to perform these fits iteratively on only a single parameter at a time, revisiting earlier parameter fits after fixing other parameters to updated models. The results of this process are shown in Figs. 4.6, 4.7, 4.8, and 4.9.

It is useful to consider how well this empirical response function works to model the spectra. One can see clearly from Figs. 4.1, 4.2, 4.3, 4.4, and 4.5 that the fit residuals appear noticeably *worse* at lower initial beta energies. Fig. 4.10 shows the reduced χ^2

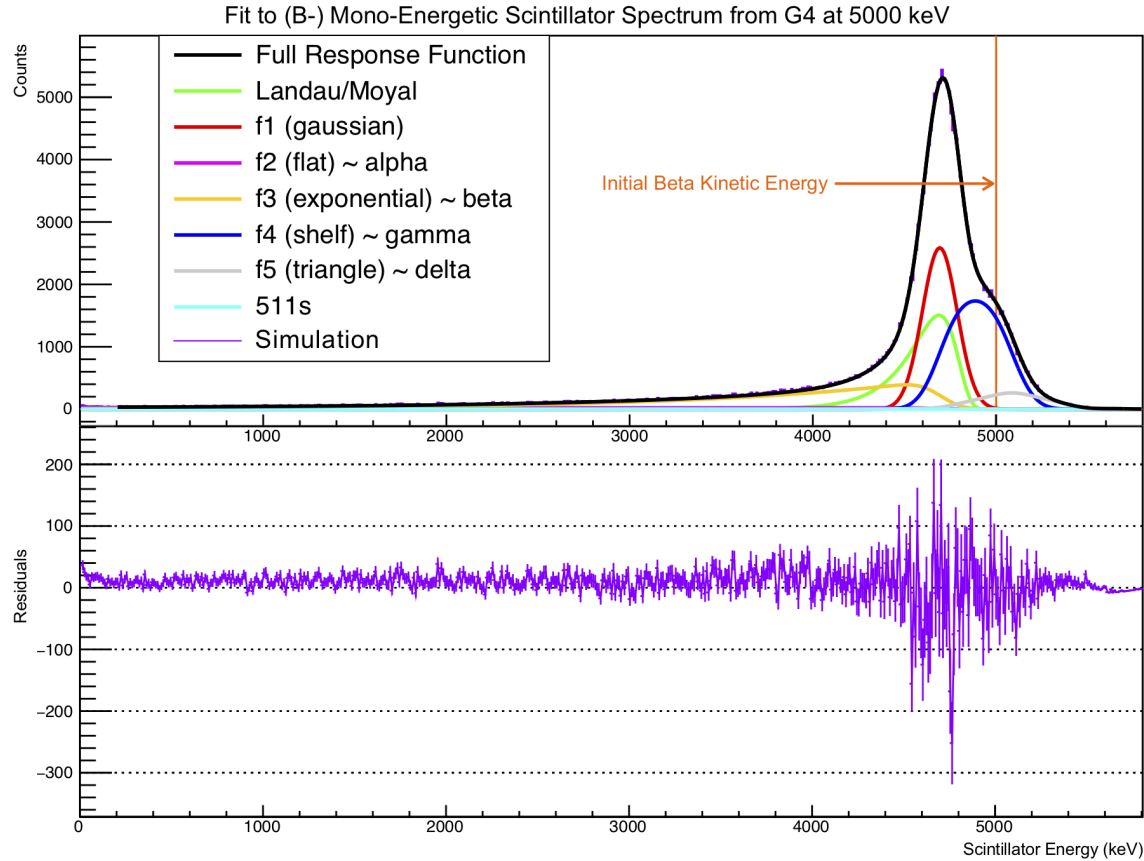


Figure 4.1: Fit to Mono-Energetic Spectrum, 5000 keV (B-)

values arising from comparing mono-energetic G4 spectra to the empirical response functions described above, for all four detector and polarization combinations.

With the energy dependence for each of the response function's parameters carefully modeled, it becomes possible to make proper use of the full response function. Given a decay event with a known beta energy from a nucleus with its initial polarization known, we can now predict a probabilistic response from *both* scintillator detectors. Obviously, for a single decay event, the full spectrum cannot be realized – however in aggregate the modeled response function agrees well with results from the full Geant4 simulation, particularly at higher beta energies.

Needs a picture of the *full* beta energy distributions that come out of the lineshape thing. To compare with (a) data and (b) G4. Probably a superratio in there somewhere too.

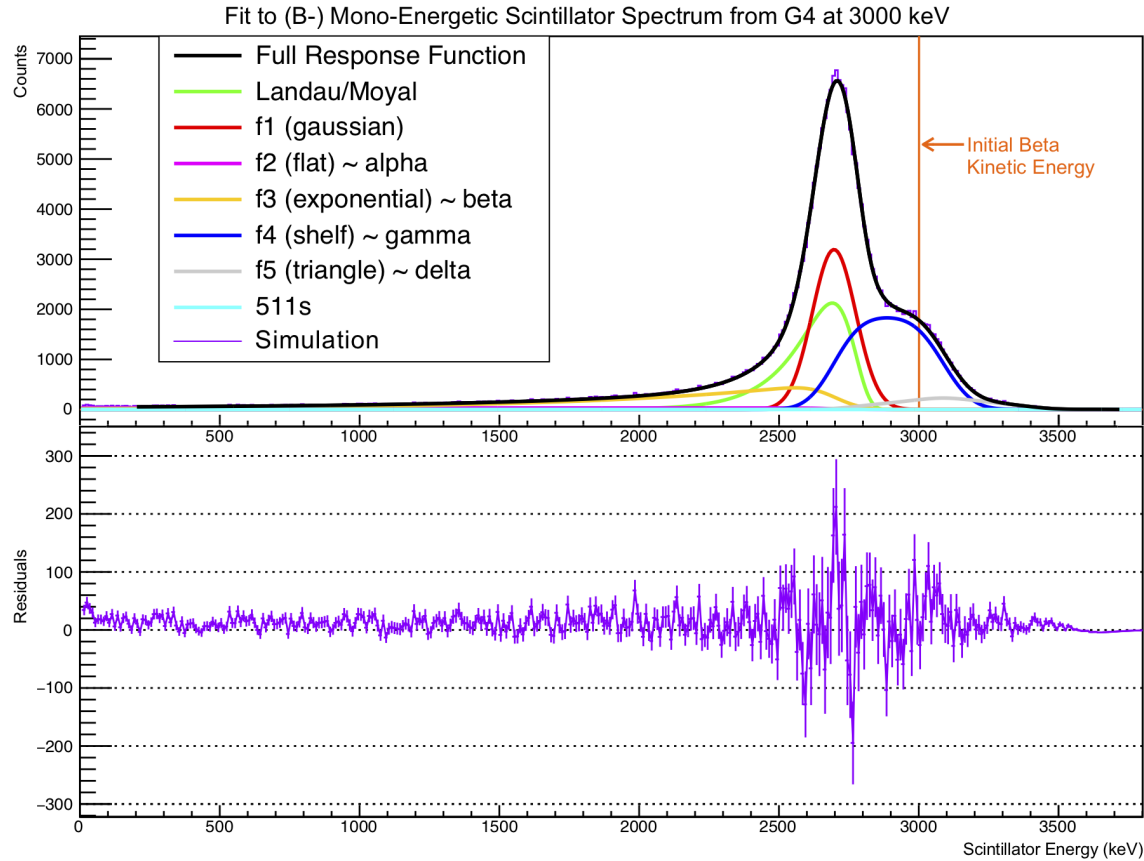


Figure 4.2: Fit to Mono-Energetic Spectrum, 3000 keV (B-)

Um. Which of the scattering things did I actually put in at the end? And when did I do it?
 Like, how did I account for (back-)scattering? I tried with/without scattering, I think? and eventually decided not to do it. for some reason. I think it breaks normalization in some way that's more subtle than you would think.

...

Do I need the angular distribution in the end? I think maybe I put in scattering later, and just used a cone for the first round. I re-did this to do the opposite thing at some point.

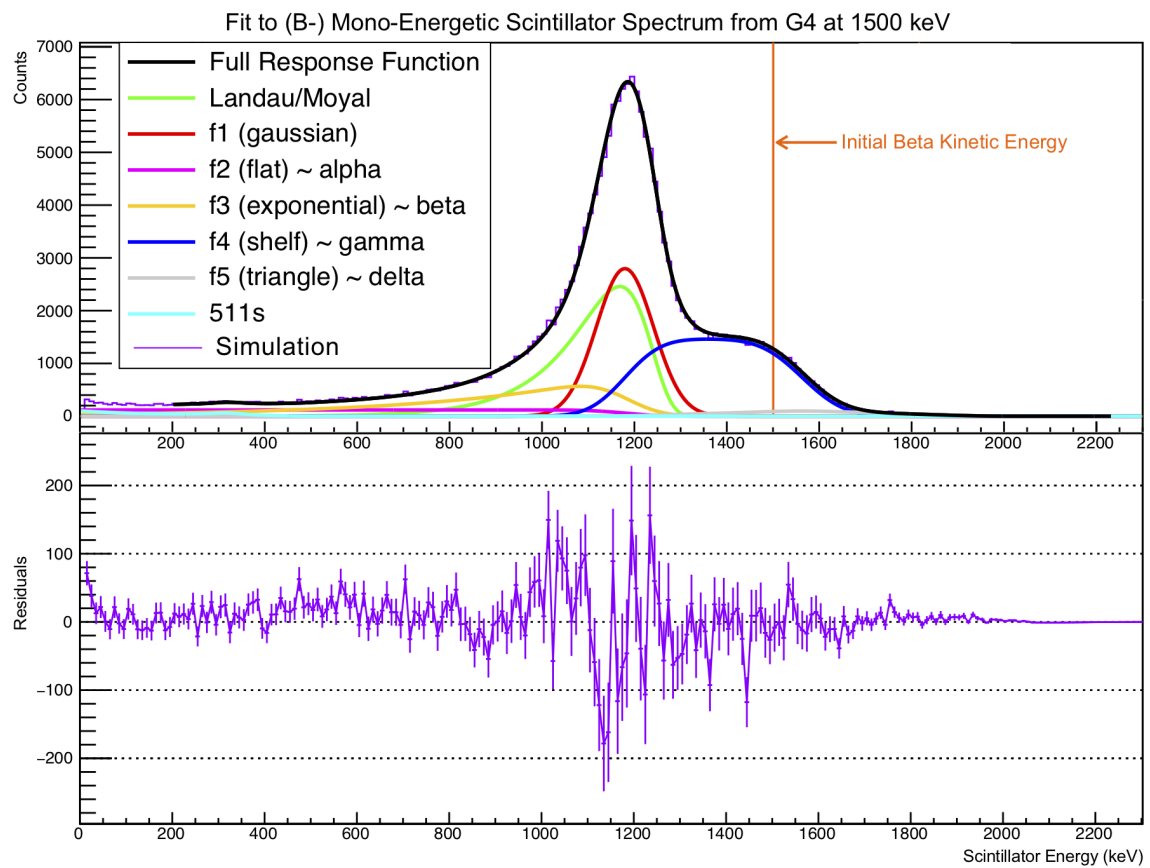


Figure 4.3: Fit to Mono-Energetic Spectrum, 1500 keV (B-)

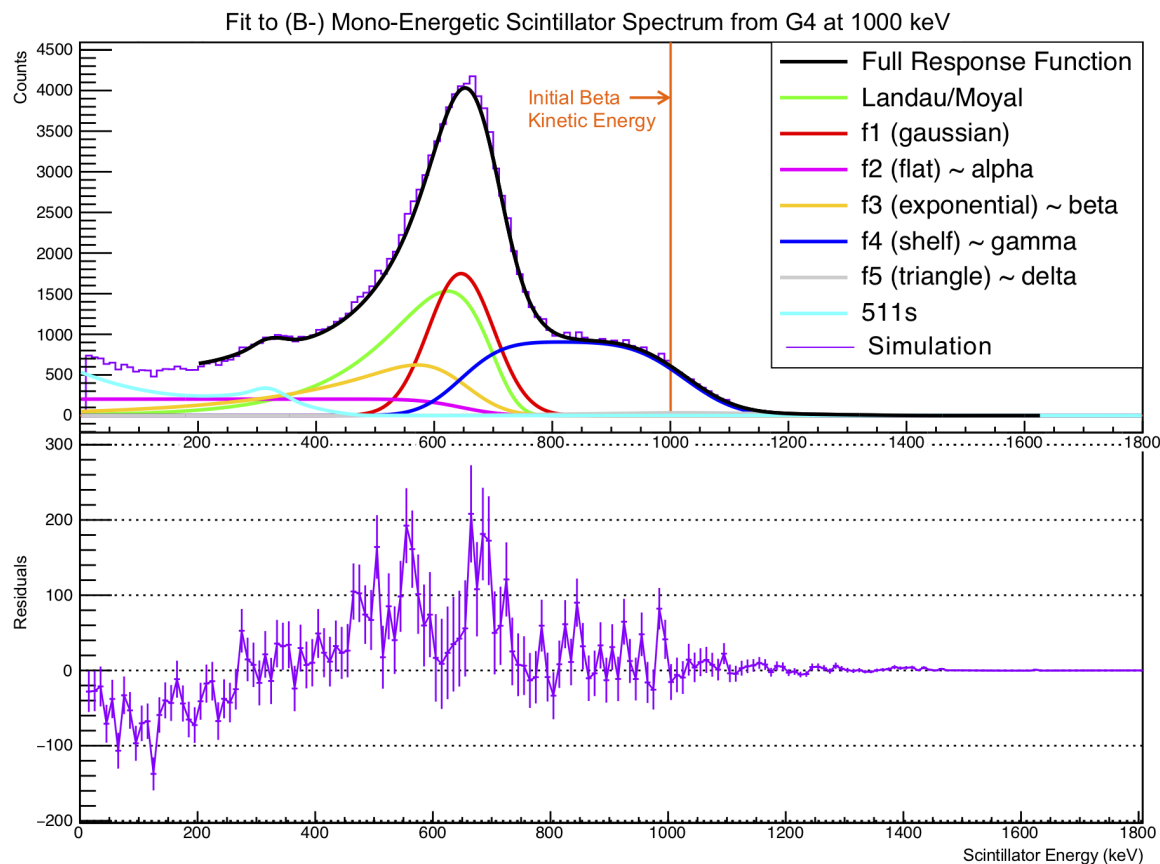


Figure 4.4: Fit to Mono-Energetic Spectrum, 1000 keV (B-)

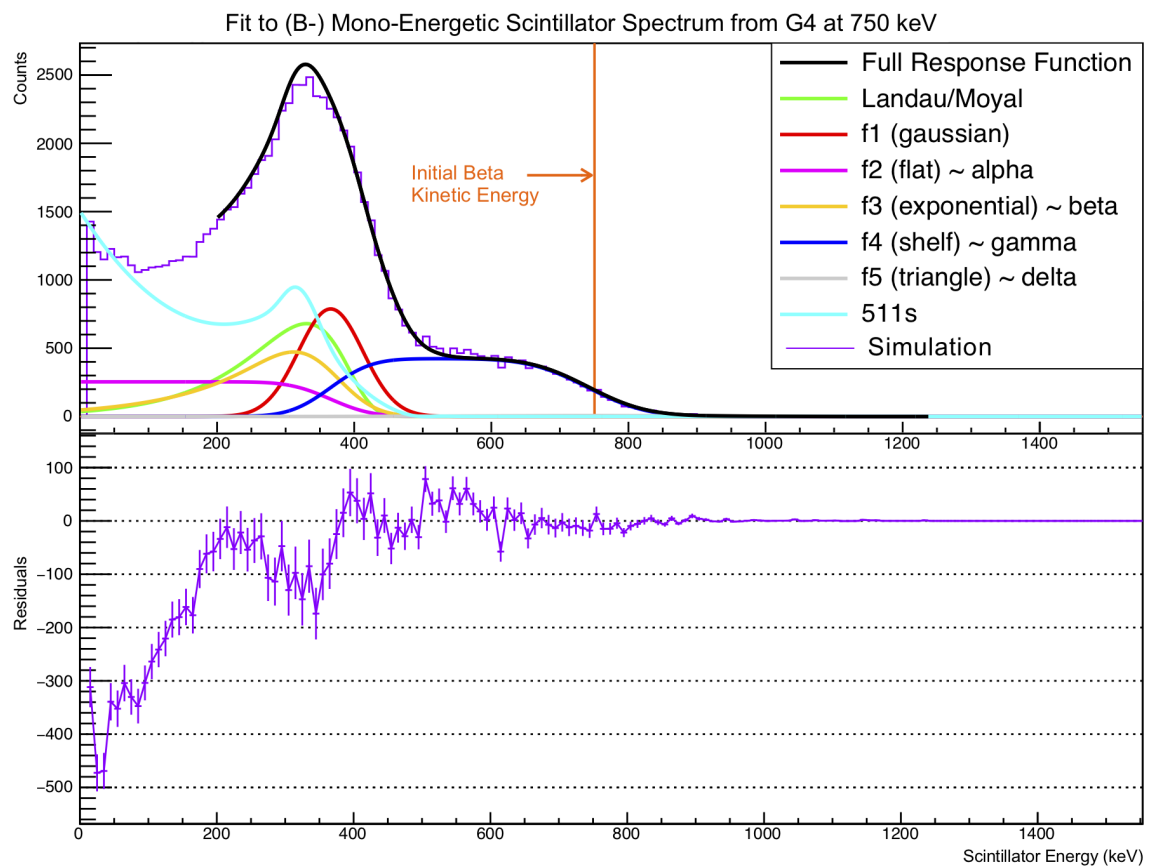
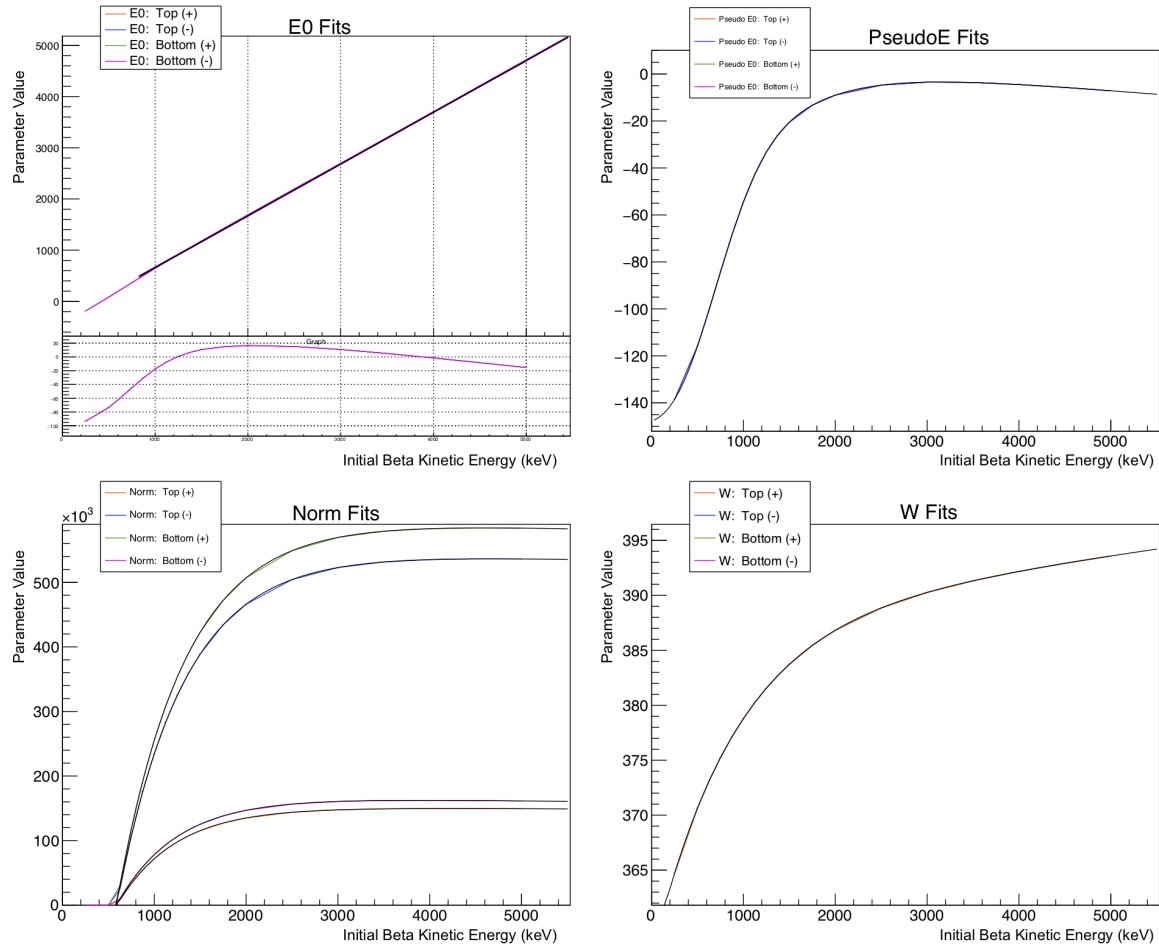


Figure 4.5: Fit to Mono-Energetic Spectrum, 750 keV (B-)



What even *is* the thing plotted below E0 in the ‘residuals’ spot, you ask? It’s ‘PseudoE’, which is describes the difference between the original input energy, E_0 , and the energy where the output spectrum is maximal. Or something. To ‘pretty good’ order, it’s a straight line. the ‘PseudoE’ plot shows what’s left after you fit it to a straight line. It’s fucking weird that it’s negative everywhere. Like, what?

Figure 4.6: Lineshape Parameter Fits (Part 1)

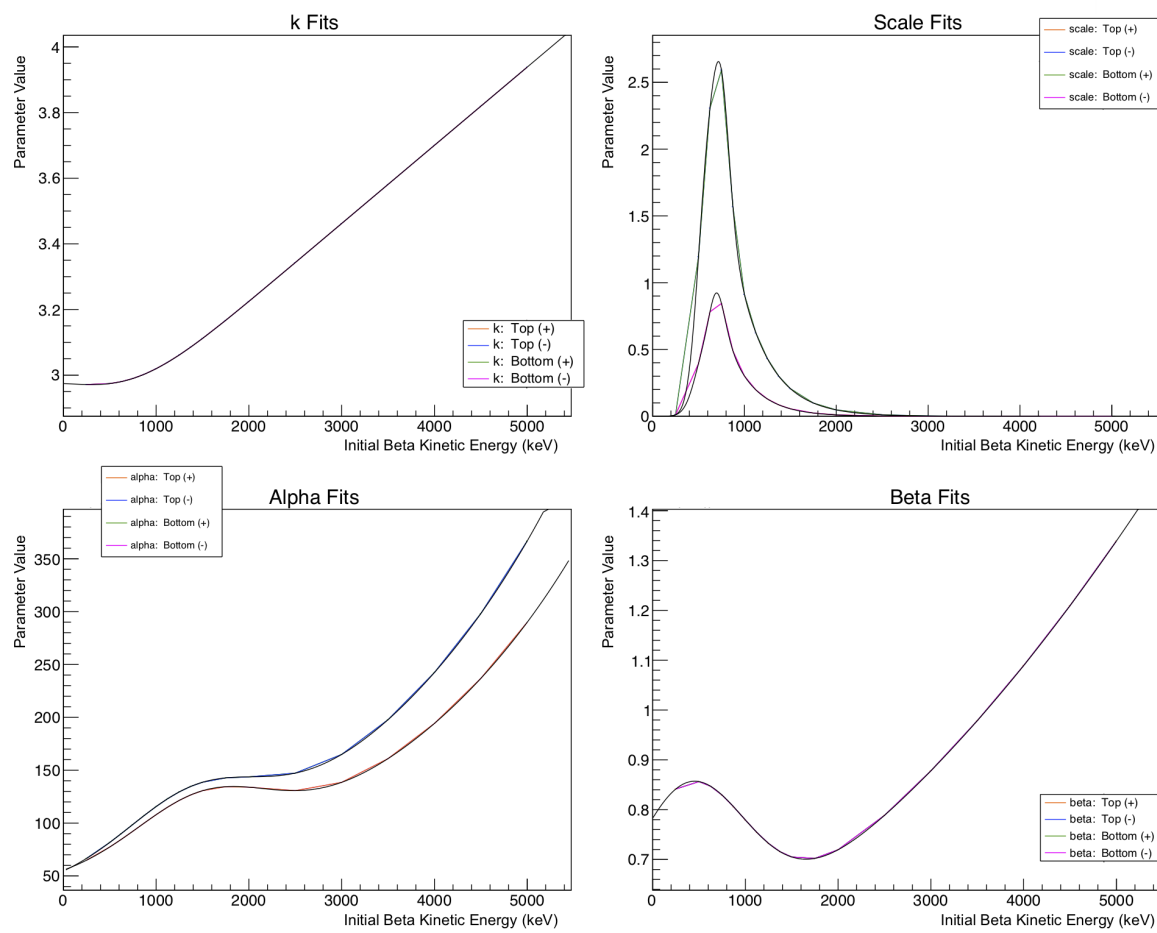


Figure 4.7: Lineshape Parameter Fits (Part 2)

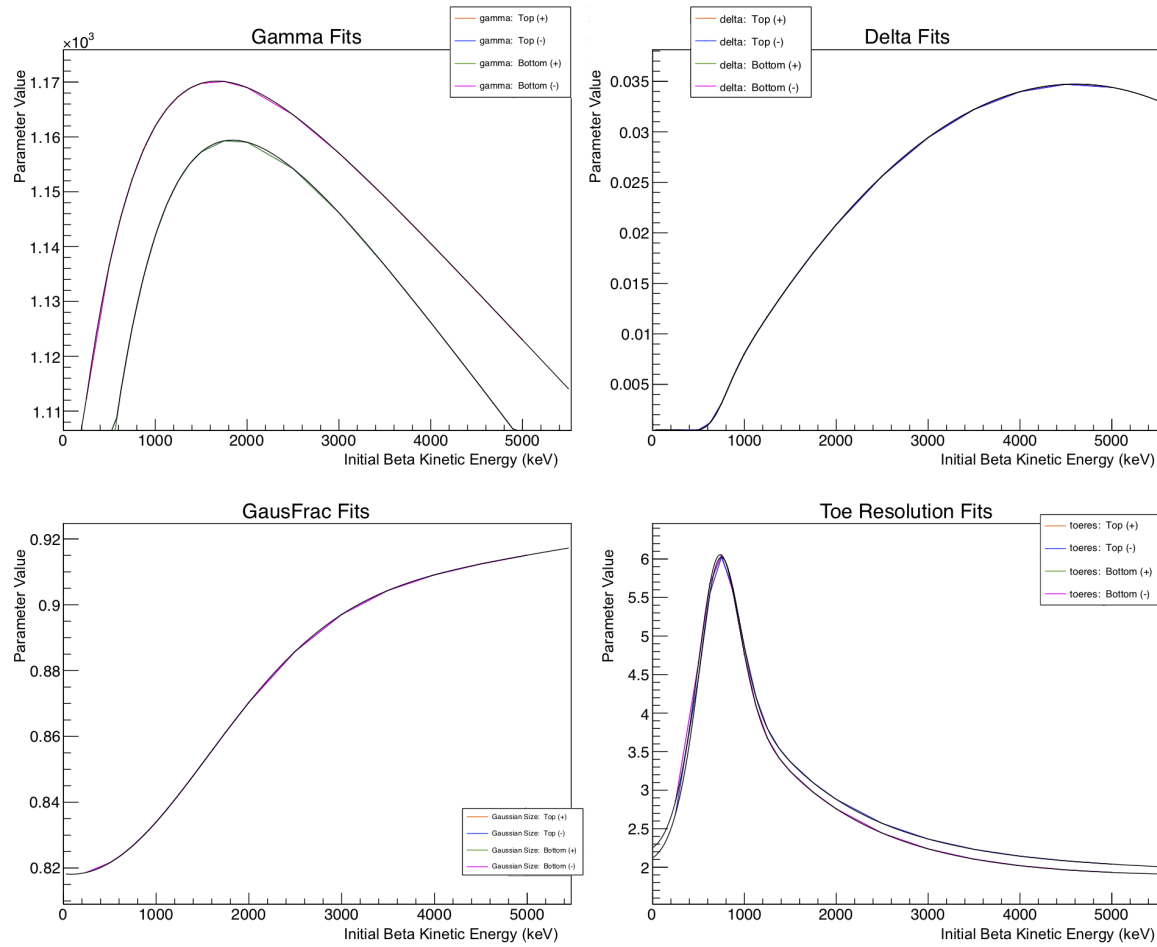


Figure 4.8: Lineshape Parameter Fits (Part 3)

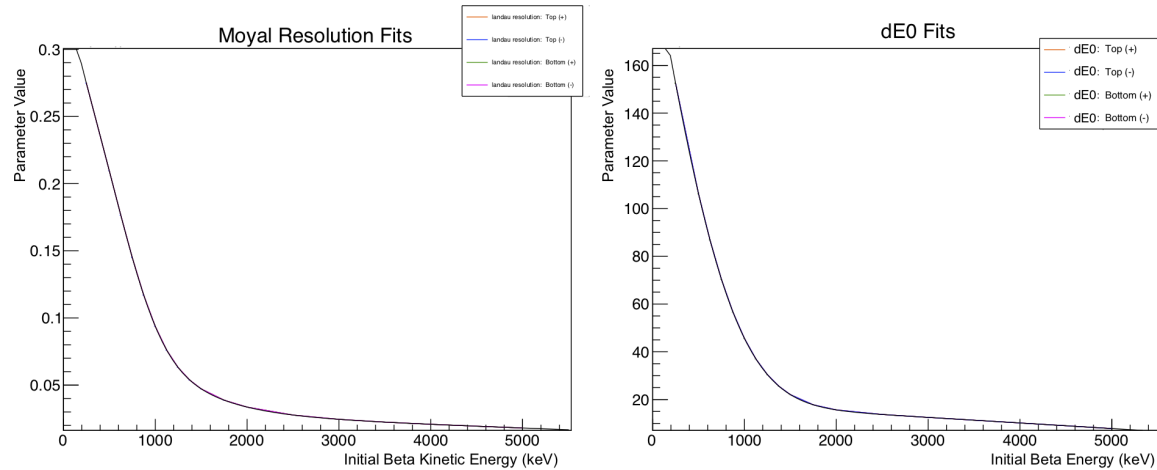
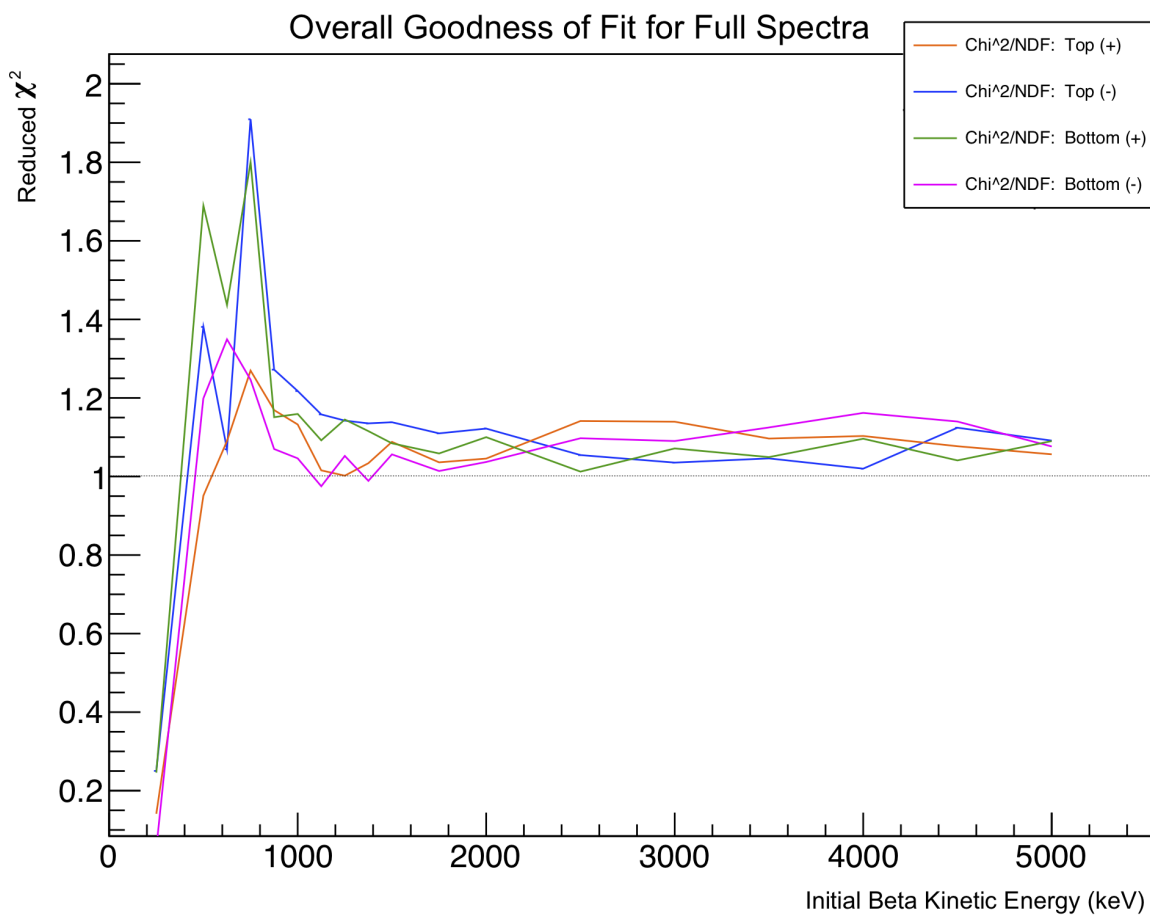


Figure 4.9: Lineshape Parameter Fits (Part 4)



How many DOF for these things? I should put it on the picture.

Figure 4.10: Goodness of fit for modeled response functions, for all four detector+polarization combinations. The models are clearly much better behaved at initial energies above ~ 1200 keV.

4.3 Evaluating Scattering Effects from the Cloud

Events from the trap aren't generated with the same position in G4 and comsol! ugh. ...but it's fine, because the betas are fast. Comsol gets the position right, which is where it actually matters.

A 'timing resolution' is *absolutely* applied to these things. Taken from the width of the prompt peak in the SOE TOF. It's believed to come from betas that hit the eMCP then scatter into a scintillator. The phase space where this could even happen isn't very big, but you can still see the peak. Probably not the other way around, because it's hard to scatter out of the whole scintillator, and if it just scattered off the DSSD then you wouldn't see it in the scintillator.

Generate a CDF for Lev and a CDF for 0eV. For events from the trap, G4 is pointlike but COMSOL has the correct cloud distribution.

For every "good" beta hit event, pick whether to use 0eV(9%) or Levinger(91%). Then, select an SOE TOF (from decay time) from the CDF. Subtract this instance of SOE TOF from this instance of beta TOF to get a thing like an experimental spectrum. Apply a detector resolution (just a gaussian) to this result. *then* we can make basically whatever spectra we like out of this. e.g., beta energy within the cut we're using.this all happens in MakeHarderMulti(...) and also MakeHarderer(...). ...also, we still haven't used the two percent branch on this.

Because there's an offset for the data that we can't measure directly to the precision needed, we simply recenter the whole SOE TOF spectrum to be centered on zero. In this way, we can more easily match it up to simulations.

Beta scattering — in which a beta originating within the atom cloud is incident on a surface within the chamber and changes its trajectory, losing some of its energy in the process — is a significant systematic within this experiment, and it must be evaluated, quantified, and corrected for. While only a small fraction of events are affected, the process results in a change to the beta energy spectrum that can easily be misinterpreted as the exact signal we are searching for. It is therefore imperative that this be well understood.

The scattering process can result both in scenarios where a beta that was initially directed away from the detectors is scattered *into* a detector, and scenarios where a beta that was initially traveling towards a detector is scattered *away* from it. Since this is a polarized decay and the beta asymmetry is not zero, the relative likelihoods of each of these two scenarios depends on whether the nuclear polarization vector is directed toward- or away from the detector in question. In either case, it is clear that some events will be removed, and other events will be added in. As a further

complication, betas that have been scattered into a detector will necessarily have a very different energy spectrum than unscattered betas, and neither are the betas that are scattered away from a detector removed uniformly from the original energy spectrum. With the four beta energy spectra comprising the essence of our observable, we must have a clear understanding of the results of this process within our data.

Despite these complications, it is clear that for events in which the beta is scattered from a surface prior to its incidence on a detector, the beta particle will take longer to travel from the position of its initial creation to the detector. Although it is not possible to fully separate scattered and non-scattered events from one another, a judicious choice of cut within the SOE-Beta TOF spectrum can still be used to lower the fraction of scattered events, improve our signal-to-noise ratio, and decrease the overall size of any systematic uncertainties associated with scattering.

It is useful to remember in the discussion that follows that a beta particle emerging from a nuclear decay is, in general, fairly energetic, with perhaps a few MeV of kinetic energy. In comparison, a shake-off-electron (“SOE” – see Chapter 1.5) typically has only a few eV of kinetic energy. As a result, within our experimental time-of-flight spectra, because it is not possible to observe the *true* time of decay, we have commonly used as a proxy the time at which a beta hit is detected. The betas are relativistic and can be treated (for these purposes) as travelling at the speed of light – therefore if we suppose that all detected betas proceed from the position at which they were created directly into a detector, then the beta hit timestamp provides an excellent proxy for the true decay time, with only a small and easily calculable timing offset. Fig. 3.10, for example, is a spectrum of this sort for the shake-off-electrons’ “times of flight”.

long high-energy tail.
it's actually critical to
the analysis.

Within this section, however, where the experimental SOE TOF spectra are examined in detail, the above assumption is insufficient, as it is necessary to consider effects from beta scattering – both to the observed beta energy spectra, and also to the observed beta time-of-flight spectra (which, of course, are only experimentally meaningful in comparison with another timed observation).

Using Geant4, a set of beta time-of-flight spectra is generated for decays originating from within the atom cloud for all four detector+polarization combinations, and it is clear that there is a small but non-negligible fraction of such events that arise from beta scattering events, as shown in Figs. 4.11 and 4.12. Even within Geant4, where *is* possible to measure the beta time of flight with respect to the initial

No, don't reference
these pictures yet –
we haven't discussed
the SOE TOF.

time of decay, the scattered and unscattered spectra cannot be fully separated from one another. The strong correlation between emission angle and time-of-flight does, however, suggest that the signal-to-noise ratio could be improved by a judicious cut on the TOF spectra.

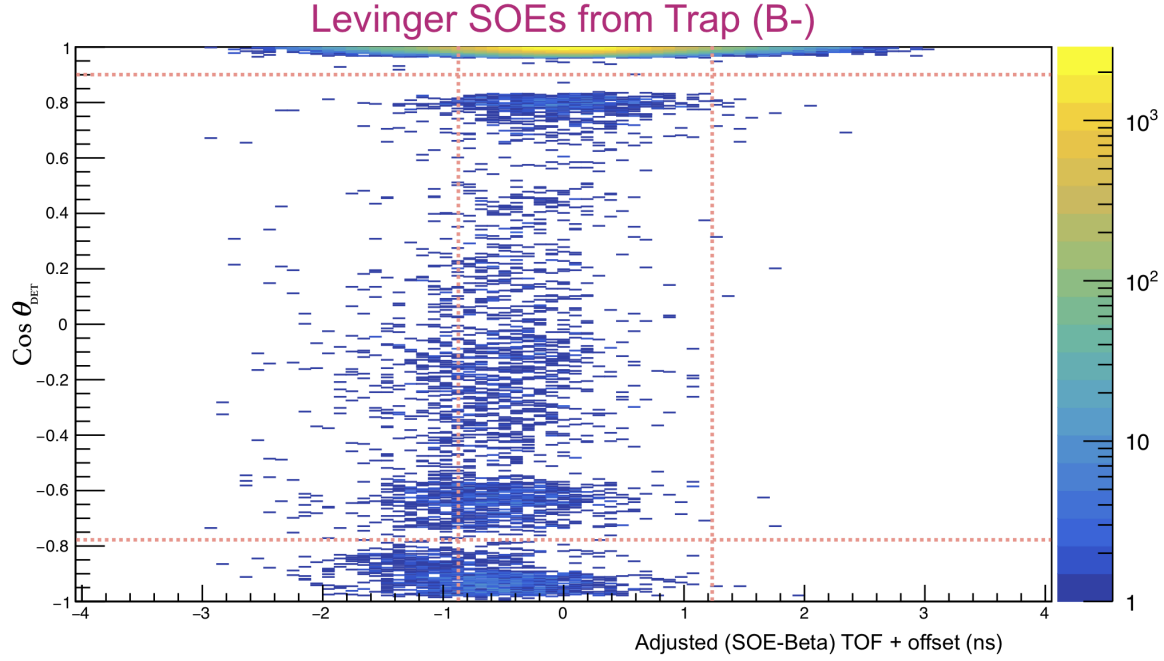


Figure 4.11: Simulated Beta emission angle w.r.t. the detector vs adjusted TOF for Levinger SOEs.

In order to produce something which can be directly compared with experimental data, a TOF spectrum for SOEs must also be produced and merged with the beta TOF spectrum. Experimentally, this is done as an event-by-event subtraction, so that is also what must be done for the simulations. Unfortunately, these two time-of-flight spectra cannot easily be produced within a single type of simulation. Because scattering is an important effect within the beta time of flight spectra (and resulting beta energy spectra), Geant4 is the tool of choice for this type of particle. For shake-off electrons, which are emitted with little energy and accelerated through the electric field within the chamber, it is much more important to have an accurate model of the electric field and its effects on charged particles. The shake-off electrons' time of flight is therefore evaluated by the TRINAT collaboration using COMSOL to track individual electrons through a model of the electric field within the experimental geometry.

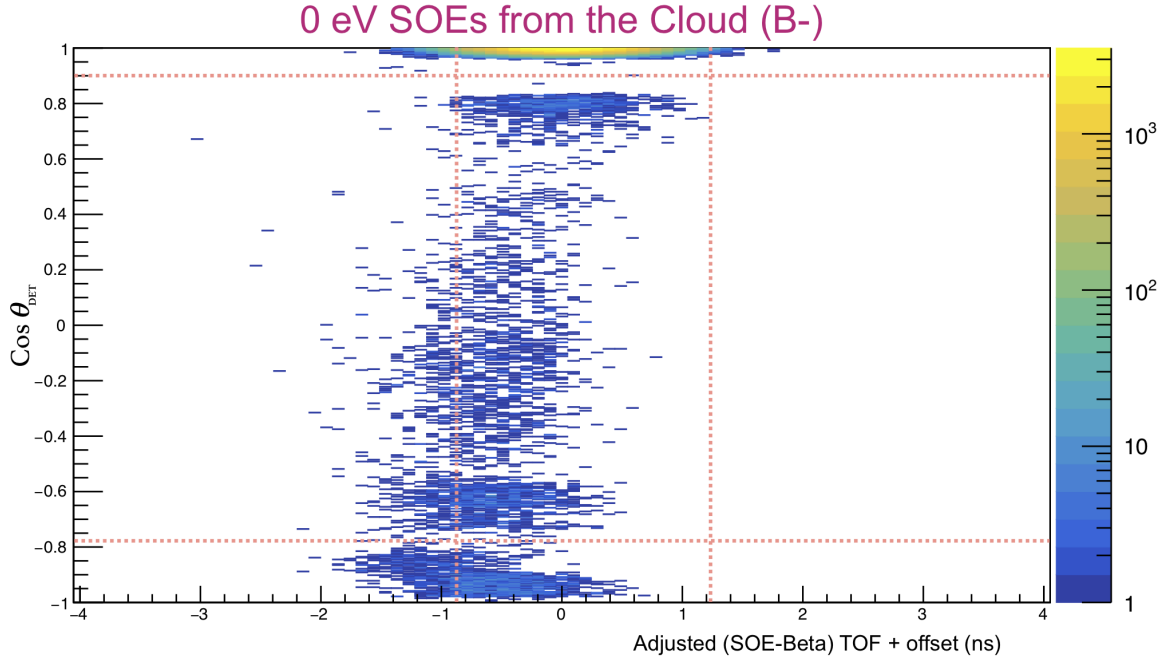


Figure 4.12: Simulated Beta emission angle w.r.t. the detector vs adjusted TOF for 0eV SOEs.

The COMSOL SOEs were generated with starting positions taken from a 3D gaussian distribution near the chamber centre, with the precise position and size parameters taken from measurements using the rMCP, as in Table 3.3. They are emitted with initial trajectories distributed isotropically. Three sets of SOE events are created: two with initial energies taken from the Levinger 4S and 3P spectra in the range of 0–100 eV, and the third with no initial kinetic energy. The origin of these SOE energy distributions is discussed in Section 1.5. A final simulated SOE TOF spectrum (relative to the time of decay) was produced as a linear combination of these spectra, comprised of 9% 0 eV events, 77% 4S events, and 14% 3P events. The relative contributions of each of these components arose from a comparison with experimental data, and the collaboration found that the distribution of hit positions on the eMCP was well modeled by Levinger’s formulae. There was only a very weak dependence on the relative number of SOEs removed from the 4S and 3P shells, though it turned out to be very important that the distributions not be truncated at too low an energy—a surprising result given the fact that both distributions are strongly peaked at much lower energies, and many of the higher energy SOEs are able to escape the central electric field region and therefore escape detection. The

addition of the 0 eV events from $^{37}\text{Ar}^-$ ions to the spectrum also greatly improved the fit.

With both a SOE TOF spectrum generated by COMSOL and a beta TOF spectrum generated by Geant4, the two spectra were combined event-by-event to produce a simulated “SOE – Beta” TOF spectrum to match the form of the data collected from the experiment. Note that although the simulated SOEs were generated from a model of the atom cloud, the betas generated by Geant4 were simply treated as originating from a pointlike distribution at the chamber centre. Since the betas are relativistic and the cloud is small, any changes to the beta spectrum as a result of this model would be too small to be seen given the timing resolution of our detectors (~ 0.1 ns).

This “SOE – Beta” spectrum is convoluted with a gaussian of width $\sigma = 0.443$ ns to model the timing jitter within our detectors. The width of this gaussian is taken from a measurement of the “prompt” peak (betas incident on the eMCP before scattering into a scintillator) within the equivalent experimental spectrum.

Is this even what these events are?

4.4 Simulating the Background and Time of Flight

One of the largest sources of background events in this experiment is from decaying ^{37}K atoms that have escaped from the trap and become stuck on the other surfaces within the chamber. The majority of these events can be eliminated simply by taking a time-of-flight cut on the eMCP relative to a scintillator hit time (as described in Section 3.7). Unfortunately, this procedure cannot remove the entirety of the background, so what remains—both background events from chamber surfaces, and events from the atom cloud itself—must be modeled and understood.

The model used for events originating from the atom cloud is described in Section 4.3, and this section will discuss events originating from other surfaces within the chamber. The methodology used is very similar.

Spectra for both the beta time of flight and shake-off electron time of flight (calculated with respect to the time of decay) were generated, using Geant4 and COMSOL, respectively. For these background events, the SOE and beta were both generated to originate on certain surfaces within the experimental chamber. Because the surfaces from which generated SOEs had a viable path through the electric field onto the

eMCP is relatively large, the SOE and beta spectrum must be generated, event-by-event, to originate at the same position. This procedure not only allows us to account for differing beta times of flight resulting from different distances to either detector, it also captures the differing energy loss from scattering for observed betas originating at different positions.

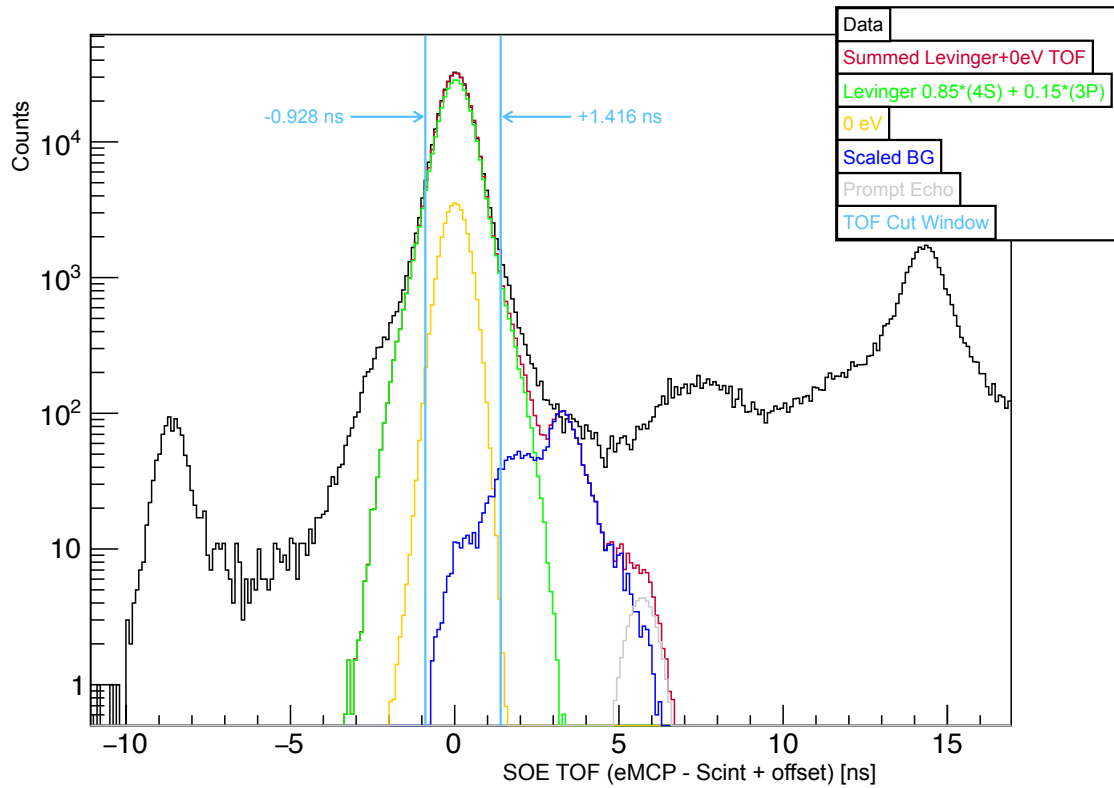
To model the distribution of atoms stuck to various chamber surfaces, we suppose that all escaped atoms were lost from the trap at the center of the chamber in an isotropic manner, so that the number of atoms on an object's (infinitesimal) surface element is given by the (infinitesimal) solid angle spanned by it. Then a set of Geant4 events are generated starting from, e.g., the surface of an electrostatic hoop, and the betas are tracked through the geometry. Only events in which a beta is incident on a scintillator are saved.

Upper limit for the fraction of events generated this way can be estimated by assuming that all losses from the trap not due to radioactive decay emerge isotropically from the trap and then stick to whatever chamber wall is in its path. This upper limit is too big by a factor of 2.

For Geant4 events in which a scintillator hit is recorded, these events' start positions are fed into COMSOL and used as start positions for SOE events, generated with the same energy spectrum that was used for events from within the cloud, as described in Sec. 4.3. For these events, only the ones in which an SOE was incident Alexandre did this. on the eMCP were preserved. This process serves to provide a normalization for the relative number of events from each surface, and for the relative number of events on each part of a surface. With a “SOE – Beta” TOF spectrum to compare with experimental data, it is possible to estimate how many such events remain (and what their energy distribution looks like) after a cut on the experimental spectrum is performed. The results are shown in Fig. 4.13.

In order to check this model's performance, the energy-averaged superratio asymmetry is assembled for each time-of-flight bin within both our simulated and experimental spectra, as in Fig. 4.14. Although the two plots diverge rapidly outside this TOF range, an evaluation of the χ^2 statistic within this range produces a result that fits almost *too* well.

SOE TOF, Both Detectors (400 - 5000 keV)

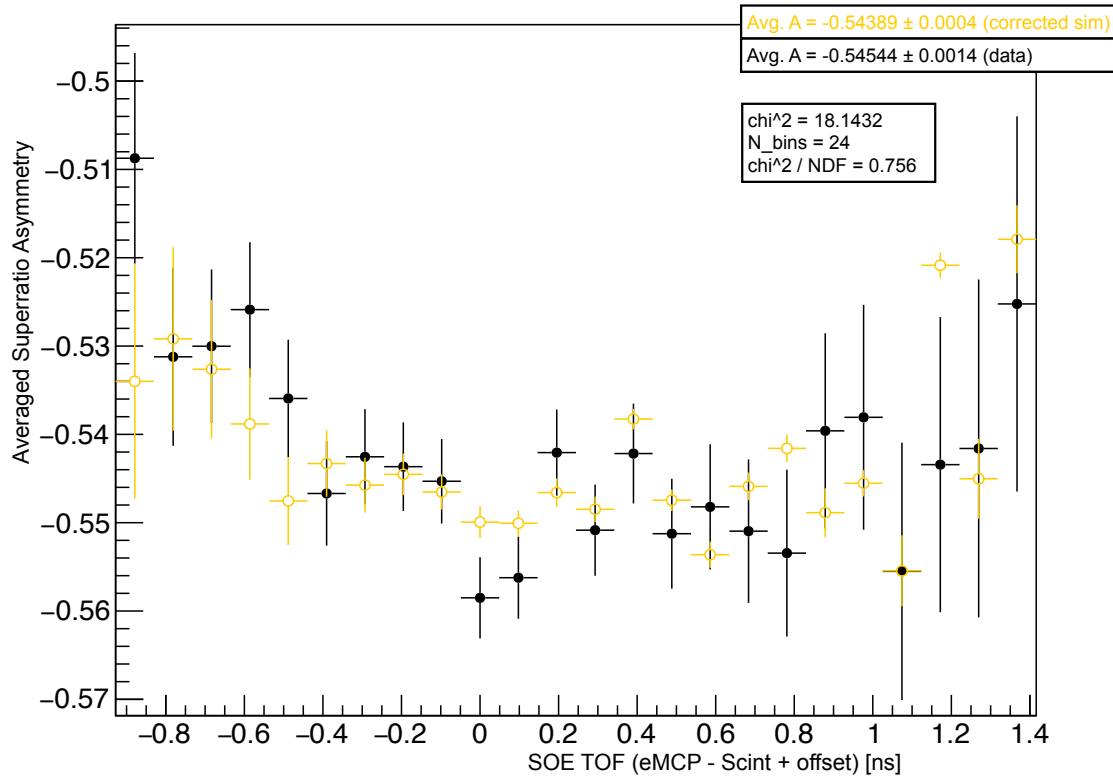


Rephrase.

Reference Section 3.7, probably.

Figure 4.13: SOE TOF, with both model and data. In the end, the data was cut to use only events with a TOF between -0.928 ns and +1.416 ns. Max. possible background is like a factor of two too big. Similar quality results no matter how you distribute the Levinger spectra between 4S and 3P, however adding the 0 eV electrons makes a big improvement to the agreement.

Superratio Asymmetry



Show the "average asymmetry" (all energies) as a function of TOF, with real data, best model normalization, and extrema of model normalizations. Show our cut. Turns out, it's a lot of work for a really tiny correction. Oh well.

JB on the *actual* figure I had been planning to put here, and my remarks about it: Indeed it will be critical to show a clear compelling version of this figure in thesis and in a paper. It was vital to minimize and determine this background to avoid fitting a polynomial to it from the wings, even more so for the energy dependence of A than for its average – you should say so.

...

The reason the correction is small is because of all your hard work.

Figure 4.14: The superratio asymmetry, averaged over all scintillator energies between 400-4800 keV, is used to compare the experimental data and simulated TOF model as a proxy for the quality of the model to estimate the background. All other cuts have been applied.

Chapter 5

Analysis and Estimates of Systematic Effects

Missing figure

Show simulated spectra separated by scattering category.

Missing figure

Show SimpleMC spectra, show the supersum, show the superratio, show the superratio asymmetry. Maybe do some simple fits to show how much better the superratio asymmetry is than *not* the superratio asymmetry.

John proposes an intro statement for this chapter (by which I really mean that other chapter, but I'm pretty sure it goes here now). But anyway, the following two paragraphs are a direct quote from him:

Analysis is critical to a precision measurement, as most of the research is in determining systematic uncertainties by self-consistent analysis and simulations. Each detector in this experiment is critical and has independent calibrations and cuts. Full explanation is here (and in two following chapters) justifying choice of the deterministic cuts, because in the analysis in this thesis the data was not blinded. The main goal

of blinding was nevertheless achieved— to make sure all analysis is done completely with full redundancy of checks wherever possible— so the discipline entailed must be described in full detail. Here there are details of detectors: eMCP rMCP beta DSSD scintillator.

The collaboration has done an independent analysis fixing bFierz to zero. Differences with that analysis are interleaved in this section. Critical physics improvements concern an emcp-beta timing walk correction which enabled an improved cut against background, also incorporating a more complete modelling of decay backgrounds from untrapped atoms. Technical corrections include a correct treatment of the polarization cycle. An arbitrary change in the deltaE radius cut is kept self-consistent.

JB: "I doubt I will have further useful comments on the Ch. (((this chapter))) as they are now.

JB:

I've tried to email you the paragraphs on "collaboration determination of uncertainties" for (((Ch. 5)))

My intent of all that other advice was to keep your time spent on Chs 1-4 ((Now Ch. 1-2)) concise, so you could concentrate on these real jobs. (n.b.: the advice he's already sent was almost all about chapters 1-4, which are the various intros/background info and experimental setup stuff)

...

I can only say that if you have an equal choice between including a detail or not, pick "not."

JB: I will try to schedule meeting with Dan for you to show us the final version of (((Ch. 5)))

Estimating systematic effects soon.

JB says:

A simple estimate from the collaboration that builds intuition for this result: Scatter in the SiC mirrors and DSSD actually produces an efficiency change at low beta energy. Energy loss is not minimally ionizing in these structures, and instead will have a long Landau tail that can take events below energy threshold in the scintillator. The collaboration has modelled explicitly the false asymmetry as a function of Kbeta between 600 and 1300 keV, producing roughly $(K-0.6 \text{ MeV})/(0.7 \text{ MeV})$, i.e. 50% at $K\beta=0.95 \text{ MeV}$. This efficiency degradation would be distributed roughly equally between the SiC and DSSD. If completely ignored, this would introduce by inspection a false bFierz of approximately 0.5. Scattering effects will vary between linear and sqrt of thickness, so assuming worst case of linear, the mechanical thickness uncertainty of 5 micron/300 micron and 6 micron /275 micron, an average of 2%, making a random contribution of order 0.01 each. The Be window has larger mechanical thickness uncertainty of 23micron/229 micron, but energy loss and scattering in this material is 5x smaller, so the net effect would be similar.

...

To minimize this systematic for future experiments, the collaboration has implemented pellicle mirrors of negligible thickness, 100 nm Au on 4 micron kapton. The collaboration is also implementing Be-windowed wire chambers in place of the DSSD.

...

MJA:huh?

5.1 Overview

A summary of systematics goes here. In words, yes, but also in table form.

Choice of low-energy scintillator threshold has a large systematic effect...

from John: "I used Ben's threshold when determining the uncertainty from the lineshape tail (UFTLT). If you're saying the UFTLT depends on the threshold used, ok, of course it does. But if you're claiming that UFTLT depends on the **uncertainty** of the threshold, that's manifestly smaller than the UFTLT itself, and I'm going to assert it isn't worth evaluating."

It's actually not nearly as big as I'd originally expected. It's huge in the line-shape thing, but pretty tiny in everything else.

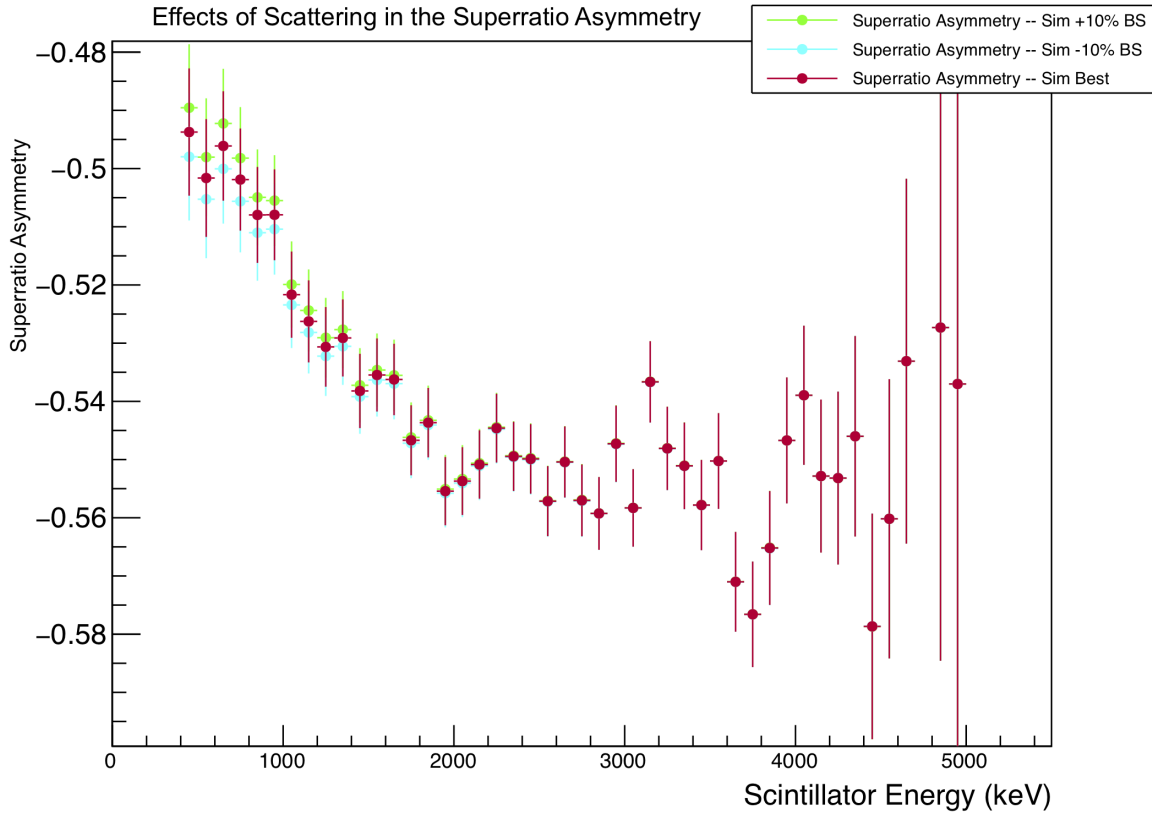
Source	Uncertainty	
	b_{Fierz}	A_β
Scintillator Calibration	0.003	0.0003
Scintillator Threshold	0.004	0.0004
DSSD Individual Strip SNR	0.006	0.0007
DSSD Energy Agreement	0.005	0.0006
DSSD Detection Radius	0.006	0.0017
DSSD Energy Threshold	0.005	0.0005
Atomic Cloud	0.002	0.0002
Background	0.004	0.0003
Beta Scattering	0.031	0.0025
Low Energy Tail	0.008	0.0007
Mirror Thickness	0.013	0.0017
DSSD Thickness	0.013	0.0017
Beryllium Foil Thickness	0.004	< 0.0001
Total Systematics	0.039	0.0041
Statistics	0.084	0.0082

Table 5.1: Error budget for the two-parameter analysis. Final results: $b_{\text{Fierz}} = 0.033 \pm 0.084(\text{stat}) \pm 0.039(\text{syst})$ and $A_\beta = -0.5743 \pm 0.0082(\text{stat}) \pm 0.0041(\text{syst})$

5.2 Comparing Simulations to Experimental Data

That old list:

- Run 3 sets of G4 simulations with a bunch of statistics (N events, for data with like N/10 events). Each one has the same nominal value of A_β , but with 3 different values of the scalar coupling C_S : zero, and +/- (whatever). Keep $C_T = 0$. Because reasons, we're not really able to distinguish between C_S and C_T in this experiment anyway, so might as well keep the analysis simple.
- Just run one set of 0.02*N events for the two percent branch. We can't neglect it, but it isn't going to change much when we adjust BSM couplings. Just use the old event generator from Holstein Eq. (51).
- generate beta-SOE TOF spectra for simulated data.
- generate background spectra and the TOF spectra to go with them.



I got it out of the Sim_to_Asym directory, so that's where I have to go looking to see how I made it and/or make a new one.

Figure 5.1: Here's what happens to the asymmetry when you adjust the scattering by the amount we decided on in the thingy. I think it's actually \pm (one sigma), despite the titles on this thing.

- make the same TOF cut on the simulated data and the experimental data.
- In fact, make all the same cuts on the experimental and simulated data. DSSD cut, DSSD energy, one hit DSSD, one hit scint. TOF cut, which requires a whole extra model of background in the TOF spectrum (see Section 4.4).
- For each of those 3 simulations, sort the “good” data according to emission angle relative to the detector. Do each detector individually. For both polarizations.
- Assemble the (simulated) superratio asymmetry. We'll compare it to data, and the χ^2 from that comparison will be our figure of merit.

- We can make a whole 2D parameter space for different values of A_β and b_{Fierz} , and compare them all (via their superratio asymmetries) to the experimental data. We get the “best” values of A_β and b_{Fierz} , where χ^2 is minimized.
- We can do this whole thing again for simulated data sets with different values of parameters that we vary as systematics. Note how the best values of A_β and b_{Fierz} change when each of the systematics are varied.

5.3 BB1 Radius, Energy Threshold, Agreement

BB1 radius cut can help to eliminate scattered events. Energy threshold selection and statistical agreement between BB1 detectors’ energies only makes a small effect on results. BB1 radius itself has a pretty big effect on the result, but we can at least just G4 it away. The remaining systematic effect is pretty small.

JB: I hope the discussion is clear in your head. Any effect that relies on scattering computation in G4 should have an uncertainty on order 10% of the correction – hopefully you are keeping a distinction here between the finite geometry acceptance (which I guess is exact) scattering off the collimator.

As per JB’s comment in section 3.6: “statistical agreement between BB1 X and Y detectors’ energies only makes a small effect on results” does not need the technical details beyond that statement.”

 Missing figure

Surely this requires at *least* one image of the pixelated BB1 data. Maybe some of a few waveforms and energy distributions too.Feels like cheating to include some of that stuff, since Ben was the one who actually used it mostly.

JB on missing figure: “if you used such an image as part of your uncertainty estimate, yes [include it]”

Remember: There’s noise applied to simulated BB1s, matching some spectrum.

In the end, we get our results from the scintillator energy only, without summing the BB1 energy back in. Energy absorbed in DSSDs is only used as (a) a tag for events, and (b) contributing to the total beta energy loss before the beta arrives at the scintillator.

JB: The simulations of course include it event-by-event, not just a minimally ionizing average loss.

5.4 Background Modeling – Decay from Surfaces within the Chamber

This content got moved to Ch. 4.4.

5.5 Quantifying the Effects of Backscatter with Geant4

This content got moved over *there*. (ie, Section 4.3.)

5.6 Lineshape Reconstruction

A lot of this content has gone into (Section 4.2) instead. I really need to just mention it here (Sec. 5.6) and give an indication of how good the result is. Then evaluate stuff.

Clifford tells us what to do. [26].

5.6.1 What is it and how does it work?

Mono-energetic beta decay events are generated in GEANT4, which outputs an energy spectrum for unscattered and forward-scattered beta events in the detector. These spectra are fit to a function to model the scintillator resolution, as well as energy loss in materials that the beta passed through before arriving at the scintillator. These spectrum fits are performed for a set of beta energies, and parameters are extrapolated to be applied to betas emitted at intermediate energies. Thus, the whole spectrum can be modeled. Pictures will make this clearer.

5.6.2 The Results – Things That Got Evaluated This Way

As it turns out, only cloud parameters were evaluated this way. Trap position, size, sail velocity, temperature. But then we varied the lineshape anyhow, to account for G4 doing a bad job of modelling the bremsstrahlung (sp?).

JB: so it's still critical to write down more of the lineshape work.

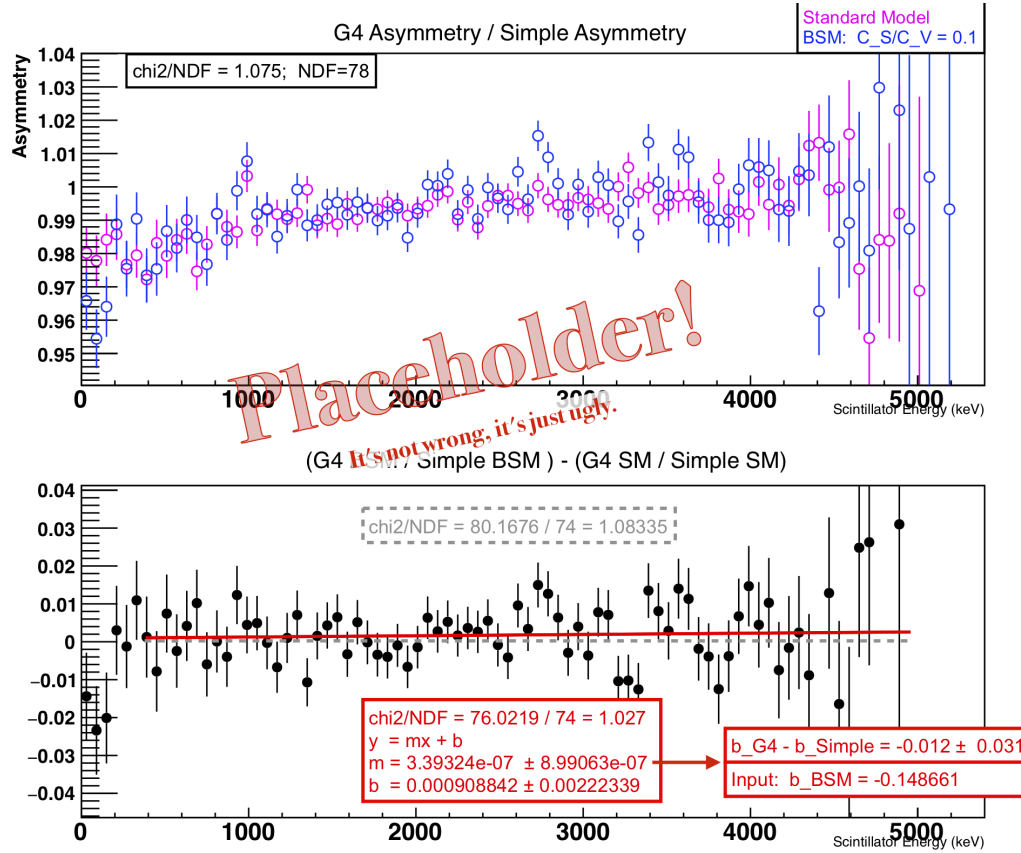


Figure 5.2: I'm not actually sure if this picture shows what I want it to. The point is, if I apply this rough lineshape to stuff that I SimpleMC-ed, then I can evaluate that way various systematic effects that would be time-consuming to actually simulate with G4. This picture is *supposed* to be a demonstration that this approach actually works...

JB: yes, brems strahlung is 'braking radiation' so gets 2 ss's. the lineshape tail in any scintillator also includes backscattered events – we are not claiming the 2-pixel cut is complete

5.6.3 The low-energy tail uncertainty, and what it does

Bremsstrahlung. It does Bremsstrahlung.

Here is Subsection 9.5.5 "The low-energy tail uncertainty, and what it does" complete. There should be no figure.

Direct quote from John follows in the next two paragraphs. Maybe I should paraphrase, but it's so nicely written!

This subsection has the collaboration's evaluation of the uncertainty from the

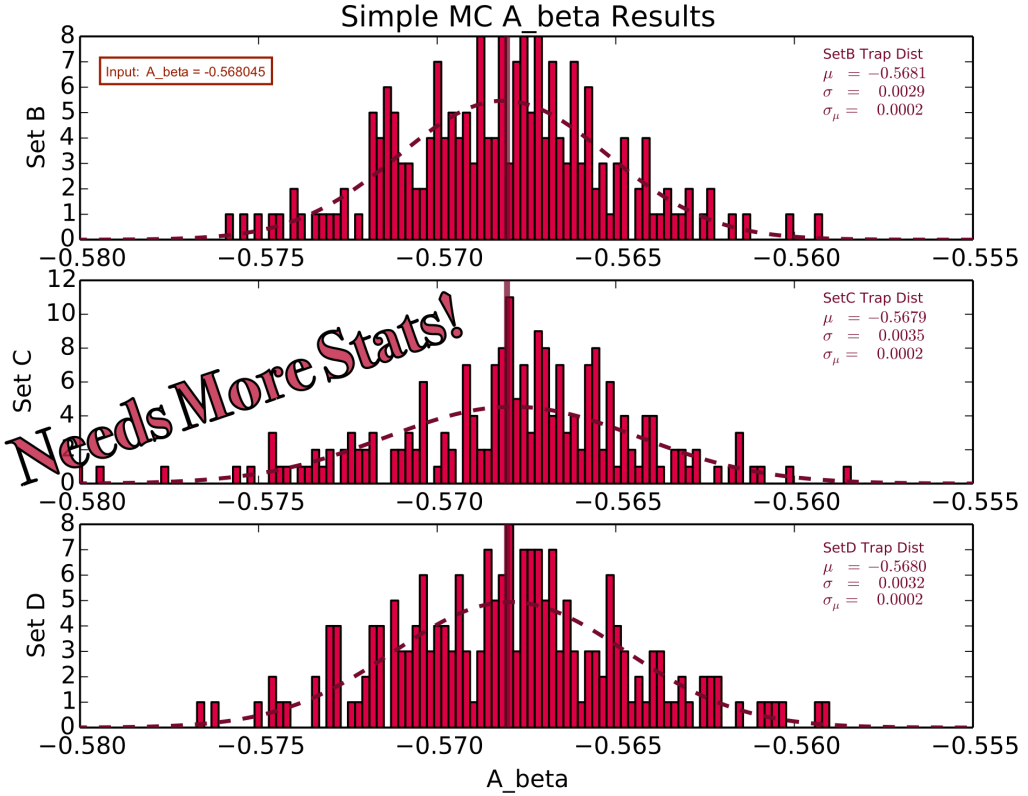


Figure 5.3: Estimated uncertainty in A_{β} resulting from uncertainty and variation in the cloud parameters. Evaluated by the lineshape reconstruction method.

scintillator detector's lineshape tail. The energy from a monoenergetic beta is not always fully absorbed in a plastic scintillator. Although most backscattered betas are vetoed by the DSSD, some produce bremsstrahlung photons, and these frequently escape low-Z plastic scintillator— all cross-sections are known to high accuracy, but there is always uncertainty entailed in the MC implementation. This lineshape tail will then effectively move events from higher to lower measured energy, artificially altering the lower-energy asymmetries and mimicking the effects of a Fierz term.

Since this detector effect is difficult to disentangle from the other scattering effects off volumes, the collaboration adds a linear function down to zero for the tail to a Gaussian for the peak, with linewidth varying by photon statistics [26]. The convolution of this simple detector response function with v/c then scales the centroid MC, with the lineshape tail varied by $\pm 10\%$ of its value, a generic uncertainty accepted by

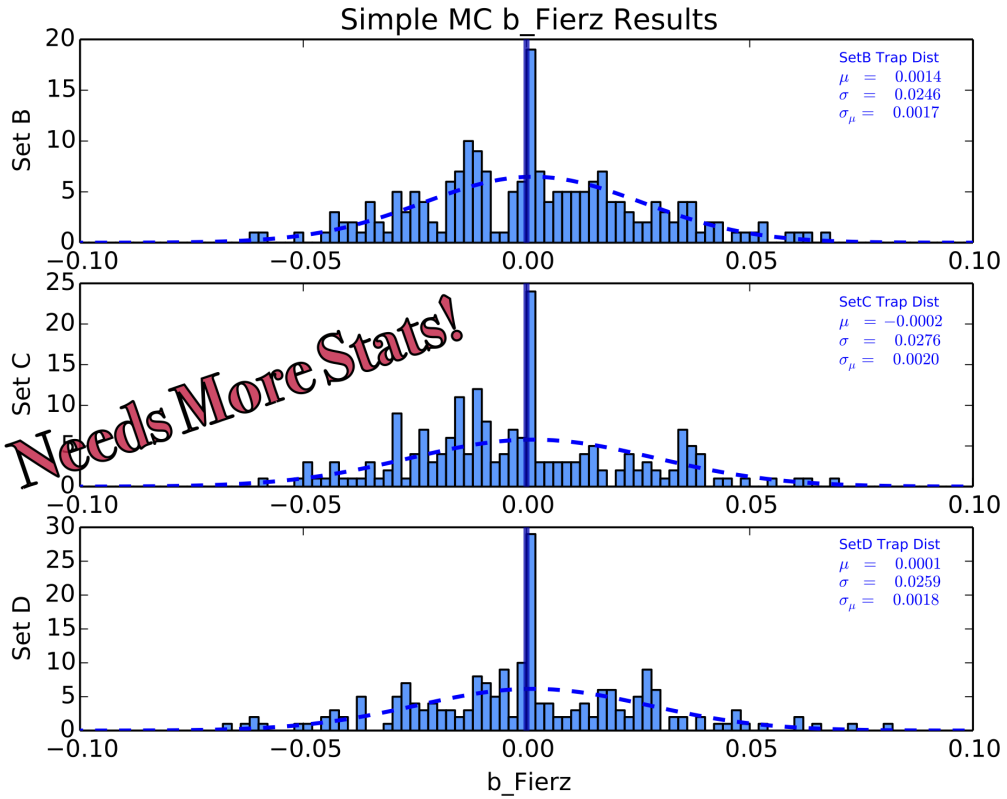


Figure 5.4: Estimated uncertainty in b_{Fierz} resulting from uncertainty and variation in the cloud parameters. Evaluated by the lineshape reconstruction method.

the community for MC electromagnetic simulations. The fit b_{Fierz} centroid changes by ± 0.0076 , summarized as the 0.008 “Low Energy Tail” in the systematics table at the start of this chapter. Compared to other uncertainties of the present data set, this is small enough that the accuracy of this estimate is adequate.

Chapter 6

Results and Conclusions

JB: Dan and I independently discussed (((Ch. 6))) yesterday, and he has suggestions to help. So I will also schedule a meeting with Dan and you to discuss (((Ch. 6))) Results and whether the S,T part must be deleted and left to a paper. You don't have enough time, and although this should be quite straightforward, it is not your critical result and it's the only thing that can go.

6.1 Measured Limits on b_{Fierz} and A_β

Results go here, with measured limits described and quantified in all formats anyone could ever care about.

John says to just skip doing the C_S and C_T stuff, for now. No time. Really, C_S is already basically done, but then that'll lead to awkward questions about C_T .

Info on the A_β measurement goes here too. In particular, you set $b_{Fierz} = 0$ and see what happens to A_β .

6.2 Discussion of Corrections and Uncertainties

Just write a blurb to qualitatively summarize a bunch of the stuff in Ch. 5. Do I want to put my error budget table here? If not, here it is! (5.1).

Other things to discuss here: which things are dominant error sources, and how viable it would be to improve those for future experiments.

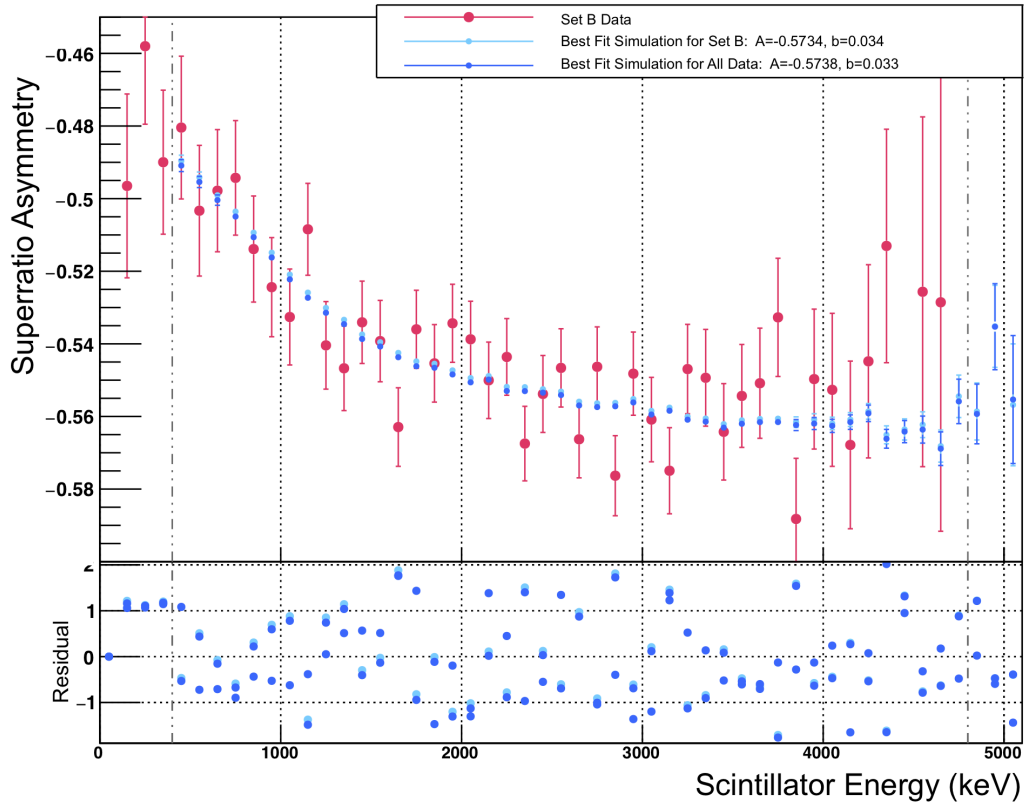


Figure 6.1: A superratio asymmetry from Dataset B, and the best fits from simulations.

6.3 Relation to Other Measurements and New Overall Limits

In which I'll show exclusion plots and write down new limits, combining my result with results from the literature. Or, y'know, maybe I'll just talk about doing that.

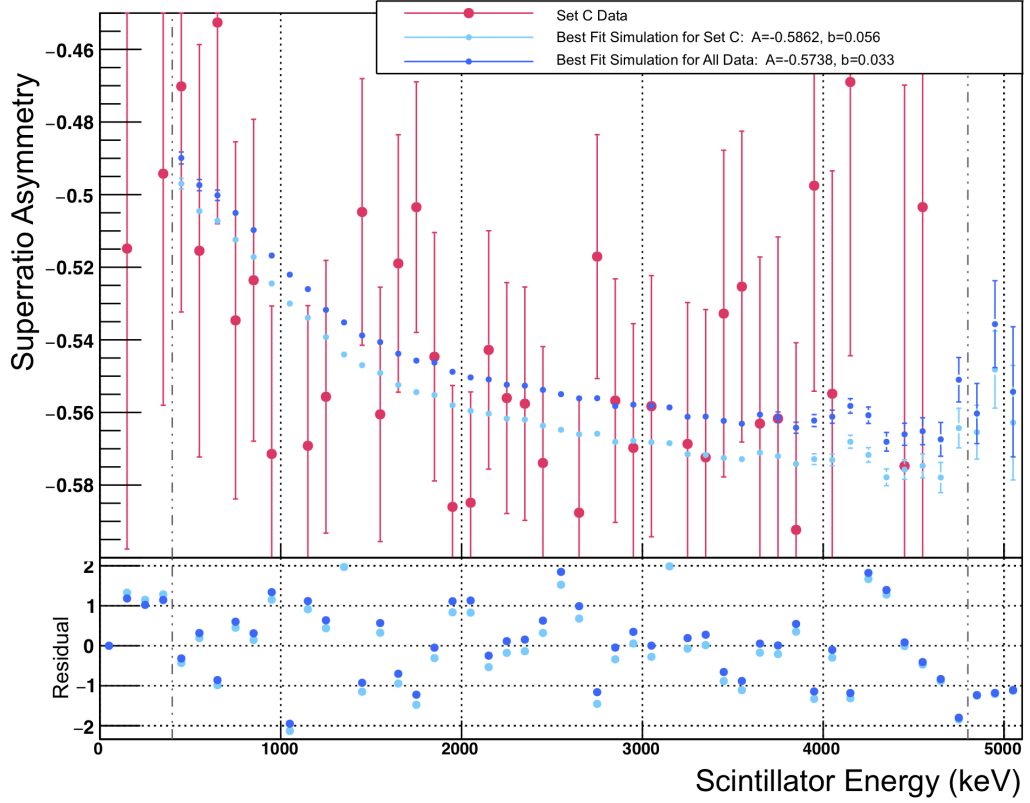


Figure 6.2: A superratio asymmetry from Dataset C, and the best fits from simulations.

JB says: To put your work in context, please add at the end of that minimal S,T section, or at the end of "Our Decay" section

...

The best existing measurement of b_{Fierz} is in the decay of the neutron [8], $b_{\text{Fierz}} = 0.017 \pm 0.021$, consistent with the Standard Model prediction of zero. Our measurement is strongly related, yet complementary. In terms on non-Standard Model Lorentz current structures, to lowest order in the non-SM currents the same equation applies:

$$b_{\text{Fierz}} = \pm (C_S + C'_S + (C_T - C'_T)\lambda^2)/(1 + \lambda^2)$$

(the plus is for β^- decay and the - for β^+ decay) [6]. [to be continued...]

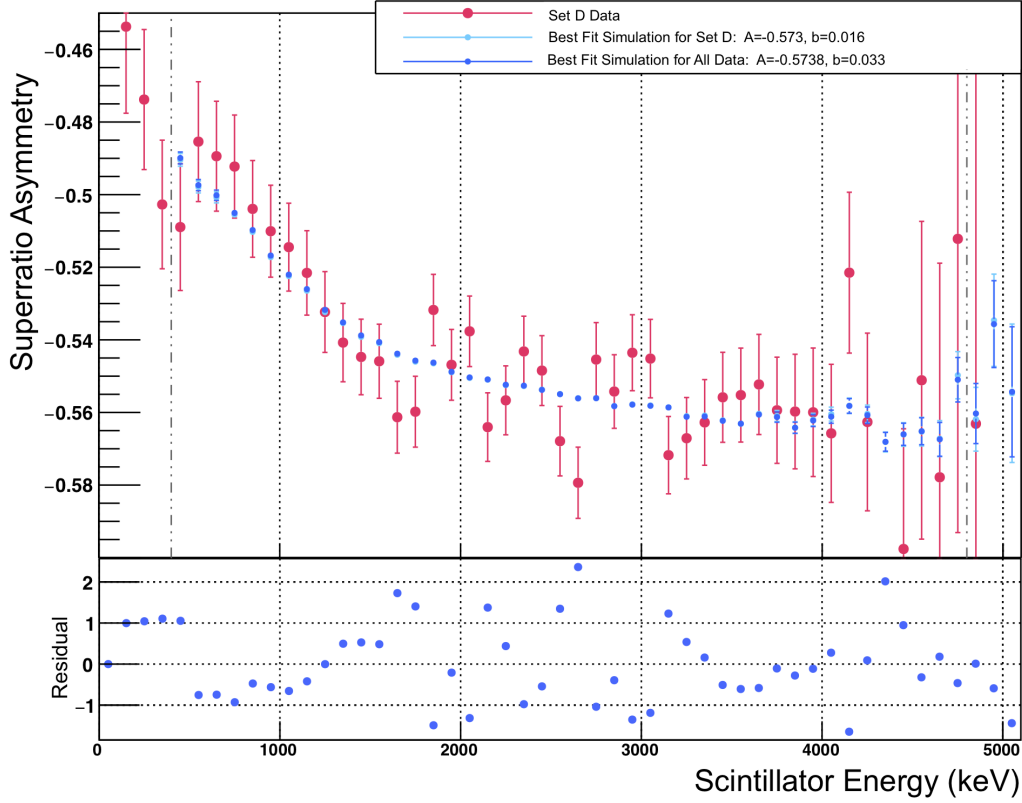


Figure 6.3: A superratio asymmetry from Dataset D, and the best fits from simulations.

[...continued from prev.]

In our ^{37}K case, $\lambda^2 = |M_{\text{GT}}|^2 / |M_F|^2$ is close to $3/5$ (the expected value $j/(j+1)$ for a single $j=3/2$ d $3/2$ nucleon) [11], while for the neutron λ^2 is close to 3 (the expected value for an $(j+1)/j$ $j=1/2$ s $1/2$ nucleon). $|M_F|$, the Fermi matrix element, is nearly the same for both of these isospin = $1/2$ decays (the largest correction is the larger isospin mixing of ~ 0.01 in ^{37}K). So our observable is relatively less sensitive to Lorentz tensor currents, and will predominantly constrain or discover Lorentz scalar currents.

...

Full considerations would require a weighted fit of b_{Fierz} experiments and similar observables [12], and are beyond the scope of this thesis. The info from this thesis, values of A_β and b_{Fierz} with their uncertainties, can together with the known fT value (lifetime and branching ratio) allow the community and/or the collaboration to include the results in a future constraint or discovery of scalar and tensor Lorentz currents contributing to β decay.

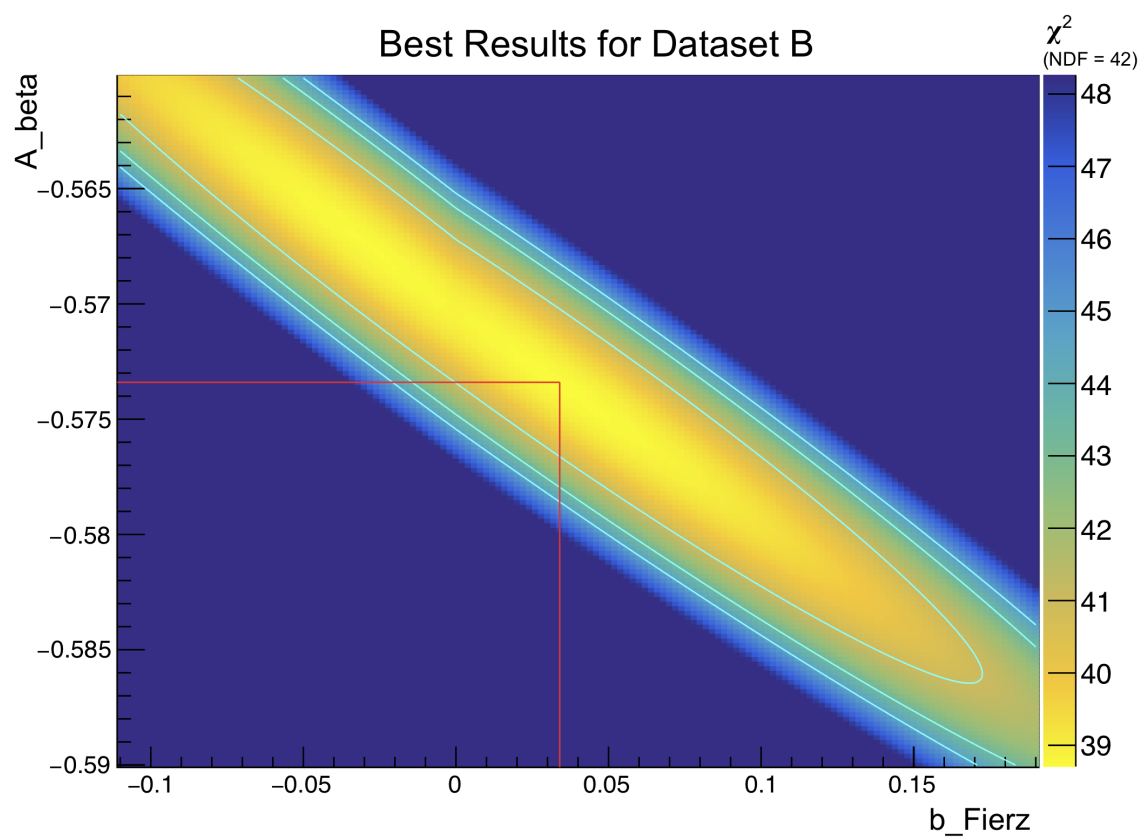


Figure 6.4: A χ^2 map to compare data from Runset B to a parameter space of A_β and b_{Fierz} values.

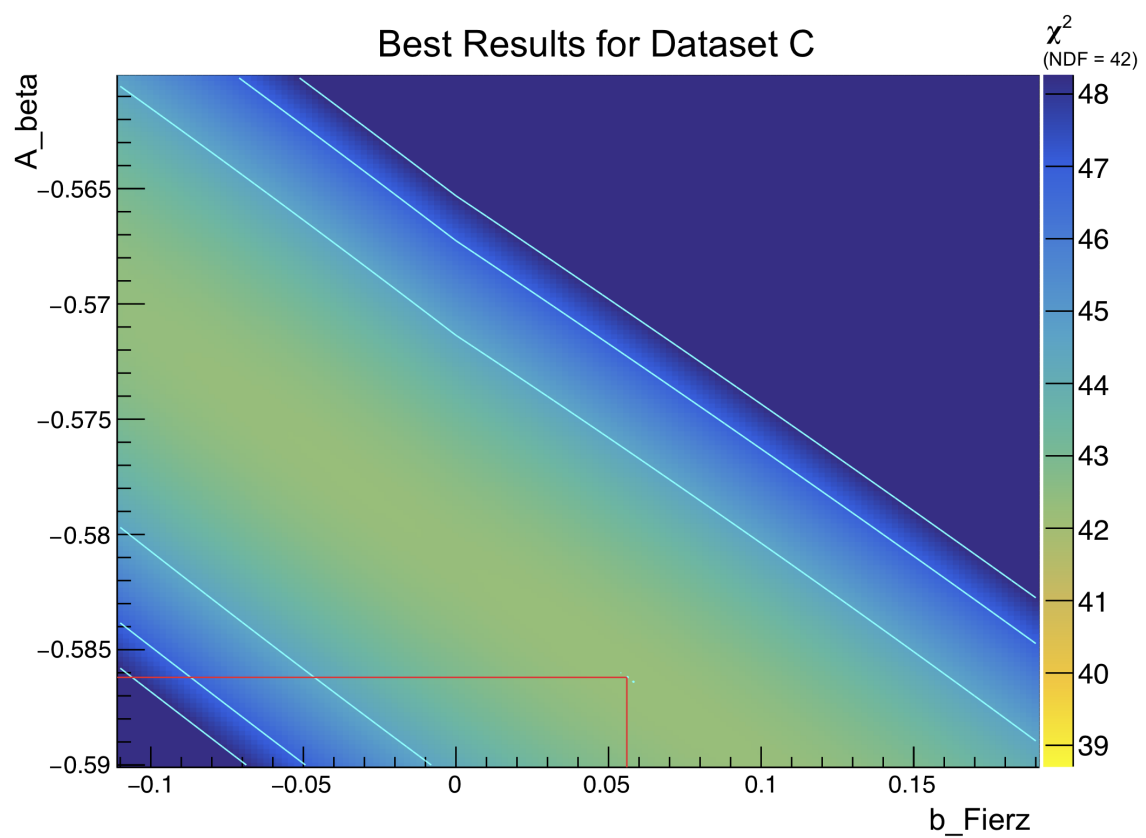


Figure 6.5: A χ^2 map to compare data from Runset C to a parameter space of A_β and b_{Fierz} values.

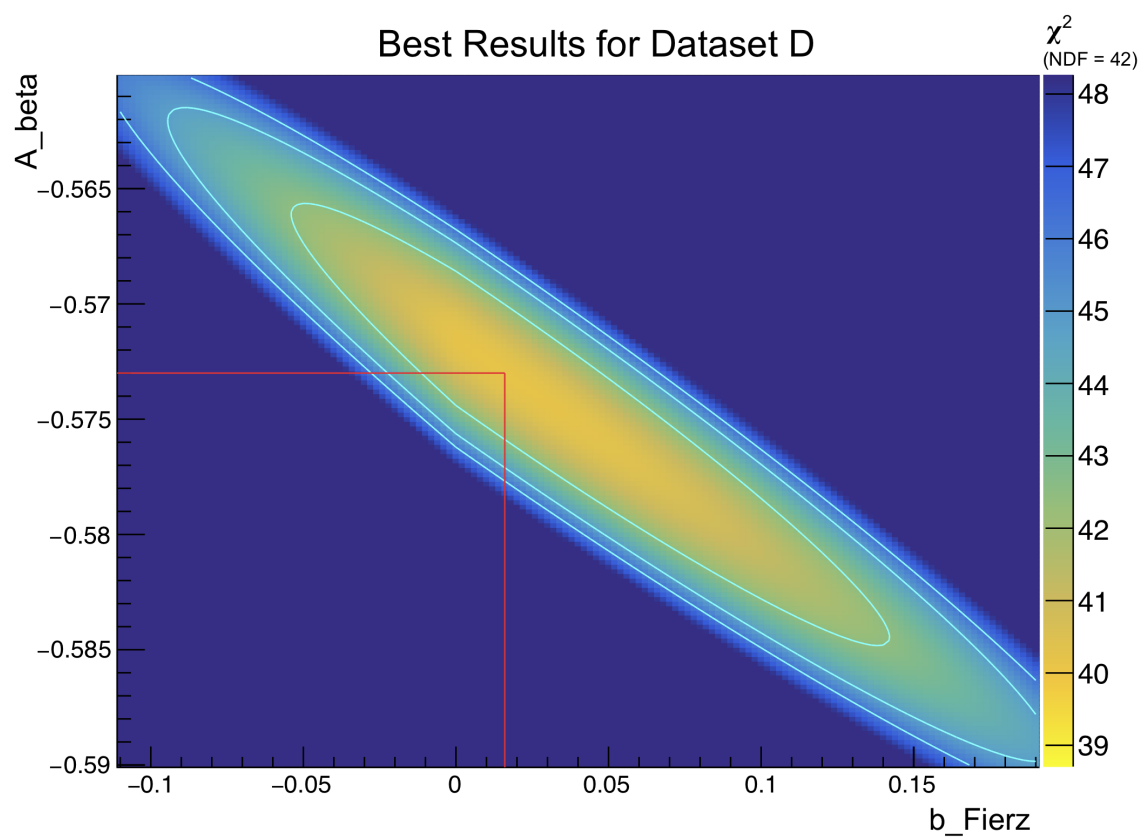


Figure 6.6: A χ^2 map to compare data from Runset D to a parameter space of A_β and b_{Fierz} values.

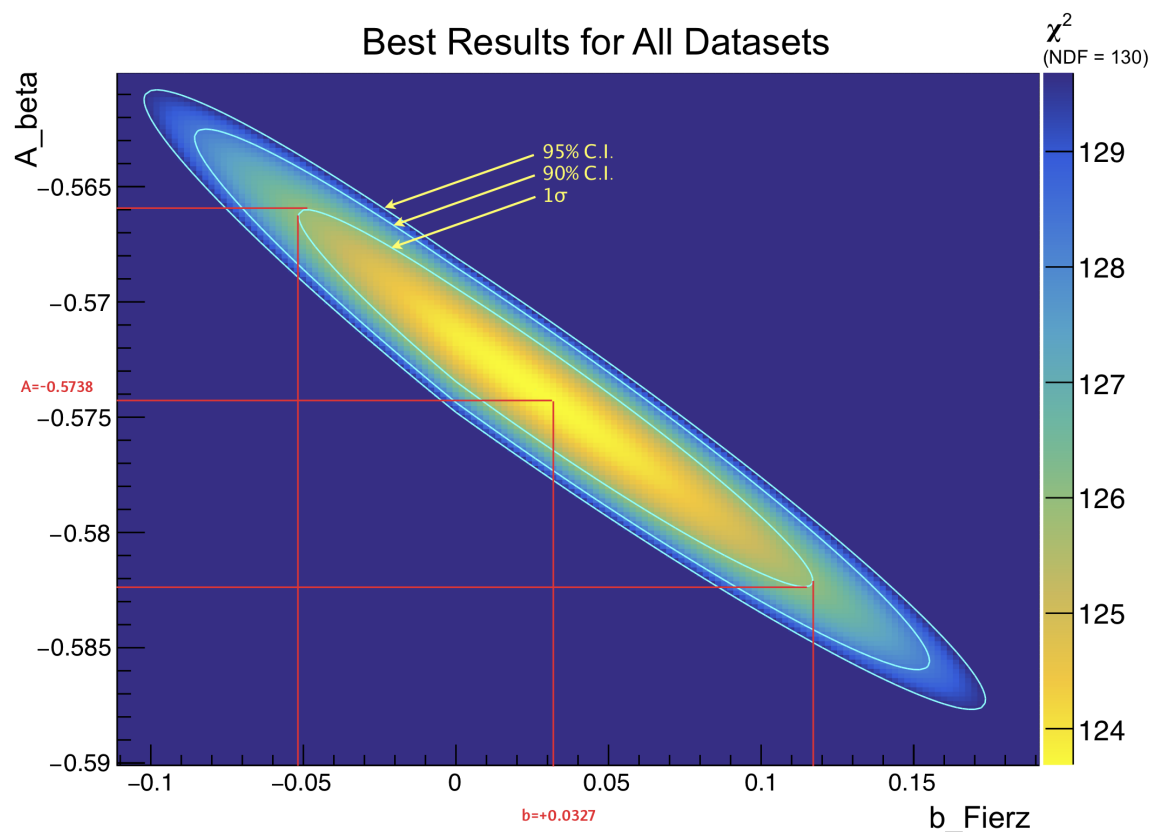


Figure 6.7: A χ^2 map to compare all data to a parameter space of A_β and b_{Fierz} values.

6.4 Other Possible Future Work for the Collaboration: R_{slow}

Probably shouldn't get a clearpage in the end. It's for my sanity during writing.

John says the whole R_{slow} thing should go in here somewhere.

Appendix I keep, it's excellent. It should be moved as is to Conclusions under "Future Experiment for the collaboration"! so people know you worked so hard on it!!

The nuclear weak force is known to be a predominantly left-handed vector and axial-vector (V-A) interaction. An experiment is proposed to further test that observation, constraining the strength of right-handed (V+A) currents by exploiting the principle of conservation of angular momentum within a spin-polarized beta decay process. Here, we focus on the decay ${}^{37}\text{K} \rightarrow {}^{37}\text{Ar} + \beta^+ + \nu_e$. The angular correlations between the emerging daughter particles provide a rich source of information about the type of interaction that produced the decay.

6.4.1 Motivation

The nuclear weak force has long been known to be a predominantly left-handed chiral interaction, meaning that immediately following an interaction (such as a beta decay) with a weak force carrying boson (W^+ , W^- , Z), normal-matter leptons (such as the electron and electron neutrino) emerge with left-handed chirality while the anti-leptons (e.g. the positron and electron anti-neutrino) emerge with right-handed chirality. In the limit of massless particles, the particle's chirality is the same as its helicity. Thus, in a left-handed model, the direction of an (ultrarelativistic) normal lepton's spin is antiparallel direction of its motion, and the direction of spin for an anti-lepton is parallel to its direction of motion. For a non-relativistic particle the property of chirality is fairly abstract, and describes the appropriate group representation and projection operators to be used in calculations. It should be noted that a fully chiral model is also one which is maximally parity violating.

This odd quirk of the nuclear weak force is not only *predominantly* true, but it is, to the best of our current scientific knowledge, *always* true – that is, attempts to measure any right-handed chiral components of the weak force have produced results consistent with zero [14][29]. This project proposes a further measurement to constrain the strength of the right-handed component of the weak interaction.

6.4.2 The Decay Process

The kinematics of nuclear β^+ decay are described by the following probability density function:

$$\begin{aligned}
W(\langle I \rangle | E_\beta \hat{\Omega}_\beta \hat{\Omega}_\nu) = & \left(\frac{1}{2\pi} \right)^5 F(-Z, E_\beta) p_\beta E_\beta (E_0 - E_\beta)^2 dE_\beta d\hat{\Omega}_\beta d\hat{\Omega}_\nu \xi \\
& \times \left[1 + a_{\beta\nu} \frac{\vec{p}_\beta \cdot \vec{p}_\nu}{E_\beta E_\nu} + b_{\text{Fierz}} \frac{m_e}{E_\beta} \right. \\
& + c_{\text{align}} \left(\frac{\frac{1}{3} \vec{p}_\beta \cdot \vec{p}_\nu - (\vec{p}_\beta \cdot \hat{j})(\vec{p}_\nu \cdot \hat{j})}{E_\beta E_\nu} \right) \left(\frac{I(I+1) - 3\langle (\vec{I} \cdot \hat{i})^2 \rangle}{I(2I-1)} \right) \\
& \left. + \frac{\langle \vec{I} \rangle}{I} \left(A_\beta \frac{\vec{p}_\beta}{E_\beta} + B_\nu \frac{\vec{p}_\nu}{E_\nu} + D_{\text{TR}} \frac{\vec{p}_\beta \times \vec{p}_\nu}{E_\beta E_\nu} \right) \right], \quad (6.1)
\end{aligned}$$

where \vec{I} is the nuclear spin-polarization, $F(-Z, E_\beta)$ is the Fermi function, and parameters ξ , $a_{\beta\nu}$, b_{Fierz} , c_{align} , A_β , B_ν , and D_{TR} are functions that vary with the strengths of the vector, axial, scalar, and tensor couplings (constant throughout nature), as well as the Fermi and Gamow-Teller nuclear matrix elements (specific to the individual decay) [6][16].

The decay may be treated as a three-body problem in which the available kinetic energy is divided up between the beta, the neutrino, and the recoiling ^{37}Ar nucleus, and (of course) the total linear and angular momentum are conserved. While the neutrino cannot be detected directly, its kinematics may be reconstructed from observations of the beta and the recoiling daughter nucleus. By placing detectors above and below the decaying atom along the axis of its polarization, we are able to obtain information about the outgoing beta's energy and momentum, in the cases of interest to us, where it is emitted along (or close to) the axis of polarization.

The recoiling ^{37}Ar nucleus is a bit trickier to work with, but the task is not impossible. One useful feature of the $^{37}\text{K} \rightarrow {}^{37}\text{Ar}$ transition is that, in addition to the β^+ emitted in the decay itself, one or more *orbital* electrons from the parent atom are typically lost. In the majority of decay events only one orbital electron is ‘shaken off’ and so the daughter ^{37}Ar atom is electrically neutral [20][30]. In the remaining cases, two or more orbital electrons are lost this way, and the daughter atom is positively charged. If we apply an electric field perpendicular to the direction of polarization,

these positively charged $^{37}\text{Ar}^{(+n)}$ ions may be collected into a detector, from which hit position and time of flight information may be extracted. These shake-off electrons are emitted with an average energy of only $\sim 2\text{ eV}$ so to a very good approximation the other decay products are not perturbed by the presence of shake-off electrons.

It should be noted that for the class of decays of greatest interest, where the beta and the neutrino emerge back-to-back along the polarization axis, the recoiling daughter nucleus will have zero momentum along the directions perpendicular to this axis, and on average less total energy than if the beta and neutrino were emitted in a parallel direction. Henceforth, daughter nuclei from a back-to-back decay as shown in Figure ?? will be described as ‘slow’ recoils. In terms of observables, this means that if the electric field is configured to point along one of the axes perpendicular to the polarization direction, then when the recoiling ion is swept away into a detector, the slow recoil’s hit position should be exactly along the projection of the polarization axis. Furthermore, the slow recoil’s time of flight should be in the middle of the time of flight spectrum, since other recoils will be emitted with momentum towards or away from the detector.

6.4.3 Status of the R_{slow} Measurement

In June 2014, after several years of preparatory work beforehand (the author has been continuously involved with this project since 2010), approximately 7 days of beam time at TRIUMF was dedicated to the TRINAT ^{37}K beta decay experiment. Approximately half of this data is suitable for use in this project. During this period, approximately 10,000 atoms were held within the trap at any given time. The cleaned spectra show around 50,000 polarized beta-recoil coincidence events in total, divided among measurements at three different electric field strengths (535 V/cm, 415 V/cm, 395 V/cm).

A fit to simulation has shown that the data that has already been collected has sufficient statistical power to measure the *fractional* contribution of any polarized ‘new physics’ beta decay parameter (ie right-handed, scalar, and tensor currents within the weak interaction) to a sensitivity of $\sim 2\%$ of its true value. Systematic limitations are still being assessed.

6.5 Conclusions

Conclusions go here.

Bibliography

- [1] Anholm, M., Characterizing the AC-MOT, Master's thesis, University of British Columbia, 2014.
- [2] Fenker, B., Behr, J. A., Melconian, D., Anderson, R. M. A., Anholm, M., Ashery, D., Behling, R. S., Cohen, I., Craiciu, I., Donohue, J. M., Farfan, C., Friesen, D., Gorelov, A., McNeil, J., Mehlman, M., Norton, H., Olchanski, K., Smale, S., Thériault, O., Vantyghem, A. N. and Warner, C. L., *Precision measurement of the nuclear polarization in laser-cooled, optically pumped ^{37}K* , New Journal of Physics, Vol. 18, No. 7, pp. 073028, 2016.
- [3] Wu, C. S., Ambler, E., Hayward, R. W., Hopps, D. D. and Hudson, R. P., *Experimental Test of Parity Conservation in Beta Decay*, Phys. Rev., Vol. 105, pp. 1413–1415, Feb 1957.
- [4] Lee, T.-D. and Yang, C.-N., *Question of parity conservation in weak interactions*, Physical Review, Vol. 104, No. 1, pp. 254, 1956.
- [5] Hong, R., Sternberg, M. G. and Garcia, A., *Helicity and nuclear β decay correlations*, American Journal of Physics, Vol. 85, No. 1, pp. 45–53, 2017.
- [6] Jackson, J. D., Treiman, S. B. and Wyld, H. W., *Possible Tests of Time Reversal Invariance in Beta Decay*, Phys. Rev., Vol. 106, pp. 517–521, May 1957.
- [7] Sun, X., Adamek, E., Allgeier, B., Bagdasarova, Y., Berguno, D. B., Blatnik, M., Bowles, T. J., Broussard, L. J., Brown, M. A.-P., Carr, R., Clayton, S., Cude-Woods, C., Currie, S., Dees, E. B., Ding, X., Filippone, B. W., García, A., Geltenbort, P., Hasan, S., Hickerson, K. P., Hoagland, J., Hong, R., Holley, A. T., Ito, T. M., Knecht, A., Liu, C.-Y., Liu, J., Makela, M., Mammei, R., Martin,

- J. W., Melconian, D., Mendenhall, M. P., Moore, S. D., Morris, C. L., Nepal, S., Nouri, N., Pattie, R. W., Pérez Gálvan, A., Phillips, D. G., Picker, R., Pitt, M. L., Plaster, B., Salvat, D. J., Saunders, A., Sharapov, E. I., Sjue, S., Slutsky, S., Sondheim, W., Swank, C., Tatar, E., Vogelaar, R. B., VornDick, B., Wang, Z., Wei, W., Wexler, J. W., Womack, T., Wrede, C., Young, A. R. and Zeck, B. A., *Improved limits on Fierz interference using asymmetry measurements from the Ultracold Neutron Asymmetry (UCNA) experiment*, Phys. Rev. C, Vol. 101, pp. 035503, Mar 2020.
- [8] Saul, H., Roick, C., Abele, H., Mest, H., Klopff, M., Petukhov, A. K., Soldner, T., Wang, X., Werder, D. and Märkisch, B., *Limit on the Fierz Interference Term b from a Measurement of the Beta Asymmetry in Neutron Decay*, Phys. Rev. Lett., Vol. 125, pp. 112501, Sep 2020.
- [9] Harvey, M. and Murray, A. J., *Cold Atom Trap with Zero Residual Magnetic Field: The AC Magneto-Optical Trap*, Phys. Rev. Lett., Vol. 101, pp. 173201, Oct 2008.
- [10] Levinger, J. S., *Effects of Radioactive Disintegrations on Inner Electrons of the Atom*, Phys. Rev., Vol. 90, pp. 11–25, Apr 1953.
- [11] de Shalit, A. and Talmi, I., Nuclear Shell Theory, Nuclear Shell Theory, Academic Press, 1963.
- [12] Falkowski, A., González-Alonso, M. and Naviliat-Cuncic, O., *Comprehensive analysis of beta decays within and beyond the Standard Model*, Journal of High Energy Physics, Vol. 2021, No. 4, pp. 1–36, 2021.
- [13] Krane, K. S., Introductory Nuclear Physics, Wiley, New York, 1988.
- [14] Severijns, N., Beck, M. and Naviliat-Cuncic, O., *Tests of the standard electroweak model in nuclear beta decay*, Rev. Mod. Phys., Vol. 78, pp. 991–1040, September 2006.
- [15] Wong, S., Introductory Nuclear Physics, Prentice Hall Advanced Reference Series Prentice Hall Labora, Prentice Hall, 1990.

- [16] Jackson, J. D., Treiman, S. B. and Wyld, H. W., *Coulomb Corrections in Allowed Beta Transitions*, Nuclear Physics, Vol. 4, pp. 206–212, Nov. 1957.
- [17] Holstein, B. R., *Recoil effects in allowed beta decay: The elementary particle approach*, Reviews of Modern Physics, Vol. 46, No. 4, pp. 789–814, Oct. 1974.
- [18] Raab, E. L., Prentiss, M., Cable, A., Chu, S. and Pritchard, D. E., *Trapping of Neutral Sodium Atoms with Radiation Pressure*, Phys. Rev. Lett., Vol. 59, pp. 2631–2634, Dec 1987.
- [19] Corney, A., Atomic and Laser Spectroscopy, Oxford University Press, New York, 1977.
- [20] Gorelov, A., Behr, J., Melconian, D., Trinczek, M., Dubé, P., Häusser, O., Giesen, U., Jackson, K., Swanson, T., D'Auria, J., Dombsky, M., Ball, G., Buchmann, L., Jennings, B., Dilling, J., Schmid, J., Ashery, D., Deutsch, J., Alford, W., Asgeirsson, D., Wong, W. and Lee, B., *Beta-neutrino correlation experiments on laser trapped ^{38m}K , ^{37}K* , Hyperfine Interactions, Vol. 127, No. 1, pp. 373–380, 2000.
- [21] Swanson, T. B., Asgeirsson, D., Behr, J. A., Gorelov, A. and Melconian, D., *Efficient transfer in a double magneto-optical trap system*, J. Opt. Soc. Am. B, Vol. 15, No. 11, pp. 2641–2645, Nov 1998.
- [22] Fenker, B., Gorelov, A., Melconian, D., Behr, J. A., Anholm, M., Ashery, D., Behling, R. S., Cohen, I., Craiciu, I., Gwinner, G., McNeil, J., Mehlman, M., Olchanski, K., Shidling, P. D., Smale, S. and Warner, C. L., *Precision Measurement of the β Asymmetry in Spin-Polarized ^{37}K Decay*, Phys. Rev. Lett., Vol. 120, pp. 062502, Feb 2018.
- [23] Audi, G., Wapstra, A. and Thibault, C., *The AME2003 Atomic Mass Evaluation*, Nuclear Physics A, Vol. 729, No. 1, pp. 337 – 676, 2003.
- [24] Fenker, B. B., Precise measurement of the β -asymmetry in the decay of magneto-optically trapped, spin-polarized ^{37}K , Ph.D. thesis, 2016.
- [25] Behling, R. S., Measurement of the Standard Model Beta Asymmetry Parameter, β , in ^{37}K , Ph.D. thesis, 2015.

- [26] Clifford, E., Hagberg, E., Koslowsy, V., Hardy, J., Schmeing, H. and Azuma, R., *Measurements of the response of a hybrid detector telescope to mono-energetic beams of positrons and electrons in the energy range 0.8–3.8 MeV*, Nuclear Instruments and Methods in Physics Research, Vol. 224, No. 3, pp. 440–447, 1984.
- [27] Landau, L. D., *On the energy loss of fast particles by ionization*, J. Phys., Vol. 8, pp. 201–205, 1944.
- [28] Moyal, J., *XXX. Theory of ionization fluctuations*, The London, Edinburgh, and Dublin Philosophical Magazine and Journal of Science, Vol. 46, No. 374, pp. 263–280, 1955.
- [29] Severijns, N. and Naviliat-Cuncic, O., *Symmetry tests in nuclear beta decay*, Annual Review of Nuclear and Particle Science, Vol. 61, pp. 23–46, 2011.
- [30] Melconian, D. G., Measurement of the Neutrino Asymmetry in the Beta Decay of Laser-Cooled, Polarized ^{37}K , Ph.D. thesis, Simon Fraser University, 2005.
- [31] Holstein, B. R., *Erratum: Recoil effects in allowed beta decay: The elementary particle approach*, Rev. Mod. Phys., Vol. 48, pp. 673–673, Oct 1976.

The citation format I'm using is really stupid. You **must** force yourself to ignore this right now, Melissa!

Appendix A

Notable Differences in Data Selection between this and the Previous Result

JB says Appendix A should all go in the analysis section, and not in an appendix at all.

JB says: Appendix A (ie, *this appendix*) is very important, and should at least be a subsection in the Analysis chapter.

...

You could condense the Appendix into a set of bullet points at the end of the intro to the Analysis section (which you still need, badly!), and then its content could be interleaved in the Analysis chapter. E.g. you already have redundancy in the LE and TE discussion vs. the Appendix, and the discussion is more complete in the Analysis chapter, which is good.

I really want this appendix to stay here. I'll make sure to mention everything in the body of the thesis though, since it *is* important. But at some point, somebody is going to really want to have this info written into a short summary.

A.1 Polarization Cycle Selection

Data used for our recent PRL article was slightly less polarized than we thought it was, due to an oversight in the data selection procedure.

A.2 Leading Edge / Trailing Edge and Walk Correction

Using the leading edge rather than the trailing edge to mark the timing of TDC pulses cleans up jitter, eliminates background, and changes the relative delays between different inputs. It is immediately relevant to the shape of the ‘walk correction’ on scintillator timing pulses, which give a different prediction for beta arrival time as a function of scintillator energy.

A.3 TOF Cut + Background Modelling

A SOE-beta time-of-flight cut is necessary to reduce background. The above mentioned walk correction directly results in an change in which specific events are selected in a given TOF cut. It further results in an adjustment to the expected fraction of background events in any such cut.

A.4 BB1 Radius

Possibly my default radius cut on the DSSDs is a bit different. The region of the parameter space that I’m taking for the systematic uncertainty on this is definitely a bit different.

Somebody will surely ask for a justification for why I did this differently, and I don’t have one beyond “this seemed more reasonable to me”, which is of course nobody will ever accept as a reason.

A.5 BB1 Energy Threshold

I use an overall 50 keV threshold, (taking +/- 10 keV from that as a systematic to be propagated/checked), but I think Ben used 60 keV.

Appendix B

A PDF For The People

John says to keep this appendix, because it's great now.

B.1 JTW

Here's a master equation from JTW to describe beta decay kinematics [6], [16]:

$$\begin{aligned} d^5\Gamma_{\text{JTW}} \equiv & \frac{F_{\mp}(Z, E_\beta)}{(2\pi)^5} p_\beta E_\beta (E_0 - E_\beta)^2 dE_\beta d^3\hat{\Omega}_\beta d^3\hat{\Omega}_\nu \\ & \times \xi \left[1 + a_{\beta\nu} \frac{\vec{p}_\beta \cdot \vec{p}_\nu}{E_\beta E_\nu} + b_{\text{Fierz}} \frac{m_e c^2}{E_\beta} + c_{\text{align}} T_{\text{align}}(\vec{J}) \left(\frac{\vec{p}_\beta \cdot \vec{p}_\nu}{3E_\beta E_\nu} - \frac{(\vec{p}_\beta \cdot \hat{\vec{j}})(\vec{p}_\nu \cdot \hat{\vec{j}})}{E_\beta E_\nu} \right) \right. \\ & \left. + \frac{\vec{J}}{J} \cdot \left(A_\beta \frac{\vec{p}_\beta}{E_\beta} + B_\nu \frac{\vec{p}_\nu}{E_\nu} + D_{\text{TR}} \frac{\vec{p}_\beta \times \vec{p}_\nu}{E_\beta E_\nu} \right) \right] \end{aligned} \quad (\text{B.1})$$

where, for convenience, we have defined a nuclear alignment term,

$$T_{\text{align}}(\vec{J}) \equiv \frac{J(J+1) - 3\langle(\vec{J} \cdot \hat{\vec{j}})^2\rangle}{J(2J-1)}. \quad (\text{B.2})$$

Note that this master equation depends on neutrino momentum, which we cannot observe directly. Furthermore, we cannot reconstruct neutrino momenta in our decay events either, because it would be necessary to account for the momentum of the recoiling daughter nucleus, treating the decay as a three-body problem. From

We have already specialized to β^+ decay.

an experimental standpoint, we failed to measure the momenta of the daughters in conjunction with the “tagged” beta decay events with which we are primarily concerned in this thesis. From a theoretical standpoint, JTW has intentionally neglected recoil-order terms – meaning that the daughter nucleus is treated, for the purpose of kinetic energy calculations, as being infinitely massive, and as such it must have no change in kinetic energy from the decay. This approximation makes it a bit tricky to correctly re-formulate Eq. (B.1) in terms of the momentum of the daughter instead of the momentum of the neutrino.

Fortunately, it is possible to simplify Eq. (B.1) by integrating over all possible neutrino directions, such that the result no longer depends on parameters that we do not observe. The neutrino energy itself is not a free variable in this equation, because the energy release in the decay is fixed, and given the approximation that none of that energy is allocated to the recoiling daughter, it is very straightforward to calculate the neutrino energy for a decay event in which the beta energy is known.

The result of performing this integration over neutrino direction is:

$$\begin{aligned} d^3\Gamma dE_\beta d^3\hat{\Omega}_\beta &= \frac{2}{(2\pi)^4} F_{\mp}(Z, E_\beta) p_\beta E_\beta (E_0 - E_\beta)^2 dE_\beta d^3\hat{\Omega}_\beta \xi \\ &\times \left[1 + b_{\text{Fierz}} \frac{m_e c^2}{E_\beta} + A_\beta \left(\frac{\vec{J}}{J} \cdot \frac{\vec{p}_\beta}{E_\beta} \right) \right], \end{aligned} \quad (\text{B.3})$$

which is a great simplification on Eq. (B.1). We still must write the remaining parameters in terms of the relevant nuclear matrix elements and fundamental coupling constants. These coupling constants are, in general, complex-valued, and JTW does not choose a phase angle for us. We write them out in Eqs. (B.4-B.6).

$$\begin{aligned} \xi &= |M_F|^2 (|C_S|^2 + |C_V|^2 + |C'_S|^2 + |C'_V|^2) \\ &+ |M_{GT}|^2 (|C_T|^2 + |C_A|^2 + |C'_T|^2 + |C'_A|^2) \end{aligned} \quad (\text{B.4})$$

$$b_{\text{Fierz}} \xi = \pm 2\gamma \text{Re} [|M_F|^2 (C_S C_V^* + C'_S C_V'^*) + |M_{GT}|^2 (C_T C_A^* + C'_T C_A'^*)] \quad (\text{B.5})$$

$$\begin{aligned} A_\beta \xi &= |M_{GT}|^2 \lambda_{J'J} \left[\pm 2\text{Re}[C_T C_T'^* - C_A C_A'^*] + 2 \frac{\alpha Z m_e}{p_\beta} \text{Im}[C_T C_A'^* + C'_T C_A^*] \right] \\ &+ \delta_{J'J} M_F M_{GT} \left(\frac{J}{J+1} \right)^{1/2} \left[2 \text{Re}[C_S C_T'^* + C'_S C_T^* - C_V C_A'^* - C'_V C_A^*] \right. \\ &\left. \pm 2 \frac{\alpha Z m_e}{p_\beta} \text{Im}[C_S C_A'^* + C'_S C_A^* - C_V C_T'^* - C'_V C_T^*] \right] \end{aligned} \quad (\text{B.6})$$

Note that JTW presents slightly different expressions for the sign convention in components of A_β within [6] and [16]. Here, we adopt the convention from the latter publication. Furthermore, we do not require that either M_F or M_{GT} be positive (which would allow us to safely drop their absolute value indicators and make the conventions of these two papers equivalent). In order to obtain the correct, physically observed value for A_β , we require that the $M_F M_{GT}$ term in Eq. (B.6) have an overall positive value. Because we know that the scalar and tensor couplings must be small, and any imaginary contributions to the term must be small, we conclude that

$$M_F M_{GT} (C_V C_A'^* + C_V' C_A^*) < 0. \quad (\text{B.7})$$

Also, $\xi = G_v^2 \cos \theta_C f_1(E)$.

B.2 Holstein

Holstein [17] [31] generously provides explicit equations to match both Eq. (B.1) (i.e. Holstein's Eq. (51), where neutrino direction is a parameter of the probability distribution) and Eq. (B.3) (Holstein's Eq. (52), where neutrino direction has already been integrated over).

Here's Holstein's Eq. (52):

$$\begin{aligned} d^3\Gamma_{\text{Holstein}} &= 2G_v^2 \cos^2 \theta_c \frac{F_\mp(Z, E_\beta)}{(2\pi)^4} p_\beta E_\beta (E_0 - E_\beta)^2 dE_\beta d^3\hat{\Omega}_\beta \\ &\times \left\{ F_0(E_\beta) + \Lambda_1 F_1(E_\beta) \hat{\mathbf{n}} \cdot \frac{\vec{p}_\beta}{E_\beta} + \Lambda_2 F_2(E_\beta) \left[\left(\hat{\mathbf{n}} \cdot \frac{\vec{p}_\beta}{E_\beta} \right)^2 - \frac{1}{3} \frac{p_\beta^2}{E_\beta^2} \right] \right. \\ &\left. + \Lambda_3 F_3(E_\beta) \left[\left(\hat{\mathbf{n}} \cdot \frac{\vec{p}_\beta}{E_\beta} \right)^3 - \frac{3}{5} \frac{p_\beta^2}{E_\beta^2} \hat{\mathbf{n}} \cdot \frac{\vec{p}_\beta}{E_\beta} \right] \right\} \end{aligned} \quad (\text{B.8})$$

A careful reader will eventually note that Holstein's spectral functions $F_i(E_\beta)$ are not the same as the $F_i(E_\beta, u, v, s)$ in any limit, despite the notational similarities. Among other rules, Holstein's spectral functions obey these:

$$F_i(E_\beta) \neq F_i(E_\beta, u, v, s) \quad (\text{B.9})$$

$$F_i(E_\beta) = H_i(E_\beta, u, v, 0) \quad (\text{B.10})$$

$$f_i(E_\beta) = F_i(E_\beta, u, v, 0). \quad (\text{B.11})$$

For the $F_i(E_\beta)$ functions of interest to us here, we find the following relationships:

$$\begin{aligned}
F_0(E_\beta) &= H_0(E_\beta, J, J', 0) = F_1(E_\beta, J, J', 0) &= f_1(E_\beta) \\
F_1(E_\beta) &= H_1(E_\beta, J, J', 0) = F_4(E_\beta, J, J', 0) + \frac{1}{3}F_7(E_\beta, J, J', 0) &= f_4(E_\beta) + \frac{1}{3}f_7(E_\beta) \\
F_2(E_\beta) &= H_2(E_\beta, J, J', 0) = F_{10}(E_\beta, J, J', 0) + \frac{1}{2}F_{13}(E_\beta, J, J', 0) &= f_{10}(E_\beta) + \frac{1}{3}f_{13}(E_\beta) \\
F_3(E_\beta) &= H_3(E_\beta, J, J', 0) = F_{18}(E_\beta, J, J', 0) &= f_{18}(E_\beta). \quad (\text{B.12})
\end{aligned}$$

Note that the $f_i(E_\beta)$ in Eq. B.12 are the same spectral functions used to describe a polarized decay spectrum when the neutrino (ie, the recoil) is also observed – though of course such a spectrum must have other terms as well. For the spectrum of interest to us here, in which the neutrino direction has already been integrated over, we can simply look up the $H_i(E_\beta, J, J', 0) = H_i(E, u, v, s=0)$ spectral functions, and leave it at that. We find:

$$\begin{aligned}
F_0(E_\beta) &= |a_1|^2 + 2 \operatorname{Re}[a_1^* a_2] \frac{1}{3M^2} \left[m_e^2 + 4E_\beta E_0 + 2 \frac{m_e^2}{E_\beta} E_0 - 4E_\beta^2 \right] \\
&\quad + |c_1|^2 + 2 \operatorname{Re}[c_1^* c_2] \frac{1}{9M^2} \left[11m_e^2 + 20E_\beta E_0 - 2 \frac{m_e^2}{E_\beta} E_0 - 20E_\beta^2 \right] \\
&\quad - 2 \frac{E_0}{3M} \operatorname{Re}[c_1^*(c_1 + d \pm b)] + \frac{2E_\beta}{3M} (3|a_1|^2 + \operatorname{Re}[c_1^*(5c_1 \pm 2b)]) \\
&\quad - \frac{m_e^2}{3ME_\beta} \operatorname{Re} \left[-3a_1^* e + c_1^* \left(2c_1 + d \pm 2b - h \frac{E_0 - E_\beta}{2M} \right) \right] \quad (\text{B.13})
\end{aligned}$$

$$\begin{aligned}
F_1(E_\beta) &= \delta_{u,v} \left(\frac{u}{u+1} \right)^{1/2} \left\{ 2 \operatorname{Re} \left[a_1^* \left(c_1 - \frac{E_0}{3M} (c_1 + d \pm b) + \frac{E_\beta}{3M} (7c_1 \pm b + d) \right) \right] \right. \\
&\quad + 2 \operatorname{Re}[a_1^* c_2 + c_1^* a_2] \left(\frac{4E_\beta(E_0 - E_\beta) + 3m_e^2}{3M^2} \right) \Big\} \\
&\quad \mp \frac{(-1)^s \gamma_{u,v}}{u+1} \operatorname{Re} \left\{ c_1^* \left(c_1 + 2c_2 \left(\frac{8E_\beta(E_0 - E_\beta) + 3m_e^2}{3M^2} \right) - \frac{2E_0}{3M} (c_1 + d \pm b) \right. \right. \\
&\quad \left. \left. + \frac{E_\beta}{3M} (11c_1 - d \pm 5b) \right) \right\} + \frac{\lambda_{u,v}}{u+1} \operatorname{Re} \left\{ c_1^* \left[-f \left(\frac{5E_\beta}{M} \right) \right. \right. \\
&\quad \left. \left. + g \left(\frac{3}{2} \right)^{1/2} \left(\frac{E_0^2 - 11E_0E_\beta + 6m_e^2 + 4E_\beta^2}{6M^2} \right) \pm 3j_2 \left(\frac{8E_\beta^2 - 5E_0E_\beta - 3m_e^2}{6M^2} \right) \right] \right\} \quad (\text{B.14})
\end{aligned}$$

$$\begin{aligned}
F_2(E_\beta) = & \theta_{u,v} \frac{E_\beta}{2M} \operatorname{Re} \left[c_1^* \left(c_1 + c_2 \frac{8(E_0 - E_\beta)}{3M} - d \pm b \right) \right] \\
& - \delta_{u,v} \frac{E_\beta}{M} \left[\frac{u(u+1)}{(2u-1)(2u+3)} \right]^{1/2} \operatorname{Re} \left\{ a_1^* \left(\left(\frac{3}{2}\right)^{1/2} f + g \frac{E_\beta + 2E_0}{4M} \right. \right. \\
& \left. \left. \pm \left(\frac{3}{2}\right)^{1/2} j_2 \frac{E_0 - E_\beta}{2M} \right) \right\} + (-1)^s \kappa_{u,v} \frac{E_\beta}{2M} \operatorname{Re} \left[c_1^* \left(\pm 3f \pm \left(\frac{3}{2}\right)^{1/2} g \frac{E_0 - E_\beta}{M} \right. \right. \\
& \left. \left. + 3j_2 \frac{E_0 - 2E_\beta}{2M} \right) \right] + \epsilon_{u,v} \operatorname{Re}[c_1^* j_3] \left(\frac{21E_\beta^2}{8M^2} \right)
\end{aligned} \tag{B.15}$$

$$\begin{aligned}
F_3(E_\beta) = & -\delta_{u,v} (3u^2 + 3u - 1) \left[\frac{u}{(u-1)(u+1)(u+2)(2u-1)(2u+3)} \right]^{1/2} \\
& \times \operatorname{Re}[a_1^* j_3] \left(\frac{E_\beta^2 \sqrt{15}}{4M^2} \right) + \frac{\rho_{u,v}}{u+1} \operatorname{Re} \left[c_1^* (g\sqrt{3} + j_2\sqrt{2}) \left(\frac{5E_\beta^2}{4M^2} \right) \right] \\
& \pm \frac{(-1)^s \sigma_{u,v}}{u+1} \operatorname{Re}[c_1^* j_3] \left(\frac{5E_\beta^2}{2M^2} \right)
\end{aligned} \tag{B.16}$$

and we might really appreciate if these things could be simplified a bit.

The terms $a_1, a_2, b, c_1, c_2, d, e, f, g, h, j_2, j_3$ are “structure functions”. Holstein gives some predictions for their form, assuming the impulse approximation holds, in his Eq. (67). For the most part, the values and form of these structure functions are beyond the scope of this thesis, so I will not re-write them all here. It should be noted that the numerical values used for these parameters came from a private communication from Ian Towner to the collaboration. However, it is important to note the expressions for a_i and c_i , because these will directly come into play when we try to reconcile Holstein’s expression with JTW’s. Therefore,

$$a(q^2) \approx \frac{g_V(q^2)}{\left(1 + \frac{\Delta}{2M}\right)} \left[M_F + \frac{1}{6}(q^2 - \Delta^2)M_{r^2} + \frac{1}{3}\Delta M_{\mathbf{r} \cdot \mathbf{p}} \right] \tag{B.17}$$

$$\begin{aligned}
c(q^2) \approx & \frac{g_A(q^2)}{\left(1 + \frac{\Delta}{2M}\right)} \left[M_{GT} + \frac{1}{6}(q^2 - \Delta^2)M_{\sigma r^2} + \frac{1}{6\sqrt{10}}(2\Delta^2 + q^2)M_{1y} \right. \\
& \left. + A \frac{\Delta}{2M} M_{\sigma L} + \frac{1}{2}\Delta M_{\sigma rp} \right]
\end{aligned} \tag{B.18}$$

There was something wrong with this assumption. Something circular. I forgot. Blah.

Somewhere I have to define q^2 and Δ are.

...where the M_{xxx} 's are certain nuclear matrix elements. However, Eqs. (B.13-B.16) are not written in terms of $a(q^2)$ and $c(q^2)$, but rather in terms of a_1 , a_2 , c_1 , and c_2 . In fact, Holstein is implicitly using series expansions to remove the dependence on recoil momentum, so that

$$a(q^2) = a_1 + \left(\frac{q^2}{M^2}\right) a_2 + \dots \quad (\text{B.19})$$

$$c(q^2) = c_1 + \left(\frac{q^2}{M^2}\right) c_2 + \dots \quad (\text{B.20})$$

Should I just list the values of things that I inherited from Ian Towner's personal communication that one time?

Next, Holstein goes and tweaks those $F_i(E_\beta)$ terms that we've already written out, by adding in an adjustment for Coulomb corrections. Those corrections have this form:

$$F_i(E_\beta) \rightarrow \tilde{F}_i(E_\beta) := F_i(Z, E_\beta) [F_i(E_\beta) + \Delta F_i(E_\beta)] \quad (\text{B.21})$$

To obtain expressions for the $\Delta F_i(E_\beta)$, Holstein invokes some Feynman diagrams and provides expressions for several integrals, all of which are both complex and complicated. The modified spectral functions are provided in terms of functions of these integrals. Since nobody wants to have to evaluate those integrals, Holstein makes a further approximation by taking only the first term in an expansion of the $\Delta F_i(E_\beta)$ in terms of $Z\alpha$, where $Z\alpha \ll 1$. Then, the resulting expressions for $\Delta F_i(E_\beta)$ can be written in terms of much more straightforward integrals over form factors for electric charge and weak charge.

If we make the further assumption that these form factors are identical, and that both types of charge are spread over a ball of uniform density with radius R , then we find:

$$X = Y = \frac{9\pi R}{140} \quad (\text{B.22})$$

and also, I think something like that the weak charge is the same distribution as the electric charge

in the Eqs. (B.23 - B.25) that follow.

Because Holstein doesn't actually write this stuff out in terms of $F_i(E_\beta)$, but rather in terms of $F_i(E_\beta, u, v, s)$, this correction presents yet another opportunity for the reader to interpret his notation incorrectly. We note that one must remember to make use of the relations in Eq. (B.12). Furthermore, Holstein notes that some of the terms $F_i(E_\beta, u, v, s)$ are suppressed already, and he does not consider those terms further. We will take this approximation to be adequate for our purposes here.

What is less clear, given the context in the paper, is whether or not when Holstein writes out his simplified expressions for $\Delta F_x(E_\beta, u, v, s)$ he actually means $F_\mp(Z, E_\beta)\Delta F_i(E_\beta, u, v, s)$. These terms are pretty small, so it probably doesn't *really* matter, but it would still be really nice to *know*, damn it.

So, we'll write out the functions for these corrections.

$$\begin{aligned}\Delta F_1(E_\beta, u, v, s) = & \mp \left(\frac{8\alpha Z}{3\pi} \right) X \left[E_\beta \left(8|a|^2 + \frac{28}{3}|c|^2 \right) + E_0 \left(|a|^2 - \frac{1}{3}|c|^2 \right) \right. \\ & \left. + 3 \left(\frac{m_e c^2}{E_\beta} \right) (|a|^2 + |c|^2) \right]\end{aligned}\quad (\text{B.23})$$

$$\Delta F_4(E_\beta, u, v, s) = \mp \left(\frac{8\alpha Z}{3\pi} \right) 9X E_\beta \left[2\delta_{u,v} \left(\frac{u}{u+1} \right)^{1/2} \text{Re}[a^*c] \mp (-1)^s \left(\frac{\gamma_{u,v}}{u+1} \right) |c|^2 \right]\quad (\text{B.24})$$

$$\begin{aligned}\Delta F_7(E_\beta, u, v, s) = & \mp \left(\frac{8\alpha Z}{3\pi} \right) X (E_0 - E_\beta) \left[2\delta_{u,v} \left(\frac{u}{u+1} \right)^{1/2} \text{Re}[a^*c] \right. \\ & \left. \mp (-1)^s \left(\frac{\gamma_{u,v}}{u+1} \right) |c|^2 \right]\end{aligned}\quad (\text{B.25})$$

We note that the above corrections have been written in terms of $a(q^2)$ and $c(q^2)$, and we must use Eqs. (B.19, B.20) to put the results in terms of a_1 , a_2 , c_1 , and c_2 so that they can be correctly combined with Eqs. (B.13-B.16).

If we evaluate Holstein's Eqs. (B8), which I will absolutely not type out here, for the case $u = v = J = J' = 3/2$, we find the following values:

$$\begin{aligned}\delta_{u,v} &= 1 & \theta_{u,v} &= 1 & \rho_{u,v} &= \frac{-41}{40} \\ \gamma_{u,v} &= 1 & \kappa_{u,v} &= \frac{1}{2\sqrt{2}} & \sigma_{u,v} &= \frac{-41}{4\sqrt{35}} \\ \lambda_{u,v} &= \frac{-\sqrt{2}}{5} & \epsilon_{u,v} &= \frac{-1}{2\sqrt{5}} & \phi_{u,v} &= 0\end{aligned}\quad (\text{B.26})$$

Furthermore, in our calculations here, we will be considering only the β^+ decay modes,

and therefore we take the *lower* sign when the option arises. We also will use $s = 0$, so that $(-1)^s = +1$.

Also, pretty sure one of those never gets used. Which one was it? idk.

- - - - -

Let's define some of that notation! Firstly,

$$\text{Holstein's } \hat{n} = \text{JTW's } \mathbf{j}, \quad (\text{B.27})$$

and the Λ_i are given by Holstein's Eq. (48):

$$\Lambda_1 := \frac{\langle M \rangle}{J} \quad (\text{B.28})$$

$$\Lambda_2 := 1 - \frac{3\langle M^2 \rangle}{J(J+1)} \quad (\text{B.29})$$

$$\Lambda_3 := \frac{\langle M \rangle}{J} - \frac{5\langle M^3 \rangle}{J(3J^2 + 3J - 1)}. \quad (\text{B.30})$$

We immediately see that Holstein's Λ_1 is closely related to JTW's $\frac{\vec{J}}{J}$, and a bit later after John points it out to us, we see that Holstein's Λ_2 is closely related to JTW's T_{align} . JTW doesn't have any equivalent to Λ_3 . In particular, we find:

$$\Lambda_1 \hat{\mathbf{j}} = \frac{\langle M \rangle}{J} \hat{\mathbf{j}} = \frac{\vec{\mathbf{J}}}{J} \quad (\text{B.31})$$

$$\Lambda_2 = T_{\text{align}} \frac{(2J-1)}{(J+1)}. \quad (\text{B.32})$$

Note: It's not the case that $|\vec{\mathbf{J}}| == J$. It's actually super fucking infuriating notation.

Appendix C

Comparing Notation between Holstein and JTW

I see some stuff in my old Appendix D that needs to be moved (in here? Or maybe in Old Appendix E) before it goes away forever.

JB: Appendix C has some redundancies with B. You will have to sort that out. (n.b.: from context, it's less clear which appendices he's actually talking about, but whatever, there's certainly redundancies all around.)

C.1 Comparison Guide

This is a short guide to differences in notation, sign convention, and normalization. There are several tables here, chosen to aid in conversion between the two conventions. This section also includes handwritten notes.

C.2 Imported from Another Appendix

Here are some equations. I want to keep these somewhere in this chapter. For the equations below, I am intentionally not including the ROC terms. We take only

Holstein	JTW	Thesis	Comments
k			Neutrino momentum 4-vector
	E_ν		Neutrino energy
\hat{k}	$\frac{\mathbf{p}_\nu}{E_\nu}$		3D Neutrino emission direction unit vector. Neutrinos are always treated as massless.
p			Beta momentum 4-vector, or sometimes the magnitude of the beta momentum 3-vector. Never the magnitude of the 4-vector.
E	E_e	E_β	Beta energy
\mathbf{p}	\mathbf{p}_e	\vec{p}_β	Beta momentum 3-vector
q			Recoil momentum 4-vector, or sometimes a magnitude.

Table C.1: A comparison of some kinematic terms in JTW [6] [16] and Holstein [17]. Yes, the bolding/italicization carries meaning.

Holstein	JTW	Comments
u	J	Initial state total nuclear angular momentum.
v	J'	Final state total nuclear angular momentum.
s	No equivalent?	Umm... I should check on this.

Table C.2: A comparison of some angular momenta in JTW [6] [16] and Holstein [17].

enough Holstein terms to construct the expressions JTW gives us.

$$\xi = G_v^2 \cos \theta_C f_1(E) \quad (\text{C.1})$$

$$a_{\beta\nu} = f_2(E) / f_1(E) \quad (\text{C.2})$$

$$\frac{\langle \vec{J} \rangle}{J} \cdot \frac{\vec{p}}{E} A_\beta = \Lambda_1 \hat{n} \cdot \frac{\vec{p}}{E} f_4(E) / f_1(E) \quad (\text{C.3})$$

$$\frac{\langle \vec{J} \rangle}{J} \cdot \frac{\vec{p}_\nu}{E_\nu} B_\nu = \Lambda_1 \hat{n} \cdot \vec{k} f_6(E) / f_1(E) \quad (\text{C.4})$$

$$\frac{\langle \vec{J} \rangle}{J} \cdot \frac{(\vec{p} \times \vec{p}_\nu)}{EE_\nu} D_{\text{TR}} = \Lambda_1 \hat{n} \cdot \left(\frac{\vec{p}}{E} \times \hat{k} \right) f_8(E) / f_1(E) \quad (\text{C.5})$$

Holstein	JTW	Thesis	Comments
$G_v^2 \cos \theta_C f_1(E)$	ξ	$\xi(E_\beta)$	Normalization. Proportional to the fractional decay rate.
\hat{n}	\mathbf{j}	$\hat{\mathbf{j}}$	Nuclear polarization unit vector. Also the axis of quantization.
J	J		Total nuclear angular momentum quantum number
$\langle M \rangle$	$ \langle \mathbf{J} \rangle $		Angular momentum projection along the axis of quantization
$\Lambda^{(1)} \hat{n} = \frac{\langle M \rangle}{J} \hat{n}$	$\frac{\langle \mathbf{J} \rangle}{J}$	$\Lambda_1 \hat{n}$	Dipole element vector. Proportional to nuclear polarization. <i>(Rephrase this.)</i>
$\Lambda^{(1)} = \frac{\langle M \rangle}{J}$...	Λ_1	...
$\Lambda^{(2)}$	$\frac{J(J+1)-3\langle(\vec{J}\cdot\hat{j})^2\rangle}{J(2J-1)} \frac{(2J-1)}{(J+1)}$	$T_{\text{align}}(\vec{J}) \frac{(2J-1)}{(J+1)}$	Quadrupole element
$\Lambda^{(3)}$	No equivalent	Λ_3	Octopole element
$\Lambda^{(4)}$	No equivalent	Λ_4	Hexadecapole element

Table C.3: A comparison of the multipole elements and their normalizations (and some other stuff) in JTW [6] [16] and Holstein [17].

$$\begin{aligned}
& \left[\frac{J(J+1)-3\langle(\vec{J}\cdot\hat{j})^2\rangle}{J(2J-1)} \right] \left[\frac{1}{3} \frac{\vec{p}\cdot\vec{p}_\nu}{EE_\nu} - \frac{(\vec{p}\cdot\hat{j})(\vec{p}_\nu\cdot\hat{j})}{EE_\nu} \right] c_{\text{align}} \\
&= \Lambda_2 \left[(\hat{n}\cdot\frac{\vec{p}}{E})(\hat{n}\cdot\hat{k}) - \frac{1}{3} (\frac{\vec{p}}{E}\cdot\hat{k}) \right] f_{12}(E) / f_1(E) \quad (C.6)
\end{aligned}$$

Term	Integral
$f_1(E_\beta)$	$\int 1 \mathrm{d}\hat{\Omega}_k = 4\pi$
$f_2(E_\beta)$	$\int \left(\frac{\vec{p}_\beta \cdot \hat{k}}{E_\beta} \right) \mathrm{d}\hat{\Omega}_k = 0$
$f_3(E_\beta)$	$\int \left(\left(\frac{\vec{p}_\beta \cdot \hat{k}}{E_\beta} \right)^2 - \frac{1}{3} \frac{p_\beta^2}{E_\beta^2} \right) \mathrm{d}\hat{\Omega}_k = 0$
$f_4(E_\beta)$	$\int \left(\hat{n} \cdot \frac{\vec{p}_\beta}{E_\beta} \right) \mathrm{d}\hat{\Omega}_k = 4\pi \left(\hat{n} \cdot \frac{\vec{p}_\beta}{E_\beta} \right)$
$f_5(E_\beta)$	$\int \left(\hat{n} \cdot \frac{\vec{p}_\beta}{E_\beta} \right) \left(\frac{\vec{p}_\beta \cdot \hat{k}}{E_\beta} \right) \mathrm{d}\hat{\Omega}_k = 0$
$f_6(E_\beta)$	$\int \left(\hat{n} \cdot \hat{k} \right) \mathrm{d}\hat{\Omega}_k = 0$
$f_7(E_\beta)$	$\int \left(\hat{n} \cdot \hat{k} \right) \left(\frac{\vec{p}_\beta \cdot \hat{k}}{E_\beta} \right) \mathrm{d}\hat{\Omega}_k = \frac{1}{3} 4\pi \left(\hat{n} \cdot \frac{\vec{p}_\beta}{E_\beta} \right)$
$f_8(E_\beta)$	$\int \hat{n} \cdot \left(\frac{\vec{p}_\beta \times \hat{k}}{E_\beta} \right) \mathrm{d}\hat{\Omega}_k = 0$
$f_9(E_\beta)$	$\int \hat{n} \cdot \left(\frac{\vec{p}_\beta \times \hat{k}}{E_\beta} \right) \left(\frac{\vec{p}_\beta \cdot \hat{k}}{E_\beta} \right) \mathrm{d}\hat{\Omega}_k = 0$
$f_{10}(E_\beta)$	$\int T_2(\hat{n}) : \left[\frac{\vec{p}_\beta}{E}, \frac{\vec{p}_\beta}{E} \right] \mathrm{d}\hat{\Omega}_k = 4\pi T_2(\hat{n}) : \left[\frac{\vec{p}_\beta}{E}, \frac{\vec{p}_\beta}{E} \right]$
$f_{11}(E_\beta)$	$\int T_2(\hat{n}) : \left[\frac{\vec{p}_\beta}{E}, \frac{\vec{p}_\beta}{E} \right] \left(\frac{\vec{p}_\beta \cdot \hat{k}}{E} \right) \mathrm{d}\hat{\Omega}_k = 0$
$f_{12}(E_\beta)$	$\int T_2(\hat{n}) : \left[\frac{\vec{p}_\beta}{E}, \hat{k} \right] \mathrm{d}\hat{\Omega}_k = 0$
$f_{13}(E_\beta)$	$\int T_2(\hat{n}) : \left[\frac{\vec{p}_\beta}{E}, \hat{k} \right] \left(\frac{\vec{p}_\beta \cdot \hat{k}}{E} \right) \mathrm{d}\hat{\Omega}_k = \frac{1}{3} 4\pi T_2(\hat{n}) : \left[\frac{\vec{p}_\beta}{E}, \frac{\vec{p}_\beta}{E} \right]$
$f_{14}(E_\beta)$	$\int T_2(\hat{n}) : \left[\hat{k}, \hat{k} \right] \mathrm{d}\hat{\Omega}_k = 0$
$f_{15}(E_\beta)$	$\int T_2(\hat{n}) : \left[\hat{k}, \hat{k} \right] \left(\frac{\vec{p}_\beta \cdot \hat{k}}{E} \right) \mathrm{d}\hat{\Omega}_k = 0$
$f_{16}(E_\beta)$	$\int T_2(\hat{n}) : \left[\frac{\vec{p}_\beta}{E}, \frac{\vec{p}_\beta}{E} \times \hat{k} \right] \mathrm{d}\hat{\Omega}_k = 0$
$f_{17}(E_\beta)$	$\int T_2(\hat{n}) : \left[\hat{k}, \frac{\vec{p}_\beta}{E} \times \hat{k} \right] \mathrm{d}\hat{\Omega}_k = 0$
$f_{18}(E_\beta)$	$\int T_3(\hat{n}) : \left[\frac{\vec{p}_\beta}{E}, \frac{\vec{p}_\beta}{E}, \frac{\vec{p}_\beta}{E} \right] \mathrm{d}\hat{\Omega}_k = 4\pi T_3(\hat{n}) : \left[\frac{\vec{p}_\beta}{E}, \frac{\vec{p}_\beta}{E}, \frac{\vec{p}_\beta}{E} \right]$

Table C.4: Integrals of terms from Holstein's Eq. (51) [17].

$C_A = C'_A$; $g = \pm \frac{1}{\sqrt{2}} M_{GT} (C_A + C'_A)$ ← prefer \oplus
 $C_V = C'_V$; $a_1 = \pm \frac{1}{\sqrt{2}} M_F (C_V + C'_V)$ ← depends on above sign.

In our code:
 $M_F = 1.0$
 $M_{GT} = -0.62376$

Also in our Code:
 $g_V = 1.00$
 $g_A = 0.91210$

* Really, the conversion above doesn't include the extra terms in a_1 and g that couple to ^{nuclear} matrix elements other than M_F and M_{GT} .

I think the point is that I should actually interpret:

$$g_V = \pm \frac{1}{\sqrt{2}} (C_V + C'_V) = 1.0 \rightarrow a_1 = g_V M_F \Rightarrow C_V = C'_V = \frac{1}{\sqrt{2}}$$

$$g_A = \pm \frac{1}{\sqrt{2}} (C_A + C'_A) \approx 0.91210 \rightarrow C_1 = g_A M_{GT} \Rightarrow C_A = C'_A = \frac{-0.91210}{\sqrt{2}} \approx -0.644952$$

* Check: with $C_A = C'_A$ and $C_V = C'_V$, does JTW give the right A_β ?

~~$A_\beta = 0.323683$; $A_\beta = 0.496903 \rightarrow A_\beta = \underline{\underline{0.375394}}$ (bad!)~~

$A_\beta = 0.763671$ ← Allow M_{GT} and M_F to have opposite signs. (Bad!)
 $A_\beta = -0.568045$ ← enforce $\oplus M_{GT}$. Or earlier JTW "convention".

* Because Holstein insists on his own sign convention, we get $M_{GT-Holstein} = -M_{GT-JTW}$

Figure C.1: "Notes 0"

In our code:

$$\boxed{\begin{array}{lll} M_F = 1.0 & ; g_V = 1.0 & \rightarrow g_V M_F = 1.0 \\ M_{GT} = -0.62376 & ; g_A = 0.91210 & \rightarrow g_A M_{GT} = -0.568931 \end{array}} \Rightarrow \rho \equiv \frac{g_A M_{GT}}{g_V M_F} \approx -0.568931_{\text{Holstein}}$$

* If we require that $C_A, C_A', C_V, C_V', M_F, M_{GT}$ are all real, and enforce that these can all take values which allow for Holstein and JTWW to be equivalent in some limits, we require:

$$\begin{array}{lll} \text{JTWW} & \text{Holstein} & \text{Holstein} \quad \text{JTWW} \\ \left\{ \begin{array}{l} f_1(E) \\ f_4(E) \end{array} \right. & \rightarrow \begin{array}{l} |a_1|^2 = |M_F|^2 (|C_V|^2 + |C_V'|^2) \\ |C_1|^2 = |M_{GT}|^2 (|C_A|^2 + |C_A'|^2) \end{array} \\ \downarrow \quad \downarrow & & \downarrow \quad \downarrow \\ \rightarrow |a_1|^2 = 2|M_{GT}|^2 \cdot \text{Re}[C_A C_A'^*] \end{array}$$

$$\begin{aligned} \text{Re}[a_1^* C_1] &= -\text{Re}[M_F M_{GT} (C_V C_A'^* + C_V' C_A^*)] \leftarrow \text{later} \\ \text{Re}[a_1^* C_1] &= -\text{Re}[|M_F| |M_{GT}| (C_V C_A'^* + C_V' C_A^*)] \leftarrow \text{earlier.} \end{aligned}$$

The Results:

$$\begin{array}{lll} C_V = C_V' & \text{Holstein} & \text{JTWW} \\ C_A = C_A' & a_1 = \pm \frac{1}{\sqrt{2}} M_F (C_V + C_V') = \pm M_F (\pm \sqrt{2}) (C_V) \\ & C_1 = \pm \frac{1}{\sqrt{2}} M_{GT} (C_A + C_A') = \pm M_{GT} (\pm \sqrt{2}) (C_A) \end{array}$$

$$a_1 \approx g_V M_{F,H}; \quad C_1 \approx g_A M_{GT,H};$$

$$\boxed{M_{GT, \text{Holstein}} = -M_{GT, \text{JTWW}}}$$

which sign?!

$$a_1 \approx g_V M_F; \quad g_V = \pm \frac{1}{\sqrt{2}} (C_V + C_V') = 1.0; \quad M_F = 1.0; \quad ; \quad C_V = C_V'$$

$$C_1 \approx g_A M_{GT}; \quad g_A = \pm \frac{1}{\sqrt{2}} (C_A + C_A') \approx 0.91210; \quad M_{GT,H} = -0.62376; \quad C_A = C_A'$$

↑ ↑
JTWW terms!

Figure C.2: "Notes 1"

$$\begin{aligned}
b \cdot \bar{z} &= \pm 2\gamma \operatorname{Re} \left[|M_F|^2 (C_S C_V^* + C'_S C_V'^*) + |M_{GT}|^2 (C_T C_A^* + C'_T C_A'^*) \right] \\
&= -2\gamma \left[|M_F|^2 (C_S C_V^* + C'_S C_V'^*) + |M_{GT}|^2 (C_T C_A^* + C'_T C_A'^*) \right] \\
&= -2\gamma |M_F|^2 (C_S + C'_S) C_V^* + -2\gamma |M_{GT}|^2 (C_T + C'_T) C_A^* \\
&= -2\gamma |M_F|^2 \cdot \frac{1}{\sqrt{2}} g_V \underbrace{(C_S + C'_S)}_{+\sqrt{2} g_S} + -2\gamma |M_{GT}|^2 \frac{(-1)}{\sqrt{2}} g_A \underbrace{(C_T + C'_T)}_{-\sqrt{2} g_T} \\
&= -2\gamma |M_F|^2 \cdot g_V \cdot g_S - 2\gamma |M_{GT}|^2 \cdot g_A \cdot g_T \\
\boxed{b \cdot \bar{z} = -2\gamma [|M_F|^2 g_V g_S + |M_{GT}|^2 g_A g_T]}
\end{aligned}$$

~~BYE~~ $\gamma = (1 - \alpha^2 z^2)^{1/2}$

Figure C.3: "Notes 2"

To Match Up Holstein and JT W:

$$g_V = \frac{1}{\sqrt{2}}(C_V + C_V') ; \quad C_V = C_V' = \frac{+1}{\sqrt{2}} g_V = \frac{1}{\sqrt{2}}$$

$$a_1 \approx g_V M_F$$

$$g_A = \frac{-1}{\sqrt{2}}(C_A + C_A') ; \quad C_A = C_A' = \frac{-1}{\sqrt{2}} g_A \approx \frac{-1}{\sqrt{2}}(0.91210) \quad c_1 \approx g_A M_{GT}$$

Also define:

$$g_S \equiv \frac{1}{\sqrt{2}}(C_S + C_S') ; \quad C_S = C_S' = \frac{1}{\sqrt{2}} g_S \approx 0$$

$$g_T \equiv \frac{-1}{\sqrt{2}}(C_T + C_T') ; \quad C_T = C_T' = \frac{-1}{\sqrt{2}} g_T \approx 0$$

Then, we find:

$$\dot{\xi} = |M_F|^2(g_V^2 + g_S^2) + |M_{GT}|^2(g_A^2 + g_T^2)$$

$$A_p \dot{\xi} = \frac{2}{5} |M_{GT}|^2(g_A^2 + g_T^2) + 2(\frac{3}{5})^{\frac{1}{2}} M_F M_{GT} (g_V g_A - g_S g_T)$$

$$b \cdot \ddot{\xi} = -2\gamma [|M_F|^2 g_V g_S + |M_{GT}|^2 g_A g_T] ; \quad \gamma \equiv (1 - \alpha^2 \zeta^2)^{\frac{1}{2}}$$

$$F_0(E) \rightarrow F_0(E) + |M_F|^2 g_S^2 + |M_{GT}|^2 g_T^2$$

$$F_i(E) \rightarrow F_i(E) + \delta_{uv} \left(\frac{u}{u+v} \right) (-2) \cdot M_F M_{GT} \cdot g_S g_T + \alpha_{uv} \left(\frac{1}{u+v} \right) |M_{GT}|^2 g_T^2$$

Figure C.4: "Notes 3"

- * In some limits, Holstein and JT_W are equivalent. For simplicity, we will require that JT_W's terms $C_A, C_A', C_V, C_V', M_F$, and M_{GT} are entirely real.
- * The physical interpretation of this is that we ~~do not~~ require time-reversal symmetry to be obeyed.
- * We use the following relationships:

$$\begin{aligned} \zeta &= f(E) \rightarrow |C_V|^2 = |M_F|^2 \cdot (|C_V|^2 + |C_V'|^2) \\ A_B \zeta &= f'(E) \rightarrow |C_V'|^2 = |M_{GT}|^2 \cdot (|C_A|^2 + |C_A'|^2) \\ \end{aligned}$$

use the later JT_W sign convention.

$$\begin{aligned} |C_V|^2 &= 2 \cdot |M_{GT}|^2 \cdot \operatorname{Re}[C_A C_A'^*] \\ \operatorname{Re}[a_i^* C_V] &= -M_F M_{GT} \cdot \operatorname{Re}[C_V C_A'^* + C_V' C_A] \end{aligned}$$

- * Then, via trial and error, we find that the following set of relationships gives consistent results:

$$\begin{aligned} C_V &= C_V'; & a_i &= \pm \frac{1}{\sqrt{2}} M_F (C_V + C_V') \\ C_A &= C_A'; & g_i &= \pm \frac{1}{\sqrt{2}} M_{GT} (C_A + C_A') \end{aligned} \quad \left. \begin{array}{l} \text{Thus far, either set of} \\ \text{signs is consistent. But they} \\ \text{must be opposite.} \end{array} \right\}$$

- * In our code, which evaluates Holstein, we use these:

$a_i \approx g_V M_F$	$M_F = 1.0$	$g_V = 1.0$	Note that we believe we know M_F better than we know g_A . So, to measure " A_B ", we vary g_A and leave M_{GT} fixed.
$g_A \approx g_A M_{GT}$	$M_{GT} = -0.62376$	$g_A \approx 0.91210$	

- * We'll define some quantities, ρ :

$$\rho_{JT\bar{W}} = \frac{C_A \cdot M_{GT}}{C_V \cdot M_F}; \quad \rho_{\text{Holstein}} = \frac{g_A \cdot M_{GT}}{g_V \cdot M_F} \approx -0.568931$$

* This $\rho_{JT\bar{W}}$ uses our own definition from PRL.

* Note that A_B comes out physically wrong unless $\rho_{JT\bar{W}}$ is \oplus , ie, in A_B , there's a term $\sim [C_V C_A'^* + C_V' C_A]$ and we need the whole thing to come out \oplus . $\therefore C_V$'s and C_A 's must have opposite signs.

- * We'll take the convention that every body has the same matrix elements:

$$\begin{aligned} M_{GT, JT\bar{W}} &= M_{GT, \text{Holstein}} \\ M_{F, JT\bar{W}} &= M_{F, \text{Holstein}} \end{aligned}$$

- * Then:

$$\begin{aligned} C_V &= C_V' \Rightarrow \oplus \\ C_A &= C_A' \Rightarrow \ominus \end{aligned} \quad \left. \begin{array}{l} \text{This because at the end of the day, we want Holstein's} \\ \text{to be } \oplus, \text{ and } C_A \text{ to be } \ominus, \text{ or else we don't} \\ \text{produce the right physics.} \end{array} \right\}$$

$g_V = \frac{1}{\sqrt{2}} (C_V + C_V') = 1.0$	$C_V = C_V' = \frac{+1}{\sqrt{2}} g_V = \frac{1}{\sqrt{2}}$
$g_A = \frac{-1}{\sqrt{2}} (C_A + C_A') \approx +0.91210$	$C_A = C_A' = \frac{-1}{\sqrt{2}} g_A \approx \frac{-1}{\sqrt{2}} (0.91210)$

Figure C.5: "Notes 4"

- * In some limits, Holstein and JTW are equivalent. We require that JTW's terms $C_A, C_A', C_V, C_V', M_F$, and M_{GT} must all be entirely real. We can probably do this WLOG. (Or without very much loss of generality, at least.)
- * Use the following relationships:

$$\xi = f_x(E) \rightarrow |q_i|^2 = |M_F|^2 (|C_V|^2 + |C_V'|^2)$$

$$|C_V|^2 = |M_{GT}|^2 \cdot (|C_A|^2 + |C_A'|^2)$$

$$A \cdot \xi = f_x(E) \rightarrow |C_V|^2 = 2 \cdot |M_{GT}|^2 \cdot \text{Re}[C_V C_A'^*]$$

$$\text{Re}[C_V] = -\text{Re}[M_F M_{GT} (C_V C_A'^* + C_V' C_A)] \leftarrow \text{later JTW convention.}$$

we'll only use this.

- * Then, the following relationships give us internally consistent results:

$$\begin{aligned} C_V &= C_V' ; & a_i &= \pm \frac{1}{\sqrt{2}} M_F (C_V + C_V') \\ C_A &= C_A' ; & c_i &= \pm \frac{1}{\sqrt{2}} M_{GT} (C_A + C_A') \end{aligned} \quad \begin{array}{l} \text{either set of signs is consistent.} \\ \text{But they must be opposite.} \end{array}$$

Code has these signs for q_i and c_i .
Do I know why?

- * In our code (which evaluates Holstein), we use these values:

\oplus	$a_i \approx g_V M_F$	$M_F = 1.0$	$g_V = 1.0$
\ominus	$C_i \approx g_A M_{GT}$	$M_{GT} = -0.62376$	$g_A = -0.91210$

- * We can also define:

$\rho_{\text{Holstein}} \equiv \frac{g_A M_{GT}}{g_V M_F} \approx -0.568931$	$\rho_{\text{JTW}} \equiv \frac{C_A M_{GT}}{C_V M_F} = \oplus$	$\leftarrow \text{we use } \rho_{\text{JTW}} \text{ def. in PRL.}$
--	--	--

- * We do not get the correct JTW A_B unless we require that ρ_{JTW} is \oplus . Equivalently, we require that $\text{Re}[M_F M_{GT} (C_V C_A'^* + C_V' C_A)]$ must be \oplus . But M_{GT} is \ominus ! \rightarrow Option 1: Take $M_{GT, \text{JTW}} = -M_{GT, \text{Holstein}}$. \rightarrow Option 2: Take $C_A = C_A'$ to be \ominus , and $C_V = C_V'$ to be \oplus .

(really, there are other options.
But let's leave M_F and C_V alone.)

- * For Holstein to come out right, we need c_i to be \ominus , and q_i to be \oplus . I think.

$\bullet g_V = \frac{1}{\sqrt{2}} (C_V + C_V') = 1.0$
 $g_A = \frac{-1}{\sqrt{2}} (C_A + C_A') = 0.91210 \Rightarrow C_A \text{ must be } \ominus \text{ then, bc } g_A \text{ is } \oplus \text{ and } M_{GT, \text{Holstein}} \text{ is } \ominus, \text{ and we need } C_A \text{ to be } \ominus.$

- * OK. Now what do I do with C_S and G ? \rightarrow can't just stick them into M_F and M_{GT} . even in JTW it doesn't come out consistent.
- * Have to write JTW in Holstein notation so I can figure out where to put C_S, G in.

Figure C.6: "Notes 5"

Appendix D

Derivation of the b_{Fierz} Dependence of the Superratio Asymmetry

Appendix KLM you have to pick what you want— I hope that's Appendix K (that's this one!) – and remove the rest as you say they're "old". Appendix K could be moved to the end of Experimental Methods because it's absolutely critical and helpful!! but if you want to reference it there and leave it as an Appendix, it's up to you.

Recall the integrated JTW probability distribution for outgoing beta particles from Eq. (B.3):

$$\begin{aligned} d^3\Gamma(E_\beta, \hat{\Omega}_\beta) dE_\beta d^3\hat{\Omega}_\beta &= \frac{2}{(2\pi)^4} F_\mp(Z, E_\beta) \xi p_\beta E_\beta (E_0 - E_\beta)^2 dE_\beta d^3\hat{\Omega}_\beta \\ &\times \left[1 + b_{\text{Fierz}} \frac{m_e c^2}{E_\beta} + A_\beta \left(\frac{\vec{J}}{J} \cdot \frac{\vec{p}_\beta}{E_\beta} \right) \right]. \end{aligned} \quad (\text{D.1})$$

We note that the only angular dependence remaining in this equation is the dot product between the direction of beta emission and the direction of nuclear spin-polarization. This allows us to pull out a further factor of 2π by choosing the axis of polarization as defining our coordinate system, and integrating over the “ ϕ_β ” coordinate. The result is a bit more friendly to work with:

$$d^2\Gamma(E_\beta, \theta) dE_\beta d\theta = W(E_\beta) \left[1 + b_{\text{Fierz}} \frac{m_e c^2}{E_\beta} + A_\beta \frac{v_\beta}{c} |\vec{P}| \cos \theta \right] dE_\beta d\theta, \quad (\text{D.2})$$

where θ is the angle between the beta emission direction and the polarization direc-

tion, and is the only angular dependence that remains. Here, we have grouped the overall energy dependence into $W(E_\beta)$, so that

$$W(E_\beta) = \frac{2}{(2\pi)^3} F_{\mp}(Z, E_\beta) \xi p_\beta E_\beta (E_0 - E_\beta)^2, \quad (\text{D.3})$$

where we note that the Fermi functions in the above make Eq. D.3 integrable only by numerical methods. Because it would be difficult to make this expression *more* challenging to work with, it is therefore easy enough to include in this expression any small corrections to overall energy dependence that might arise from e.g. recoil-order corrections, as described by Holstein [17].

In the TRINAT geometry with two polarization states (+/-) and two detectors (T/B) aligned along the axis of polarization, we are able to describe four different count rates, with different combinations of polarization states and detectors. Thus, neglecting beta scattering effects, we have:

$$r_{T+}(E_\beta) = W(E_\beta) \varepsilon_T(E_\beta) \Omega_T N_+ \left[1 + b_{\text{Fierz}} \frac{m_e c^2}{E_\beta} + A_\beta \frac{v}{c} |\vec{P}_+| \langle \cos \theta \rangle_{T+} \right] \quad (\text{D.4})$$

$$r_{B+}(E_\beta) = W(E_\beta) \varepsilon_B(E_\beta) \Omega_B N_+ \left[1 + b_{\text{Fierz}} \frac{m_e c^2}{E_\beta} + A_\beta \frac{v}{c} |\vec{P}_+| \langle \cos \theta \rangle_{B+} \right] \quad (\text{D.5})$$

$$r_{T-}(E_\beta) = W(E_\beta) \varepsilon_T(E_\beta) \Omega_T N_- \left[1 + b_{\text{Fierz}} \frac{m_e c^2}{E_\beta} + A_\beta \frac{v}{c} |\vec{P}_-| \langle \cos \theta \rangle_{T-} \right] \quad (\text{D.6})$$

$$r_{B-}(E_\beta) = W(E_\beta) \varepsilon_B(E_\beta) \Omega_B N_- \left[1 + b_{\text{Fierz}} \frac{m_e c^2}{E_\beta} + A_\beta \frac{v}{c} |\vec{P}_-| \langle \cos \theta \rangle_{B-} \right], \quad (\text{D.7})$$

where $\varepsilon_{T/B}(E_\beta)$ are the (top/bottom) detector efficiencies, $\Omega_{T/B}$ are the fractional solid angles for the (top/bottom) detector from the trap position, $N_{+/-}$ are the number of atoms trapped in each (+/-) polarization state, and $|\vec{P}_{+/-}|$ are the magnitudes of the polarization along the detector axis for each polarization state. $\langle \cos \theta \rangle_{T/B,+/-}$ is the average of $\cos \theta$ for *observed* outgoing betas, for each detector and polarization state combination. This latter term is approximately ± 1 as a result of our detector geometry, but contains important sign information. For a pointlike trap in the center of the chamber, 103.484 mm from either (DSSSD) detector, each of which is taken to be circular with a radius of 15.5 mm, we find that $\langle |\cos \theta| \rangle_{T/B,+/-} \approx 0.994484$, and is the same for all four cases. Note that a horizontally displaced trap will decrease the magnitude of $\langle |\cos \theta| \rangle$, but as it is an expectation value of an absolute value,

Does this even agree with whatever I wrote about the geometry in the other section?

Not quite true. Some strips are missing.

This is only true if we neglect (back-)scatter. This is not actually a good approximation. But we have pretty good simulations to give us the real num-

all four will remain equal to one another. In the case of a vertically displaced trap, these four values will no longer all be equal, however it will still be the case that $\langle |\cos \theta| \rangle_{T+} = \langle |\cos \theta| \rangle_{T-}$, and $\langle |\cos \theta| \rangle_{B+} = \langle |\cos \theta| \rangle_{B-}$.

In the case of the present experiment, we note that $|\vec{P}_+| = |\vec{P}_-|$ is correct to a high degree of precision.

Is that definitely true, or is it only true to lowest order?

We define the ‘superratio’, s , to be:

$$s = s(E_\beta) := \frac{r_{T+} r_{B-}}{r_{T-} r_{B+}}, \quad (\text{D.8})$$

and the ‘superratio asymmetry’, A_{super} , as

$$A_{\text{super}} = A_{\text{super}}(E_\beta) := \frac{1 - \sqrt{s}}{1 + \sqrt{s}}. \quad (\text{D.9})$$

This is explicitly an experimental quantity that is measured directly by the above combination of count rates, however it is obvious that it reduces, under appropriate limits, to be equivalent to a naive asymmetry. In particular, if we require that the physical conditions and relative detector positions and sensitivities are identical when the polarization is flipped, then we have $r_{T+}(E_\beta) = r_{B-}(E_\beta)$ and $r_{T-}(E_\beta) = r_{B+}(E_\beta)$. It follows that we can simplify the superratio asymmetry into a more intuitive quantity that we might use for a measurement with only a single polarization state, e.g.,

$$A_{\text{super},+} \rightarrow \frac{r_T - r_B}{r_T + r_B}. \quad (\text{D.10})$$

While Eq. D.10 is conceptually encouraging, the assumptions that gave rise to that expression are too simplifying. We will introduce some more limited assumptions for what follows, along with shorthand notation for improved readability. First, we require that the magnitude of the polarization vector is the same for both polarization states, and also that the average of the magnitude of $\cos \theta$ for a given detector does not change when the polarization is flipped (equivalent to a requirement that the trap position doesn’t change when the polarization is flipped). Then:

$$P := |\vec{P}_+| = |\vec{P}_-| \quad (\text{D.11})$$

$$\langle |\cos \theta| \rangle_T := \langle |\cos \theta| \rangle_{T+} = \langle |\cos \theta| \rangle_{T-} \quad (\text{D.12})$$

$$\langle |\cos \theta| \rangle_B := \langle |\cos \theta| \rangle_{B+} = \langle |\cos \theta| \rangle_{B-}, \quad (\text{D.13})$$

and we can further define

$$c = \langle |\cos \theta| \rangle := \frac{1}{2} (\langle |\cos \theta| \rangle_T + \langle |\cos \theta| \rangle_B) \quad (\text{D.14})$$

$$\Delta c = \Delta \langle |\cos \theta| \rangle := \frac{1}{2} (\langle |\cos \theta| \rangle_T - \langle |\cos \theta| \rangle_B) \quad (\text{D.15})$$

and

$$\tilde{A} = \tilde{A}(E_\beta) := A_\beta \frac{v}{c} \quad (\text{D.16})$$

$$\tilde{b} = \tilde{b}(E_\beta) := b_{\text{Fierz}} \frac{mc^2}{E_\beta}, \quad (\text{D.17})$$

$$\tilde{r} = \tilde{r}(E_\beta) := 1 + \tilde{b}. \quad (\text{D.18})$$

With this new set of variables defined, we can re-write Eqs. (D.4-D.7) as

$$r_{T+}(E_\beta) = W(E_\beta) \varepsilon_T(E_\beta) \Omega_T N_+ [\tilde{r} + \tilde{A}P(c + \Delta c)] \quad (\text{D.19})$$

$$r_{B+}(E_\beta) = W(E_\beta) \varepsilon_B(E_\beta) \Omega_B N_+ [\tilde{r} - \tilde{A}P(c - \Delta c)] \quad (\text{D.20})$$

$$r_{T-}(E_\beta) = W(E_\beta) \varepsilon_T(E_\beta) \Omega_T N_- [\tilde{r} - \tilde{A}P(c + \Delta c)] \quad (\text{D.21})$$

$$r_{B-}(E_\beta) = W(E_\beta) \varepsilon_B(E_\beta) \Omega_B N_- [\tilde{r} + \tilde{A}P(c - \Delta c)], \quad (\text{D.22})$$

and the superratio becomes

$$s = \frac{(\tilde{r} + \tilde{A}Pc)^2 - (\Delta c)^2}{(\tilde{r} - \tilde{A}Pc)^2 - (\Delta c)^2} \quad (\text{D.23})$$

where all factors of $W(E_\beta)$, $\varepsilon_{T/B}(E_\beta)$, $\Omega_{T/B}$, and $N_{+/}$ have been cancelled out entirely.

For simplicity we take $\Delta c = 0$ in what follows. Although this is not strictly accurate within the present experiment, this assumption greatly simplifies the expressions that follow. Then, absent other corrections (*e.g.* backscattering, unpolarized background, ...), it is clear that if $\tilde{b} = 0$ as in the Standard Model,

$$A_{\text{super}} = \tilde{A}Pc = A_\beta \frac{v}{c} |\vec{P}| \langle |\cos \theta| \rangle \quad (\text{D.24})$$

In the case where $\tilde{b} \neq 0$, we find that

$$A_{\text{super}} = \frac{\tilde{A}Pc}{1 + \tilde{b}} \quad (\text{D.25})$$

$$\approx \tilde{A}Pc(1 - \tilde{b} + \tilde{b}^2), \quad (\text{D.26})$$

where we have utilized the assumption that $\tilde{b} \ll 1$. Thus, to leading order in terms of \tilde{b} ,

$$A_{\text{super}} \approx A_\beta \frac{v}{c} |\vec{P}| \langle |\cos \theta| \rangle \left(1 - b_{\text{Fierz}} \frac{mc^2}{E_\beta} \right). \quad (\text{D.27})$$